Contract: 031038

CELPACT

Cellular Structures for Impact Performance

FP6 - Specific Targeted Research Projects (STREP)

Priority T4 – Aeronautics

Publishable final activity report

Start date of project: 01/09/2006 **Duration:** 37 Months

Responsible partner: DLR

Contributors: All Partners

Contents

1. Project execution

I.1. Project objectives

The European aircraft industry has strong interest in **novel structural concepts** for future aircraft fuselage and wing structures with lower fabrication costs and high performance. An important class of these next generation aerospace materials will employ **advanced manufacturing techniques** for sandwich structures with cellular core materials giving high strength/weight and improved impact resistance under critical aircraft load cases such as foreign object impact from birds, tyre rubber and runway debris.

The main objective of the project is **development and design of cellular materials and twin skinned sandwich structures** made from hybrid composites and metals. CELPACT is progressing fabrication technology for **cellular metals based on selective laser melting** and developing new fabrication concepts for hybrid **composite sandwich structures with folded cellular composite cores**. Computational methods are being developed based on micromechanics cell models with multiscale modelling techniques for understanding progressive damage and collapse mechanisms and used for structural analysis. Impact performance is critical for sandwich aircraft structures and the simulation tools are being used to **design efficient impact resistant aircraft structures**. Structural integrity of these advanced cellular structures is being assessed by testing generic cellular beam and shell structures under high velocity impact conditions relevant to aircraft structures.

The CELPACT proposal focuses on basic research, for implementation by industry in an 8 to 12 year time scale. The research includes next generation manufacturing techniques for both composite hybrid and metal cellular materials and structures. There will be a wide range of candidate materials and geometries considered: Cellular Hybrid Composites (CHC) with folded composite core structures, Cellular Metal (CM) with closed cell cores and selected laser melted lattice cores.

Main Objectives

The development of new classes of materials for aeronautical structures based on:

- Cellular metallic core structures
- Cellular hybrid composite core structures.

The development of new manufacturing processes based on:

- Laser forming for manufacturing complex three dimensional metallic lattice structures

- Brazing and bonding technology for making periodic closed and open cell metallic structures
- Folded composite cell structures from aramid paper and carbon prepreg
- Fabrication of twin-walled sandwich structures with innovative cores

The development of numerical tools to:

- Predict the mechanical behaviour of the cellular materials
- Optimise the cellular and sandwich concepts with regard to applications.
- Develop design tools for predicting impact damage and failure in sandwich structures

Technology validation studies to demonstrate viability of these new materials for future aircraft structures:

- Validated design procedures for novel cellular and sandwich structures
- Impact design tools validated by low and high velocity impact test programmes on sandwich panels
- Road map for dissemination to aircraft industry design teams

CELPACT Overview

Current aircraft sandwich structures are made from CFRP skins with Nomex paper honeycomb or polymer foam cores for low weight secondary structures such as radomes, wing flaps, internal bulkheads, luggage containers, etc. More critical structures with improved energy absorption may have aluminium skins with aluminium honeycomb cores. In all cases the main function of the core is to be low weight, low cost, and stiff enough in shear and compression to maintain the separation distance between the load bearing skins. The developments being considered in CELPACT are new low weight structural cellular cores with enhanced properties made of composites and metals. New folded composite core structures are fabricated in a continuous manufacturing process which is currently under development at the University of Stuttgart. The core material for the initial state-of-the-art cell structures is aramid fibre paper preimpregnated with phenolic resin with folding patterns based on a trapeze-form zig-zag geometry, which gives an open repeating cellular structure. By varying the geometry parameters about 30 standard foldcore core materials have been defined using aramid/phenolic core material with core thickness ranging from 10 – 30 mm and core densities from 50 – 200 kg/m³, giving a wide potential range of core mechanical properties. Other composite core materials and cell geometries with carbon and aramid fabric reinforcements are also being evaluated by partners in CELPACT. Hybrid composite sandwich panels have been developed and tested with CFRP skins bonded to the foldcores. An important feature of foldcore is that it has open cells and sandwich panels can be ventilated, which is important for aircraft structures such as fuselage panels or wing flaps since there is a problem with moisture accretion in conventional Nomex honeycomb core structures.

A second group of advanced cellular materials being studied uses an open lattice geometry cellular metal (CM) core which is being developed at Liverpool University, with fabrication by selective laser melting (SLM) with stainless steel and titanium as basic core materials. With the rapid prototyping SLM technique, the realisation of metallic open cellular lattice structures at the micro scale is possible with precise microstructure geometry. Sandwich structures with CM cores have been developed with CFRP skins by directly embedding the lattice core into the carbon/epoxy prepreg before curing, which has been demonstrated to provide a strong skin-core bond. Alternative high performance CM core materials were investigated with larger scale steel struts braised together from press formed meshed sheets, and with closed cell cores consisting of hollow nickel spheres, close packed and adhesively bonded together with epoxy resin. In the latter case the aim is to replace metallic foam cores, which have variable geometry due to manufacture, with a core of consistent density and spherical pore size. In this case the CM core materials are fabricated into metallic sandwich panels with bonded aluminium skins and could be suitable for aircraft applications such as bird impact protection panels in the front cockpit. Baseline metallic cores using conventional aluminium honeycomb and new CM cores out of foldcore with aluminium replacing the aramid paper were also fabricated during the final year. This allowed impact tests to be carried out with new CM cores and compared with conventional honeycomb cores.

To support the materials developments, computational methods were developed based on micromechanics cell models with multiscale modelling techniques for understanding progressive damage and collapse mechanisms for use in structural analysis. Impact performance is critical for sandwich aircraft structures and the simulation tools were used to design efficient impact resistant

aircraft structures. For sandwich structures homogenised unit cell models which have equivalent mechanical properties to the cell microscale models were developed and implemented in FE codes. To simulate structural response under impact loads multiscale modelling techniques were proposed based on combining homogenised models away from the impact zone with microscale models in the damaged region. Finally structural integrity of these advanced cellular structures were assessed by dynamic materials tests and gas gun impact tests on cellular beam and panel structures under high velocity impact conditions relevant to aircraft structures.

Coordinator's Assessment

The CELPACT project objectives have been essentially met at the end of the project. Thus the second phase improved core materials, core specimens and sandwich element specimens were fabricated and supplied to the test partners for evaluation. Test programmes on CM and CHC core materials at the cell material and cell microstructure level have all been completed providing property data for validation of the microscale cell modelling methods. The core and sandwich plate impact tests were all completed, on the Phase 2 materials. Focus in the last year on testing was completion of low and high velocity impact test programmes on all 2nd phase core materials and sandwich panels. Many more tests were performed than in the original planning, since further core concepts were introduced such as hybrid dual foldcores with intermediate core fabric ply, and aluminium foldcore as an alternative to aluminium honeycomb. Impact test programmes also considered a wide range of projectiles, including steel balls, cubes and beams, tyre rubber fragments and gelatine to represent a synthetic bird. Extensive use was made by several partners of new DLR facilities for high definition X-ray CT scanning of structural damage. This advanced diagnostic facility was only in planning when CELPACT was proposed, but its arrival during the project allowed detailed images of microfailures within the cores of sandwich panels in a fully non-destructive test.

Modelling activities were built on the initial generic unit cell micro models, by extending them to modelling strategies for core and sandwich materials. The main thrust of modelling in the second half of the project was to complete the impact modelling techniques and validate them by careful comparison with impact test data from both CHC and CM sandwich panels in WP4. Several different impact modelling strategies were developed in the group depending on FE codes available and the type of core and sandwich structure. Core models were based on either microstruts or folded core shells, which requires different FE approaches, then another significant factor is the sandwich skin material, ductile aluminium or more brittle carbon composite laminates. For the CM panels good agreements were found with test data for both strut cores and bonded nickel microspheres, with both aluminium and carbon skins. Foldcore was only used with carbon laminate skins. Here it was seen that for several types of impact, either at lower energies or by soft bodies that skin models had to include delamination failure mechanisms to give better agreement with observed damage from CT and measured failure behaviour.

CELPACT was an upstream project looking at potential aircraft sandwich structures for applications in 10 years time. This is a challenge as until now sandwich materials are used as secondary aircraft structures and the aim of studying high performance metallic and composite cores is to develop primary sandwich structures. For composite aircraft structures foldcore now looks very promising for the future, particularly for niche applications where foldcore and hybrid foldcore concepts can be used in specific regions requiring high impact protection or crash energy absorption where a small weight penalty is permissible. For the CM structures it appears hard to overtake aluminium honeycomb which has been optimised over 20 years for low weight aircraft secondary panel structures. New core materials such as the strut cores oe microspheres have similar energy absorbing properties to honeycomb but are either heavier or more expensive at present. The SLM materials have high potential for graded density aircraft structures such as beams, frames etc rather than thin panel structures, because they employ an additive manufacturing technology, rather than a subtractive technology as in standard machining of aluminium profiles, which can lead to 90% materials wastage in extreme cases.

I.2. Contractors involved

CELPACT Coordinator

Dr Alastair Johnson
German Aerospace Center (DLR)
Institute of Structures and Design
Pfaffenwaldring 38-40
70569 Stuttgart, Germany

Tel: +49 711 6862-297
Fax: +49 711 6862-227

Email: alastair.johnson@dlr.de

CELPACT is an upstream proposal which has been prioritised by the European Aeronautical Scientific Network (EASN). The consortium from five European countries contains seven leading universities with research institutes and aircraft industry partners, as listed below:

Partic. Role*	Partic. no.	Participant name	Participant short name	Country
CO	1	German Aerospace Centre	DLR	Germany
CR	2	University of Liverpool	ULIV	UK
CR	3	University of Oxford	UOXF	UK
CR	4	University of Patras	UPAT	Greece
CR	5	University of Aachen	RWTH	Germany
CR	6	ENS de Cachan	LMT	France
CR	7	University of Stuttgart	USTU	Germany
CR	8	University of Brno	UBRN	Czech Republic
CR	9	ATECA	ATEC	France
CR	10	Airbus-Deutschland	A-D	Germany
CR	11	EADS IW F (ex CRC-F)	EADS IW F (ex CRC-F)	France
CR	12	EADS Gmbh	CRC-G	Germany
CR	13	ALMA Consulting	ALMA	France

*CO = Coordinator, CR = Contractor

I.3. Work performed and end results

WP 1: Manufacture of cellular Structures (WP Leader: ULIV)

WP Leader	ULIV
Participants	DLR, ULIV, UOXF, UPAT, RWTH, LMT, USTU, UBRN, CRC-G, EADS IW F, AD

The main aims of this work package was to define the cellular materials and to manufacture CM and CHC materials.

Cellular materials have been defined in Deliverable D11-1. 'First generation' CM and CHC materials have been manufactures for relevant partners. 'Second Generation' CM and CHC materials have been defined at mid-term of the project.

Specification of 'first' and 'Second' Generation materials

Work carried out in this Task is aimed at specifying materials, cellular geometries, sandwich constructions, and sandwich structures for manufacture, core design and analysis, impact testing and code validation studies. The specification here is a basis for initial fabrication, analysis and test programmes in the first phase of CELPACT, up to the Critical design Review (M18).

All CELPACT partners were involved in this specification activity through their contributions at the Kick-off meeting technical session (15.09.06), participation at planning Workshops for WP2 in Cachan (18.10.06), for WP1.3 in Stuttgart (18.12.06) and in the e-Workshop for WP3. The lead in the detailed specification was taken by the Coordinator (DLR), together with the WP1 Task leaders A-D, ULIV and USTU, the WP2 coordinator LMT and the WP3 coordinator UOXF. The final Specification was summarized in report D11-1.

DLR organised a Critical Design Review meeting on 21/5/08 in Brussels, which was followed by working meetings on CM and CHC materials at CRC-F and LMT, respectively. This led to an update of the Specification Report by defining core materials and sandwich concepts with improved impact resistance for study in the second phase.

Agreed 'second generation' structures are:

Table 1: Updated specification of core materials for manufacture

Material type	CM-SLM	CM-Conventional	CHC-Continuous	CHC-Discontinuous
Manufacturer	ULIV	ATECA	USTU	CRC-G (KGTU)
Cell code name			05-12.5-H10 to 05-12.5-H30 Ro 75 – 200 – Block core	Z-Crimp Dual core
Cell geometry	BCC lattice	1) Assembly of hollow spheres 2) Open truss	Folded open cell from continuous prepreg paper	Folded open cell press formed from prepreg sheets
Cell material	Laser melted Ti 64	1) Bonded or brazed hollow nickel spheres, thickness 12 µm 2) Steel	Folded aramid prepreg paper N637, thickness 0.3 mm	Carbon fabric 0.39 , 0.195 mm Aramid fabric 0.48 mm
Cell size (mm)	Cell 2.5mm, Strut diam. 200 µm Core height 20-50	1) Spheres. diam 2.5 mm 2) Strut section – not specified Core height 25 - 50	Cell variables 5 x 12.5 Core height 10 - 30	Cell variables 20 x 21 x 10 Core height 28 mm
Core Density (kg/m3)	170	200 - 400	75 - 200	60 - 120
Panel size (m)	0.25 x 0.25 (2007) 0.5 x 0.5 (2008)		Unlimited length	0.3 x 0.3
Skin material	2.1 mm Q/I UD carbon/epoxy Cytech HTS/977-2	1.2 mm alu 2024	2.1 mm Q/I UD carbon/epoxy Cytech HTS/977-2	2.1 mm Q/I UD carbon/epoxy Cytech HTS/977-2
Skin/core bonding	Bonded/co-cured	Brazed or bonded - Hysol 9321	Bonded film – Redux 319	Bonded - Epibond 1590
Core/SW production	ULIV	ATECA	USTU	33 core panels purchased CRC-G fabricates SW
Partner supplied	UOXF, ULIV, UPAT	CRC-F, UOXF, UPAT, DLR	LMT, RWTH, DLR	CRC-G, RWTH, DLR

ULIV

A schematic of the SLM manufacturing process is shown in Figure 1(a), in which a layer of powder is deposited onto a substrate and is spread uniformly by a wiper. A high power fibre laser fully melts the pre-deposited powder layer according to a specific computer-generated pattern, i.e. the geometry of the component cross-section is 'drawn' onto the powder bed by the laser. The melted particles fuse and solidify to form a layer of the component. The build platform then moves down by 50 µm and a new powder layer is spread and scanned. The process is repeated to yield a solid equivalent of the original 3D model. The excess powder is collected and reused, thereby reducing material costs. It should be noted that the open cells allow the removal of the powder. It is possible to build fine details using the SLM technique such as cylindrical struts of approximately 150 µm diameter.

The apparatus used in the present study was a MCP Realizer II (Figure 1(b)), a commercial SLM workstation with a 200 W continuous wave Ytterbium Fibre Laser operating at a wavelength of 1068-

1095 nm. The build envelope of this machine is 250x250x240 mm. The scanning system used is a Dual Axis Mirror Positioning System and a Galvanometer Optical Scanner, which directs the laser beam in the x and y axes. The variable focussing optic is a Sill 300 mm focal length f-theta lens, which produce a focussed beam spot size diameter of 90 µm. Since the powder is fully melted during the manufacturing process, protection of the parts from oxidation is essential. Therefore metal powder processing is undertaken in an inert (Argon) atmosphere.

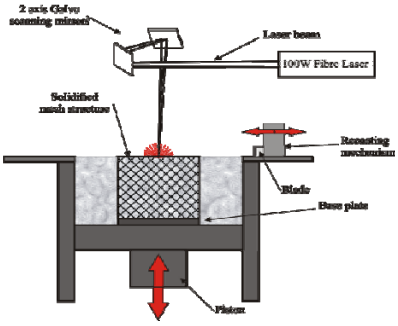

(a)

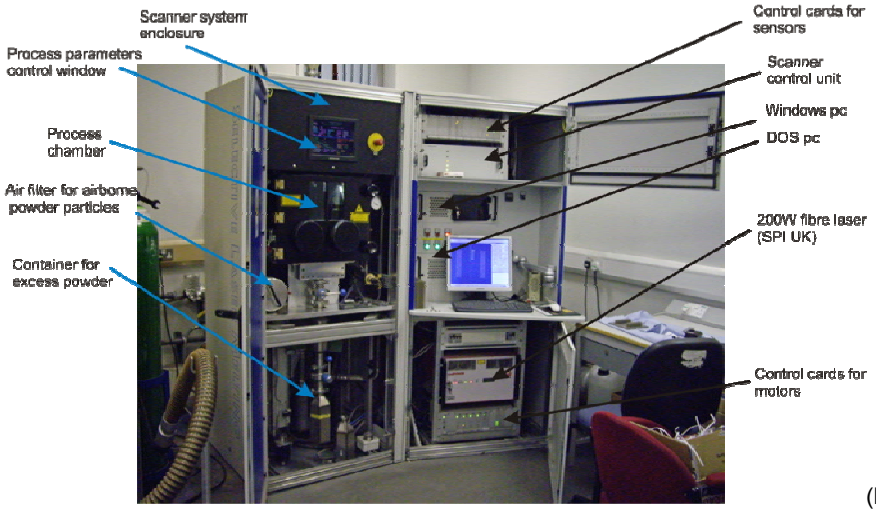

(b)

Figure 1: (a) Schematic of the SLM process, (b) the MCP Realizer II machine.

Essentially, various micro lattice configurations can be realised, covering body centred cubic (bcc) (see Figure 2), face centred cubic and other geometries. It was decided to focus on bcc here.

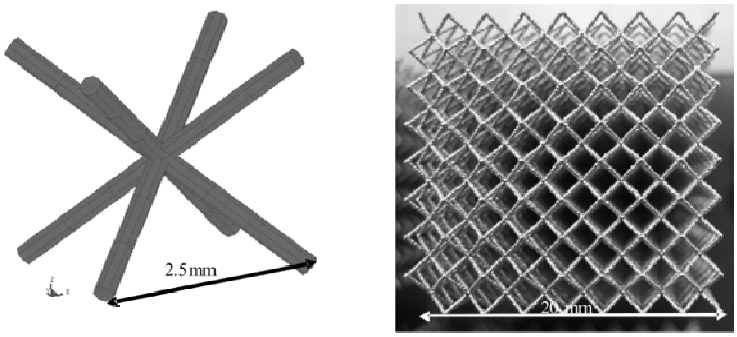

(a) (b)

Figure 2: Geometry of the BCC unit-cell and an example of a micro-lattice block.

For the purposes of Celpact, blocks of dimension 50 mm cubed, 100 x 100 x 20mm (small panel) and 150 x 150 x 50 mm (large panel) were made from both stainless steel 316L and Ti 6 4 powder.

Panels

Small panel and large panel blocks were then combined with carbon epoxy skins. Table 1 gives detail of the ULIV skins. Figure 3 shows the hot press and Figure 4 shows the resultant panel. Figure 5 gives detail of the skin core bond line.

Table 1: Skin material parameters.

Prepreg material	Skin lay-up	Areal density	Tensile modulus (8 ply laminate)	Tensile strength (8 ply laminate)
		g/m^2	GPa	MPa
Plain weave Carbon fibre / epoxy matrix	4 ply-nominal thickness 1.1mm	410 +/-15	58	850

Pressure was applied at approximately 1 bar, and a temperature of 120°C for approximately 2 hours. Careful control of the pressure was required to prevent yielding of the lattice core but was still high enough to bond the prepregs together.

Figure 3: Hot Press.

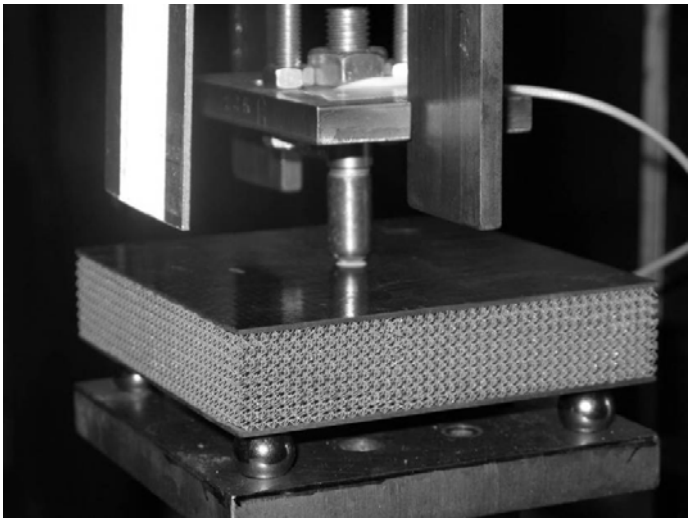

Figure 4: Small Panel in impact rig

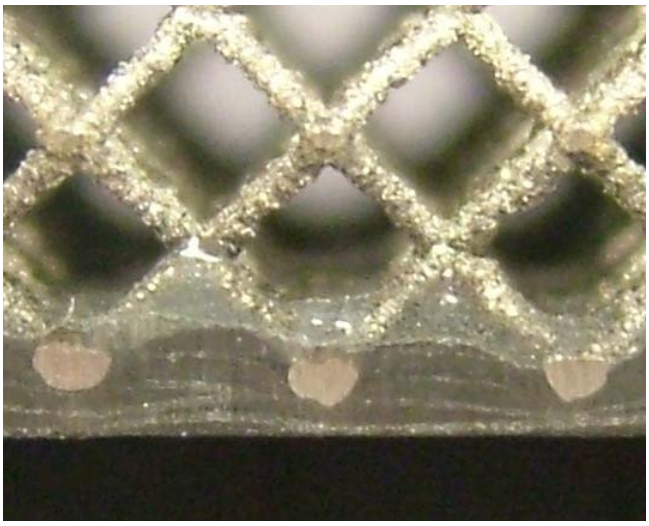

Figure 5: Core skin bond detail

From Figure 5, it can be seen that there is good bonding between core and skin.

The constraints of the manufacturing procedure are as follows. The process of SLM is time consuming – it takes about 5 hours to manufacture the small panel, but a number of cores can be made at the same time and the whole process is automated. The current build envelope is 200 x 200 x 250mm, but a larger machine (500 mm cubed build envelope) is being built.

It should be noted that 3D structures with integral metallic skins (see Figure 6) can be built.

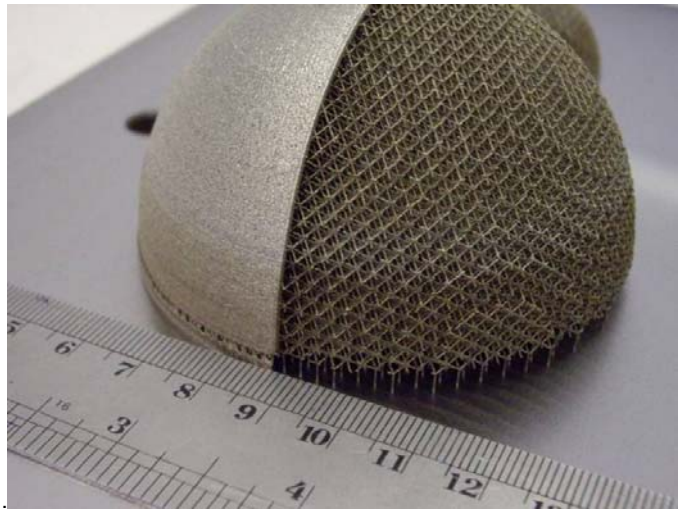

Figure 6: Example of the three dimensional complexity that can be achieved using the SLM process.

It can therefore be concluded that currently the process is most applicable to small, high value added, components. For example, the process has applicability to aero engine components. However, in the longer term, the process should become faster, more cost effective with larger panels being able to be produced. One possible item for future work is the welding together of lattice blocks to create larger structures.

It should also be noted that micro lattice configurations can be adjusted to optimise core properties [2].

References

1. Mines R, Tsopanos S, Celpact Deliverable D 123, February 2009
2. Mines R, Tsopanos S, Celpact Deliverable D 413, March 2009

ATECA

ATECA was in charge of manufacturing **closed cell periodic cellular Metals (CM) core structures** with high stiffness/weight and low density. These cellular metallic structures were manufactured starting from porous materials such as hollow spheres- **1rst generation**- and from truss core structures – **2nd generation**.

- **Work performed :**

- **First generation :**

The micro scale cell geometry is based on the hollow spheres. Their manufacturing process was patented by ATECA in 1985. No optimization was done on the manufacturing process during this project but the hollow spheres were designed to answer to the required mechanical properties.

144 Samples for static tests and impact tests were manufactured in order to evaluate the potential of this material for the targeted application.

Figure 7: Hollow Spheres produced for the CELPACT project.

- **Second generation:**

This work was based on the publications from Wadley et al.[1] . This was a totally new research activity for ATECA and a dedicated equipment was built to produce the needed specimens. A manufacturing strategy was defined to manufacture these specimens.

The process can be described as follows. A squarely perforated sheet is subject to punch loading to create a pyramidal truss layer. The different truss layers are then brazed together to form the desired 3D structure.

[1] Phil. Trans. R. Soc. A (2006) 364, 31–68

The manufacturing process was optimized thanks to the new equipment but the manufacturing time (about 6 hours for a 200 x 200 x 50 mm specimen) and the brazing time are still long.

30 Samples for static tests and impact tests were manufactured. All specimens were manufactured, supplied and tested successfully.

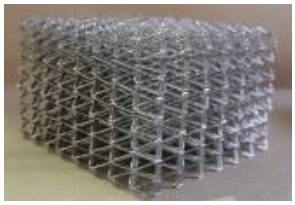

Figure 8: Metallic core made of "Wadley" Structures

- **Results :**

- **First generation:**

Adhesion between the spheres is a key point and was not really satisfying in this project. It has been seen that the impact properties were rather low compared to the other metallic cores. However this material is rather light and easy to shape and could present a good compromise for other aeronautical applications.

- **Second generation:**

Time of manufacturing has been improved and limitations like the maximum size of specimens have been overcome.

It should be noted that between the first and the last manufactured specimens, the density was decreased from 650 kg/m^3 till 540 kg/m^3. The measured densities are rather high for aeronautic applications and one optimisation should focus on the change in the raw materials and in the layers geometry.

However the 2nd route presents some improved impact properties compared to the 1rst route. The energy dissipation capacity was multiplied by 10 (see UOXF Results in WP3). These results show that this material has an interesting potential for the targeted application. Nevertheless the manufacturing parameters were not fully optimized and more work should be done based on the numerical model developed by UPAT.

USTU

A foldcore is an origami-like structural sandwich core. It is manufactured by folding a planar base material into a three dimensional structure. A foldcore panel consists of several unit cells, a typical foldcore unit cell is shown in fig. 9. This unit cell has five independent geometrical parameters, which means that the unit cell can be adjusted to specific needs. Also the base material which is used to produce foldcores can be varied.

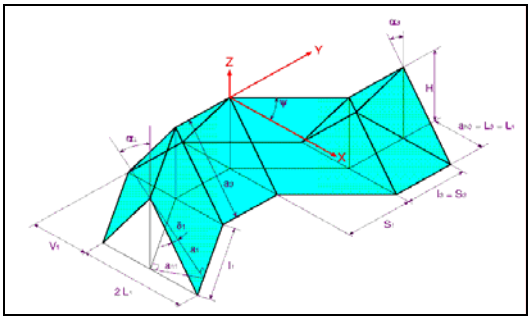

fig. 9. Foldcore unit cell with geometrical parameters

Within the project CELPACT, the goal was to characterize foldcores under static loading and impact loading and to characterize their post damage properties by performing residual strength tests. These results were then used to define a foldcore which is optimised for impact loading.

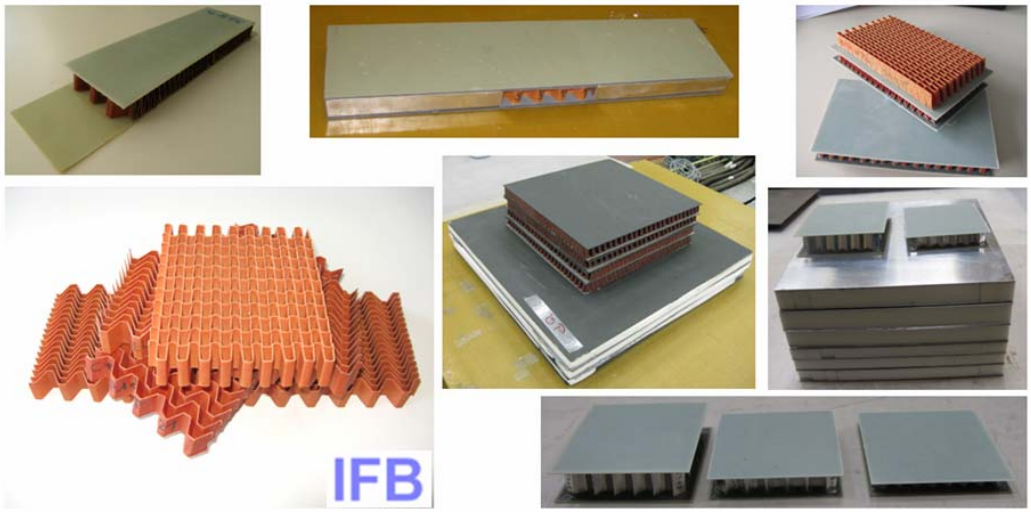

fig. 10. Some of the foldcores which were produced at USTU for CELPACT

In the first phase of the project, foldcores in different baseline unit cell geometries were produced and tested. These tests included standard static sandwich tests, impact test, dynamic tests and residual strength tests. From the results of the baseline foldcores, two improved designs (Fig 11) for the next generation foldcores with improved impact performance were defined.

One concept is to use a unit cell with high compression strength and stiffness – the blocked configuration. For comparability with the baseline foldcores, the core density, the core height and the base material were kept constant.

The second concept is to change the base material. Here aluminium is used because of its ductile material behaviour.

For both improved designs, samples for static tests and for impact tests were manufactured.

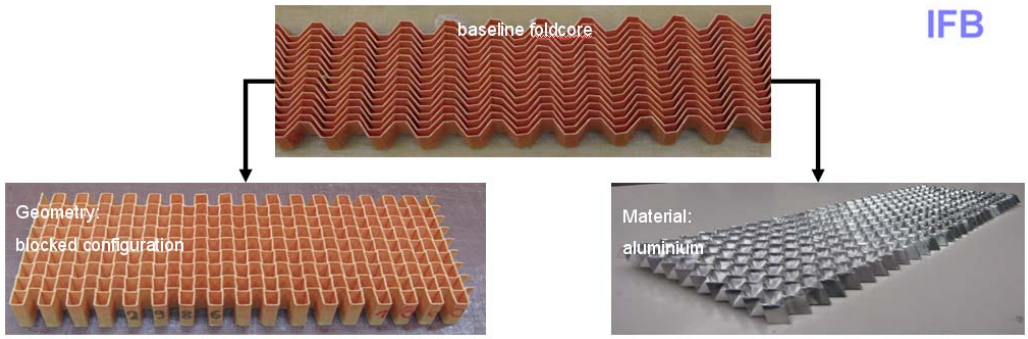

fig. 11: Two concepts for improving the impact performance of foldcores

Accompanying the production of sandwich samples, samples for material tests were also built. These were samples from both foldcore base materials - aramid fiber paper and aluminium – and from both face sheet materials – aluminium 2024 and CFRP.

- Results

Folccores were manufactured successfully in constant quality. Cores with high density and also the blocked configuration were managed. The manufacturing process was adapted to a different base material; aluminium. Manufacturing of the aluminium foldcores was successful performed with stable quality.

The test programmes on base materials and cores gave deeper inside in the mechanical properties of foldcores and their relationship to base material and unit cell geometry.

Concepts for foldcores with improved impact performance were developed.

CRC-G:

The focus of CRC-G within the CELPACT project was on folded carbon composite cores made from unidirectional and woven fabric composite prepregs, as a contrast to the random fibre aramid paper foldcores. These carbon foldcores – offering the well-known advantage of open ventilation channels – were produced and supplied by the Kazan State Technical University in Russia, using a discontinuous manufacturing process. The basic principle of this process is to convert a flat sheet of material into the final foldcore shape by folding or locally bending the material without elongating it. The folding is achieved by the use of transformable matrices (Fig. 12). Those matrices consist of flexibly joined metal plates, representing the cell wall geometry. In CELPACT the Z-crimp configuration was produced, which consists of a simple zigzag pattern. After folding, the prepreg material was cured in an autoclave.

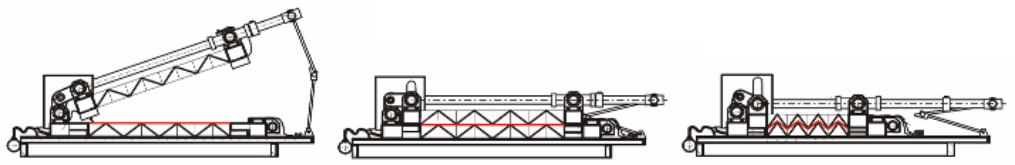

Fig. 12: Illustration of folding process with transformable matrices

In the first phase of the project, a three-ply carbon composite laminate with unidirectional plies and a stacking sequence of [0°/90°/0°] was used for the cell wall material. Based on the knowledge gained from these first specimens, some enhancements were implemented in the 2nd phase foldcore structures. First of all, woven fabric prepreg material was used for the cell walls, as it is easier to handle during manufacturing compared to the unidirectional material. The unit cell geometry was

optimised in a numerical study in order to obtain increased compressive properties while maintaining the same global density of around 110 kg/m³. Furthermore, a dual-core configuration was investigated, using two separate foldcore layers – one carbon foldcore and one aramid foldcore – and an aramid plate in-between (Fig. 13). This concept may allow for a two-phase energy absorption behaviour. All sandwich structures consisted of quasi-isotropic carbon/epoxy skins, which were bonded onto the foldcores with an epoxy-based pasty adhesive.

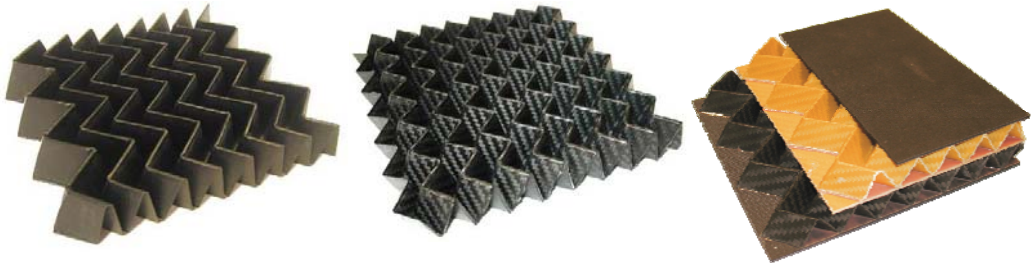

Fig. 13.: 1st phase carbon foldcore made of unidirectional plies (left), 2nd phase carbon foldcore with optimised geometry made of woven fabric (middle) and dual-core configuration (right)

The increased performance of these 2nd phase structures could be verified during the compression and impact test series, demonstrating that the foldcore structures offer the designer certain measures to tailor the core's properties for specific requirements (like the compressive behaviour). These measures are primarily the choice of cell wall material, cell geometry and single core/multi-core configuration. However, it has to be stated that the discontinuous manufacturing process, which was used for the production of these carbon foldcores, is more or less limited to the prototype level, because the final foldcore plate size is of limited dimensions, which is insufficient when it comes to the manufacturing of large quantities on an industrial level.

WP 2: Modeling and Simulation (WP Leader: LMT)

WP Leader	LMT
Participants	DLR, ULIV, UOXF, UPAT, RWTH, LMT, USTU, UBRN, CRC-G

The WP objectives were:

- To develop models for predicting the mechanical behaviour of CM and CHC cellular cores and their sandwich structures in terms of core cell geometry, core materials and sandwich skins.
- To develop numerical FE techniques for simulating damage and failure in cellular core sandwich structures under high and low velocity impact loads from hard and soft projectiles.

The WP2 work package is divided into three tasks. In task WP2.1, the unit cell modelling is developed: geometry, material behaviour and description of degradation mechanisms. In task WP2.2, homogenisation, multiscale modelling strategies and multiscale computational strategies are developed. In task WP2.3, industrial cases are treated. Note that all tools used in WP2.3 are developed and implemented in WP2.2. WP2.3 is only an application task. Note that validation is treated in WP4, thus the quality of the models developed in WP2 is assessed only in WP4.

For this simulation task, different numerical tools are used according to the partner: industrial explicit codes and in-house research codes that mainly address implicit problems. The former is dedicated to explicit problems that require high level of performances and complexities in high-speed dynamics. The latter is used to develop future computational strategies and models and to verify the accuracy of solutions given by industrial codes for simple test cases.

CHC cores

CRC-G contributions:

In this work package CRC-G focussed on the FE modelling of CFRP composite foldcore structures of the ‘Kazan’-type with LS-DYNA. Unit cell models and homogenised models were developed and multi-model coupling analyses were performed. Finally, impact simulation models were generated for low and high velocity impact simulations.

Unit cell modelling:

In order to be able to easily generate foldcore unit cell models of different geometries with the pre-processing tool PATRAN, a parametric model was developed in the command language PCL (Patran Command Language). The geometric model is defined by the foldcore height, the zigzag opening angle and two further spacing parameters. Inside the code a unit cell is generated from the geometry input and duplicated in both in-plane directions as prescribed by the model size. Overlapping cell walls are trimmed. Two sandwich faces are generated on the upper and lower side of the foldcore, where the loads are applied. The whole model is meshed with 4-node shell elements according to the defined element size and the core and the faces are connected by a contact formulation. Then the boundary conditions are applied to the face sheets.

This unit cell model so far has a uniformly perfect geometry. In reality no cellular structure is neither uniform in geometry nor free of imperfections and irregularities. This affects the buckling load of the single cell walls and the whole structure’s strength. Therefore, different approaches to account for imperfections in the FE-models were investigated. Global geometric imperfections can be modelled by randomly distorting the foldcore geometry prior to meshing. Local imperfections like uneven cell walls can be represented by randomly modifying all node’s coordinates (‘node-shaking’). Both features were included in the parametric models based on random numbers.

The next important aspect is the cell wall material modelling. In the first phase of the project laminated cell walls with [0°/90°/0°] lay-up of three unidirectional layers were used. A user-defined integration rule with three integration points across the thickness of each shell element was applied and the orthotropic composite material model MAT54 in LS-DYNA was used for the CFRP material. Each integration point represents one layer and is characterised by the respective fibre angle. Material

model MAT54 is based on a linear elastic constitutive law with failure criteria by Chang-Chang. Additionally, failure strains are introduced, which control element layer erosion. For the composite fabric material in the second phase of the project, the fabric material model MAT58 was used, which is based on continuum damage mechanics with a stiffness degradation law. Again, element erosion is controlled by failure strains.

Several modelling parameters have an influence on the structural behaviour of the folded core model and the respective simulation results, including not only the material model and geometry, but also the method of discretisation and boundary conditions: model size, element size, element type, loading rate and mass scaling. Those influences were investigated systematically by means of parameter studies.

Challenging tasks arise regarding modelling of the CFRP cell wall crushing in the post-failure region in a flatwise compression test of the foldcore (Fig. 2.1). First the cell walls slightly buckle, then the material fails under compression starting from the cell wall edges. The respective elements are eroded in a propagating horizontal crack. Once a complete row of elements is deleted, the compression force drops to zero. Due to the angular geometry of the folded core cell, the elements do not come into contact again. The force does not increase until the upper and lower halves of the failed foldcore have contact with the compression plates.

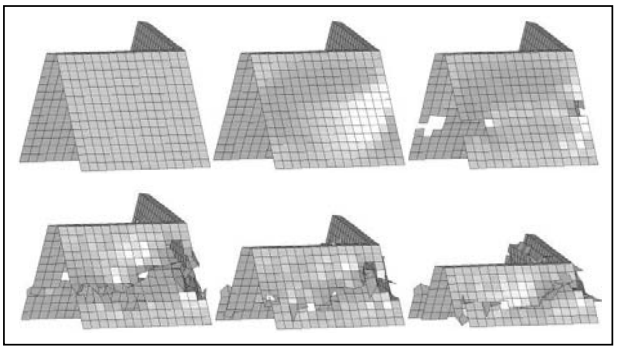

Fig. 2.1: Unit cell under compression load

Homogenised modelling and skin-core interface modelling:

A homogenisation of the cellular structure of a CFRP folded sandwich core was conducted by CRC-G. The basic idea of this homogenisation was to develop a constitutive law for a continuum solid element, so that the mechanical behaviour of this solid element is equal to the effective mechanical behaviour of the foldcore structure. This was done by performing numerical compression, tensile and shear test on a foldcore unit cell model and taking the resulting stress-strain curves as input for the orthotropic LS-DYNA material model MAT126. A validation for single elements could be conducted but for multiple elements across the thickness a localisation effect due to strain softening occurred influencing the numerical results. An improvement for this material model was proposed but not implemented yet. In the framework of this homogenisation of CHC structures, one has always to be aware of the fact that here a ‘structure’ is to be treated as a ‘material’. This can only be a rough approximation. Inside this structure local stress concentrations, local instability or local failure can occur, which can not be treated exactly in the global homogenised element. Furthermore, Poisson’s effects that can play a significant role are neglected due to a full uncoupling.

Especially for the homogenised model, modelling methods in LS-DYNA for a skin-core interface were investigated. The methods analysed were divided into two general approaches, the contact formulation with failure and the cohesive interface elements. With both approaches the crack propagation can be modelled based on linear or even nonlinear cohesive laws. A comparison of both approaches with a total of four different models was undertaken by simulating the debonding crack propagation of a CSB (cracked sandwich beam) test specimen (Fig. 2.2). Differences with respect to stability, computational cost, crack length, bending deformation and resulting energy could be identified. These models showed a good potential of covering debonding failure in a sandwich simulation model. However, no quantitative comparison or rating of these models could be done here since no experimental data for a validation were available. This should be done in further studies based on CSB tests performed on CHC sandwich structures.

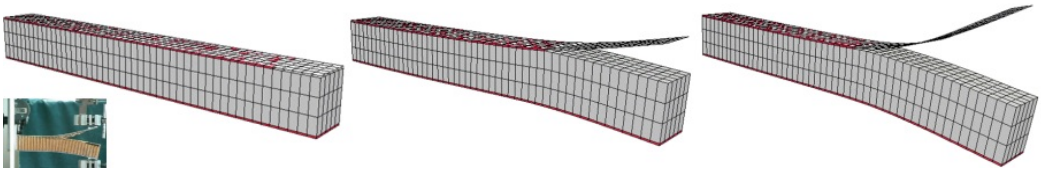

Fig. 2.2: FE simulation of CSB test

Multi-model coupling:

The combination of two different meshing domains with a higher and lower level of detail, combined in one model of a CFRP foldcore sandwich plate, was analysed by CRC-G (Fig. 2.3). The connection of both meshes, i.e. the unit cell shell elements and the homogenised solid elements, was found to play a significant role in a correct representation of the foldcore stiffness. Different methods were applied and compared in a modal analysis study that gave valuable information on the bending stiffness. The approach with nodal rigid bodies for the connection of nodal pairs led to a global stiffness closest to the homogeneous reference model. In a further study the wave propagation in this multiscale model was compared to a reference model and showed only minor differences.

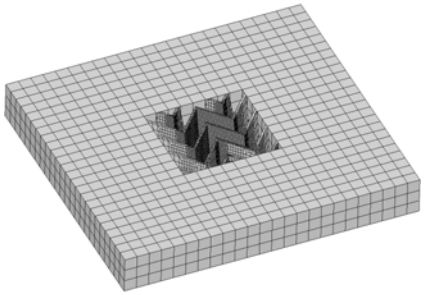

Fig. 2.3: Multi-model coupling

Impact modelling:

The first impact models of CFRP foldcore sandwich structures for the analysis of low velocity impact scenarios in LS-DYNA were based on several simplifications to limit the modelling complexity. Predominantly, a perfect skin-core bonding was assumed and the skins were modelled with only one shell element across the thickness without interlaminar failure. The simulations showed a very localised loading of the sandwich structure, which is the result of the high stiffness impeding any large bending deformations (Fig. 2.4).

In the second phase of the project the impact models were improved by adding a delamination failure in the skins and skin-core debonding. The interlaminar failure was implemented by using a stacked shell approach, where individual layers of sublaminate shell elements are separated by a cohesive interface contact. The debonding is based on a simple stress-based tiebreak contact law. Further results of this modelling approach are given in the WP4 section of this report.

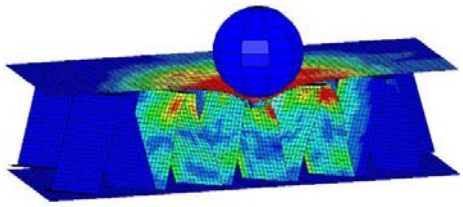

Fig. 2.4: Localised stressed area in the core due to transversal impact

DLR contributions:

Unit cell micromodels

DLR activities in WP2 have concentrated on detailed FE models for foldcore aramid composite cores. Some main features of the models are summarised here:

- Parametric generation of unit cell FE models for generalised foldore geometry
- Material model of aramid paper has been established based on paper tension and compression tests. The compressive material behaviour is difficult to measure directly. To reproduce paper folding characteristics a 4-ply layered shell model was used for the aramid paper with both outer plies elastic-plastic to represent the surface resin layers.
- FE models have been verified by study of numerical parameters: model size, element size, element type, loading rate, mesh distortions (node shaking). Results showed that element size has an influence on buckling behaviour of paper unit cells which increases with decreasing wall thickness to element size ratio. The material model was fitted to a defined element size, with appropriate element size to wall thickness ratio. The model response to quasi-static loads in compression is dependent on the loading rate.
- Virtual testing of aramid paper foldcore structure has been performed and compared to compression and shear experimental tests, see Fig. 2.5. The node shaking method was successfully applied to allow some distortion of the model to represent imperfections in fabricated structures. This method was used to improve agreement with core compression test data, Fig. 2.2. The DLR micromodel was able to simulate observed folding behaviour in compression and shear and gave good quantitative agreement to measured compression crush loads and shear failure loads.

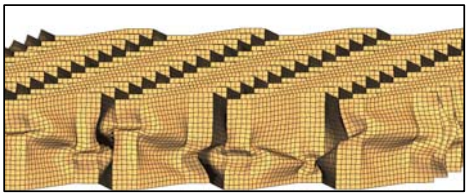

Figure 2.5: FE model of core compression test

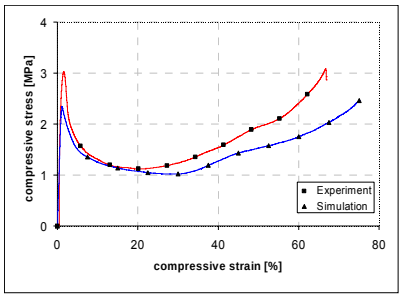

Figure 2.6: FE simulation of core compression

Multiscale modelling strategy

Work was completed on homogenised models for foldcore structures based on replacing the microscale shell models above with equivalent solid elements in the commercial PAM-CRASH code. These were satisfactory in the regions away from microfailure and collapse. Where this occurs a multiscale method was proposed. A multiscale modelling strategy was defined for foldcore sandwich structures based on domain coupling between detailed microscale shell models in regions of failure, and homogenised brick models away from the damage zone. A multimodel coupling (MMC) strategy through the domains was developed based on contact interfaces at which force compatibility is maintained by penalty forces which prevent interpenetration at the interface. The method was investigated with some idealised benchmark simulations based on sandwich beams and plates under bending loads.

To assess the feasibility of such an approach a three-point bending load was applied to a sandwich beam with CFRP skins and foldcore. Here the refined shell model for the foldcore in regions where the cellular core is under high loads, where buckling and failure may occur. Away from this region the sandwich core is modelled by solid elements with homogenised fold core properties, see Fig. 2.7. For validation purposes the behaviour of a MMC beam model was compared to a beam model which is entirely composed of the fine scale shell model. Fig. 2.8 shows a satisfactory comparison of the load deflection curve of the indenter computed with the MMC model and a full microscale model for the foldcore under constant velocity loading conditions.

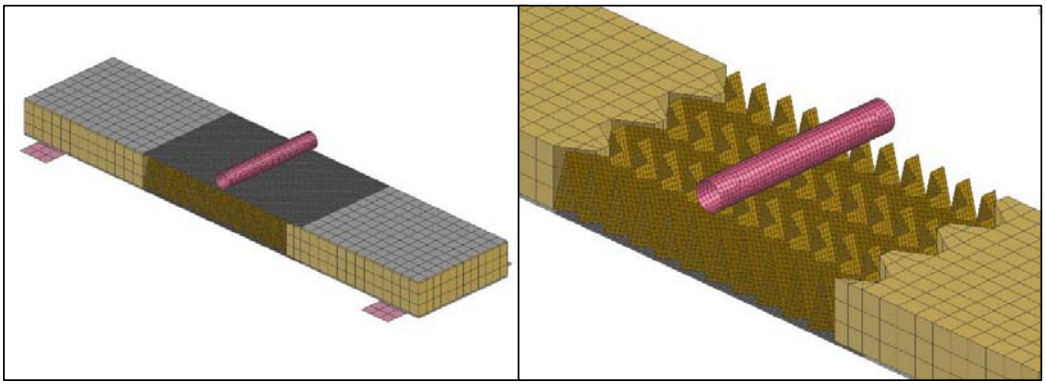

Fig. 2.7: Setup of multi-model coupling (MMC) model for a three-point bending test in foldcore sandwich

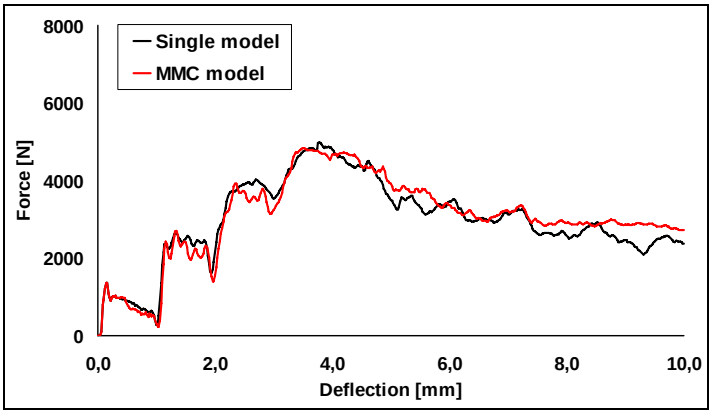

Fig, 2.8: Load-deflection curve of the cylinder indenter: comparison of MMC with core microshell model

Development of impact modelling techniques for foldcore sandwich panels

An impact model in PAM-CRASH for transverse impact loads on a foldcore sandwich plate has been developed based on the validated foldcore microscale model described above, which uses shell elements, together with a single-multilayered shell element representing the carbon skins. The model setup is depicted here in Figs. 2.9 and 2.10, with an assumed high velocity impact from a rigid projectile. Parameter studies have been carried out to verify the model. The influence of element size, the impact position in relation to foldcore microstructure, the influence of the specimen size, the loading rate and the influence of friction on the sliding interfaces have been investigated. The figures show that a 1 mm shell element size was necessary to capture the core failure in impact penetration.

The work in this task was to develop and verify numerically methods for impact analysis of foldcore sandwich panels. In WP 4 the models developed here were applied to validation studies with DLR low velocity and high velocity impact tests on foldcore sandwich panels with steel and rubber projectiles. Refinements to the basic impact modeling procedures were also presented in WP 4 such as stacked shells with cohesive interfaces to model delamination in the composite skins, in order to obtain improved models for sandwich failure under impact.

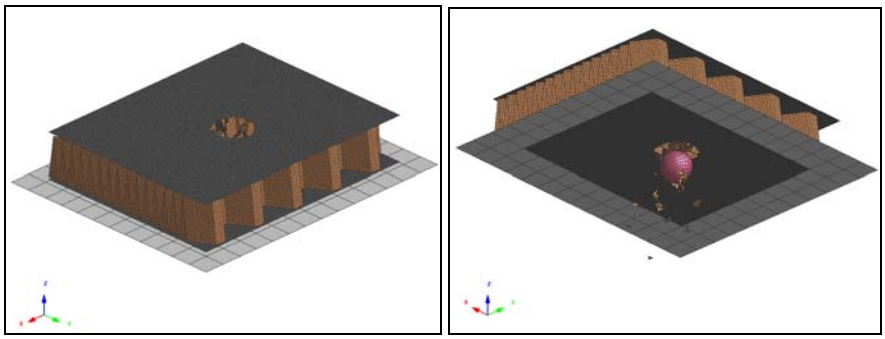

Fig.2.9: Outer and inner skin penetration of impact model with 1.0 mm element size

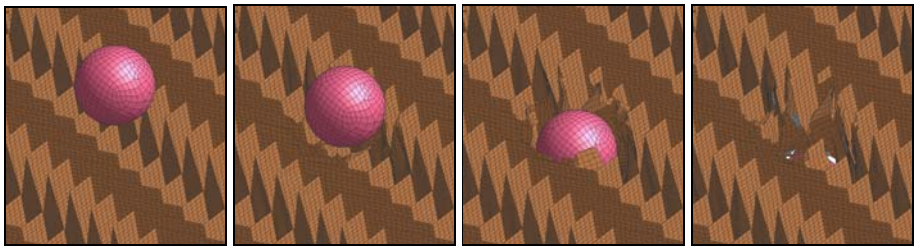

Fig. 2.10: Visualisation of core penetration for impact model with 1.0 mm element size

LMT contributions:

During the CELPACT project, the activities of LMT on numerical modelling can be divided into two major parts. The first part concerns the modelling of folded cores under crushing. The second part concerns the development of multiscale computational strategies based on domain decomposition methods (DDM).

Concerning the modelling part of the work, it is closely linked to LMT activities in WP3 (characterisation and identification) and in WP4 (validation). The developed model aims at describing a folded core from USTU at the paper scale as a shell assembly. The objective is to be able to predict the behaviour of such a core under out-of-plane compression, up to the global collapse. For that, an implicit computation using Abaqus is performed in order to control the numerical error. The two key points concern the material behaviour modelling and the geometrical imperfections modelling. Concerning the material behaviour of the paper, the paper is modelled as a three layered laminate. In each layer of this laminate, an isotropic damage evolution law is affected. These laws have been implemented in a user material subroutine UMAT. Concerning defects, the problem to solve is a stability problem (buckling, post buckling). It is well known that this kind of problem including bifurcations branches is strongly dependant of defects, as they guide the solution to go on one branch or another. The strategy developed at LMT is to numerically build geometrical imperfections. For that, the folding process has been simulated on a perturbed folding pattern. This leads to a final folded geometry in which, cell walls are already in bending and folded edges no more straight. This last point is of major importance. The entire process is parameterized using the python scripting interface available in Abaqus. The convergence of the finite element method considering the mesh size and the time steps has been studied.

Concerning multiscale computational strategies, the use of a previously developed DDM with non linear relocalization allows to simulate (for elastic materials in a first step) the behaviour of a folded core up to the global geometrical instability. This issue has been treated on a simple springs exemple and a solution proposed. Two other more fundamental topics are ongoing work and two thesis has started during CELPACT:

- Multiscale approach for coupling buckling and delamination i.e. how to handle the coupling between different kinds of non linearities (local/global, material/geometrical) in a computationally efficient domain decomposition framework;
- Non linear two scales strategy for the analysis up to collapse by buckling and post buckling of stiffened structures i.e. how to handle strong geometrical non linearities in a multiscale framework. It especially focuses on the macro representation in case of large displacements and rotations.

RWTH contributions:

Homogenisation and multiscale modelling

A homogenisation method was developed during the project to simplify the modelling of sandwich cores. Even more important is the possible reduction in computing time and in consumption of other computational resources.

The basic concept of the described procedure is to replace the fine modeled core structure by volume elements, which show a similar behavior. Only global behavior can be represented with this approach. So for example in case of impact simulations the area beneath the impact point cannot be simulated properly using the homogenised elements. The proposed elements cannot reflect effects like buckling of the core walls and other local processes, which occur during the impact in the core under the impact area. Nevertheless these volume elements may still increase the efficiency of the impact simulations if used for the core modeling around the actual impact zone.

In the described procedure the core structure with the real micro structure is replaced by an “effective” homogeneous medium. The mechanical properties of the effective medium are derived to simulate the same global mechanical behavior as for the real structure. The effective properties are derived from a representative volume.

The considered cores have two distinguished directions (L- and W-direction) with different mechanical properties. So orthotropy can be considered as the proper material law. In this material model the normal strains are independent of the shear strains. Due to this assumption 9 independent material constants are needed to describe the material.

$$\sigma_{ij} = \boldsymbol{E}_{ijkl}\varepsilon_{ij}, \qquad \varepsilon_{ij} = \boldsymbol{S}_{ijkl}\sigma_{ij}$$

$\boldsymbol{E}_{ijkl}$ is the elasticity tensor and $\boldsymbol{S}_{ijkl}$ the compliance tensor. Both of them are symmetrical.

Additionally the “in-plane” and “out-of-plane” properties of a sandwich core can be considered as independent. This approach allows the consideration of the effects caused by the connection between core and the face sheets. With this assumption the number of the needed constants can be further reduced to 7.

$$\begin{pmatrix} \sigma_{11} \\ \sigma_{22} \\ \sigma_{33} \\ \tau_{12} \\ \tau_{13} \\ \tau_{23} \end{pmatrix} = \begin{pmatrix} E_{1111} & E_{1122} & 0 & 0 & 0 & 0 \\ E_{2211} & E_{2222} & 0 & 0 & 0 & 0 \\ 0 & 0 & E_{3333} & 0 & 0 & 0 \\ 0 & 0 & 0 & E_{1212} & 0 & 0 \\ 0 & 0 & 0 & 0 & E_{1313} & 0 \\ 0 & 0 & 0 & 0 & 0 & E_{2323} \end{pmatrix} \begin{pmatrix} \varepsilon_{11} \\ \varepsilon_{22} \\ \varepsilon_{33} \\ \gamma_{12} \\ \gamma_{13} \\ \gamma_{23} \end{pmatrix}$$

The needed values of the elasticity tensor of the homogenised material are derived based on the following assumption: the average strain energy stored in a representative volume filled with the homogenised medium due to certain boundary conditions and loading is equal to the average strain energy stored in the micro-structured model which occupies an equal volume under equal conditions.

$$w_{avrg,micro} = \frac{1}{V}\int_V w_{micro}(\varepsilon_{ij,micro})dV = \frac{1}{V}\int_V w_{homog}(\varepsilon_{ij,homog})dV = w_{avrg,homog}$$

$w(\varepsilon_{ij})$ is the strain energy density stored in the structure due to the strain ε_{ij}.

The strain energies are computed for seven different strain states to derive the seven constants of the elasticity tensor. All states have to fulfil the condition $\varepsilon_{ij,micro} = \varepsilon_{ij,homog}$.

The homogenised elasticity tensor is given as:

$$\boldsymbol{E}_{ijkl,homog} = \frac{\partial^2 w_{avrg,homog}}{\partial\varepsilon_{ij,homog}\partial\varepsilon_{kl,homog}} = \frac{\partial^2 w_{avrg,micro}}{\partial\varepsilon_{ij,micro}\partial\varepsilon_{kl,micro}}$$

All the strain energies needed for the homogenisation procedure are computed numerically with the finite element method.
As solver the commercial program Nastran is used. The micro-scale model of the core is built with shell elements. All the strains are applied through displacement boundary conditions. Additionally in case of the virtual out-of-plane compression and shear tests all the rotations on the upper and lower sides of the core are blocked to include the effects of the core to face sheets bonding. For each core configuration seven virtual tests have to be performed to acquire the seven needed engineering constants:

The average strain energy density is computed by dividing the sum of the element strain energies of all elements in the investigated part of the core by the volume of this part including the empty space between the individual walls.

$$w_{avrg,micro} = \frac{\sum_{m=1}^{N} W_{el,m}}{V}$$

with *N* as the number of elements in the volume.
The effect of the usage of homogenised elements during low velocity impact simulation were investigated. Different ratios between the homogenised region and micro-structured region beneath the impact point were compared (see Fig. 2.11).
The suitable size of this region depends upon the impact energy for low velocity impacts. For very low energies (2 or 5 Joule) with small indentions the microstructured part can remain small. With higher energies this region has to be increased. For energies (≥60 Joule) at which the impactor penetrates the upper face sheet the affected area of the core does not increase any more with increasing impact energy. So the same extent of the microstructured part can be used in this energy range.

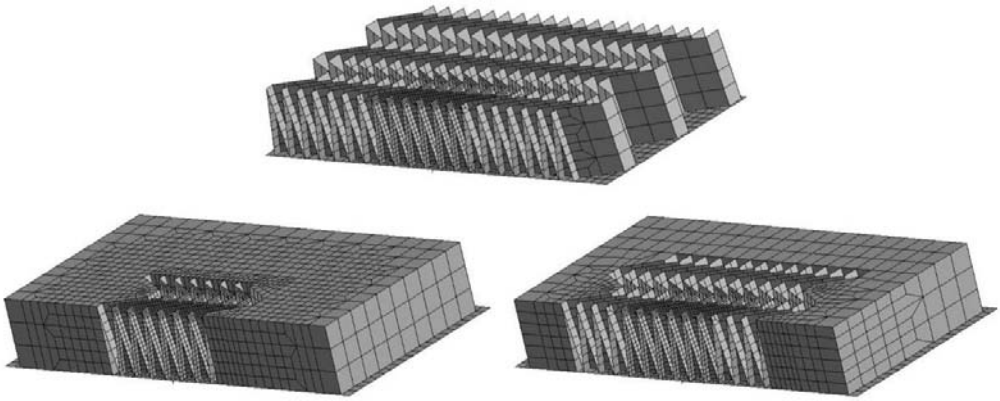

Fig. 2.11: Completely microstructured and partly homogenised models

The time step used during the simulations is dependent on the smallest element in the model, which always is in the microstructured part of the model as part of the fine mesh below the impact point. Also the ratio between the homogenised and microstructured parts is small for model sizes described here. Because of this, the computational time saved due to use of partly homogenised core models as described here is relatively small (10%-15%). However it is possible to decrease the consumption of computational resources by introducing of regions with different time steps (small time steps for the microscaled region and larger time steps for the homogenised region). Further investigations are needed to explore the potential of this method.

Residual strength simulation procedure

To avoid expensive and time-consuming test programs (impact tests, 4-point bending tests and compression after impact (CAI) tests), numerical simulations may be useful to assess the impact behaviour and also to estimate residual strength after impact.

A procedure is developed to simulate low velocity impact tests as well as the residual strength tests (e.g. 4-point bending tests or CAI tests) of the pre-damaged sandwich structures.

The impact simulations are performed using LS-Dyna. The data resulting from these simulations, especially the residual deformations and damages in the face sheets and the core can be used to establish a "pre-damaged" model for a residual strength simulation. The non-linear static residual strength simulations are performed using Abaqus. Additionally comparative simulations are done with an equivalent non damaged model to assess the drop in strength caused by the impact.

The damages occurred during the impact simulations in the plies of the composite face sheets are caused by one of the four failure modes. Each of these modes leads to a different degradation of the properties of the affected ply. For all elements of the upper face sheet where in one or more plies the condition for one of the failure modes is satisfied during the LS-Dyna computation a new element in the Abaqus model is generated. These elements are provided with degraded properties in the affected ply (or plies). For the computations described here the affected properties are reduced to a value of 10% of the original.

The procedure was validated with experimental results (impact tests and successive 4-point bending tests) in WP4. The comparison between the experimental and the simulated result is very good in most cases. However for certain critical energy there is room for improvement. A promising approach could be the introduction of inter-ply delaminations into the numerical models.

USTU contributions:

The work of USTU in WP2 can be divided into two parts. The first concerns the devolpment of an analytical design tool for zigzag cores. The second aims at modelling geometrical imperfections on folded cores.

The general purpose of the first topic is the examination of the behaviour of zigzag cores under compression. For that, the cores are assumed to be ideal, which means that there are no imperfections and the material is linear-elastic. The proposed approach relies on analytical modelling. In a first step, a zigzag core is studied numerically and in a second step, an analytical model is developed. This last one fits the numerical model developed in the first step.

The Geometrical parameters of folded cores are explained in Fig. 2.12:

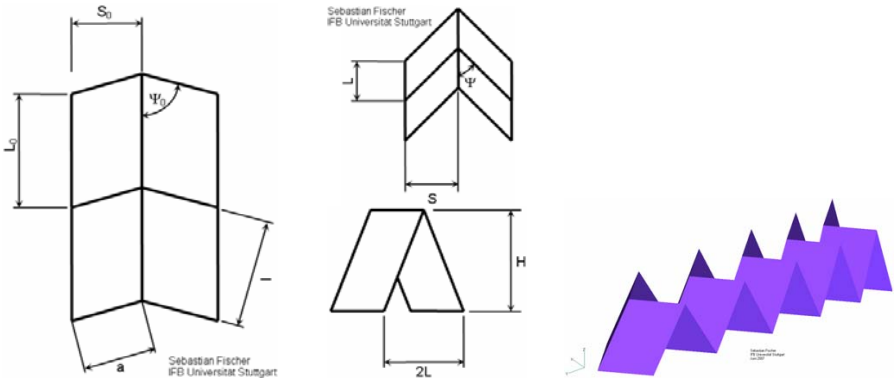

Fig. 2.12: Geometrical parameters, folded and unfolded condition

The geometries used in the study are:

No.	Ψ_0	Ψ	L_0/S_0	L_0	S_0
	[°]	[°]	[-]	[mm]	[mm]
133	80	45	1,5	21,49	14,33
233	78	45	1,5	21,49	14,33
333	75	45	1,5	21,49	14,33
433	73	45	1,5	21,49	14,33
533	70	45	1,5	21,49	14,33

The behaviour of ideal folded cores can be divided in two regions as seen in Fig. 2.13: Before and after buckling of the faces. The Point where the faces buckle is called a critical point. It is characterized by a drop in Young's Modulus E_z. After that point Young's Modulus is not constant anymore but a function of stress σ_z.

The analytical model was developed using a:

- Modified rod model for the behaviour prior to buckling
- Calculation of critical stress for face and core using formulas and diagrams from HSB
- The behaviour after buckling is described by a theory for the post-buckling behaviour of plates.

Fig. 2.13 shows the comparison of the analytical and numerical model for predicting the foldcore compression modulus. The agreement is satisfactory and shows the value of the analytical model for foldcore design studies.

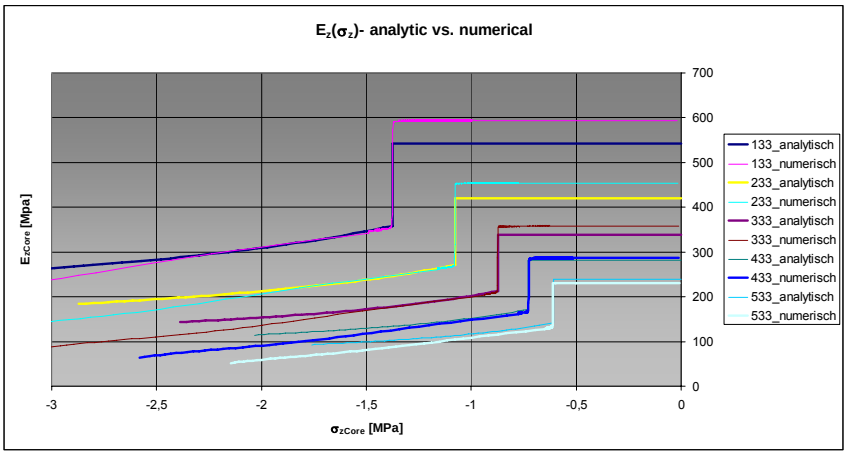

Fig. 2.13: Comparison of analytical and numerical model

Because of imperfections, which appear in real structures, this model cannot be used to predict the behaviour of an imperfect folded core.

But it is possible to compare different geometries of folded cores. So it can be seen as a Design-Tool for which helps deciding which geometry should be used for a certain application.

The general purpose of the second topic is the modelling of the real geometry of a folded core using a scanning technique. Geometrical imperfections influence the mechanical properties of foldcores. A possibility is examined how to get a FE-model of a foldcore where geometrical imperfections are included.

A manufactured foldcore is scanned with the 3d-digitizer ATOS by gom. The raw data is mainly a point cloud. Points are connected with triangles (triangulated surface).

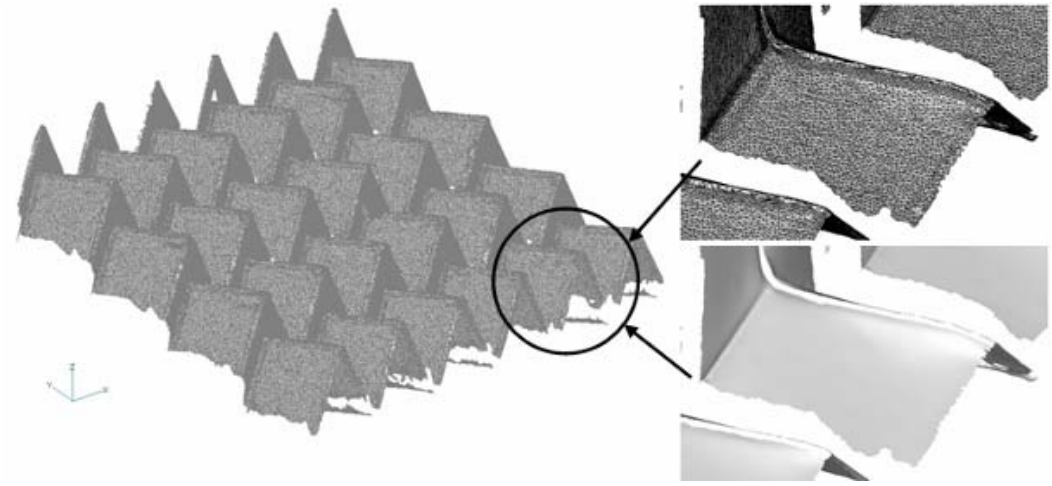

Fig. 2.14: Raw data of a 3d-digitized foldcore

Measurement data has to be remodelled to a NURBS surface or a set of surfaces. These surfaces can then be used for meshing in order to give the final FE-model with geometrical imperfections included (Fig. 2.15).

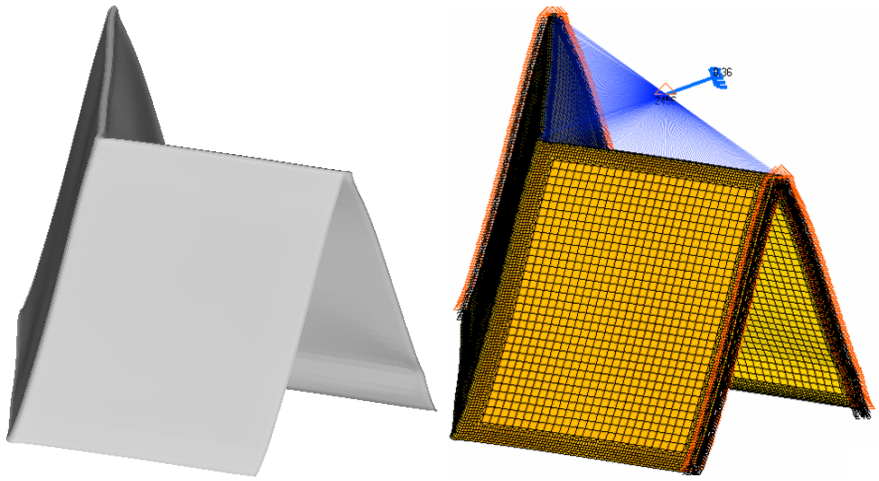

Fig. 2.15: Remodelled geometry (left) and FE-model (right)

In the example above, the method was used on a single unit cell of the foldcore sample. But of course it is also possible to work on a larger piece of the sample in this way as shown in the next picture (Fig. 2.16).

Fig. 2.16: Raw data (left), remodelled geometry (middle) and FE-model (right) of 3 unit cells out of a foldcore sample

The separations visible in the remodelled geometry are boundaries of the NURBS surfaces. The geometry is separated in order to simplify meshing. A controlled quad mesh is achieved with finer meshing at the edges and a coarser meshing in the surfaces.

CM cores

UBRN contributions:

Hollow spheres micro-models (FE modelling of closed cellular cores)

The goal of the subtask was to create the structure model describing structure behaviour under press and shear loading. At the frame WP2.1 task the three cases were solved. Firstly, there was behaviour of pure basic cells under compression. Secondary, the solving small assemblies of structures under

compression and shear loading was done. This solution was invocated by structure heterogeneity. In the last case, the optimization of cell diameter and wall thickness was done. For complete modelling a fix cell diameter 2.4 mm was chosen (It was the first value of diameter) and thickness was scaled in dependence on required rate. All solutions were done for several rates of diameter and thickness, because at the beginning of modelling, the production capabilities were not known. The microscale cell geometry is based on the production technology. The basic shape is polystyrene ball with 2.4 mm diameter at the full off volume. This ball is enwrapped with nickel. The thickness of nickel depends on the chosen structure density.

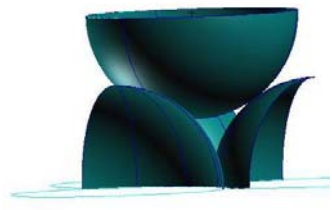

Fig. 2.17: Spheres position at cell

Fig. 2.18: Sample of Hollow spheres

During the solution of small assembling two possible theoretical layering were compared (see Fig. 2.19, where layer 3 have a spheres centre at blue point) with a result that the layering system do not have significant influence on results.

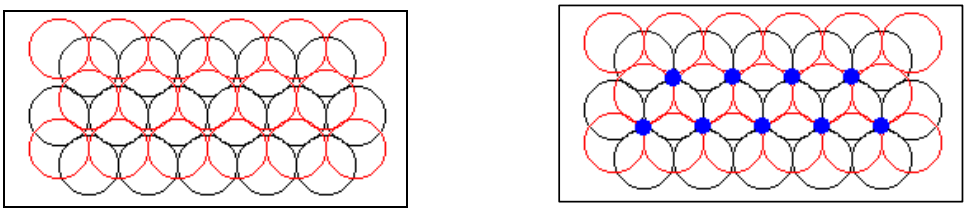

Fig. 2.19. Possible layering of spheres (1-2-1, 1-2-3-1)

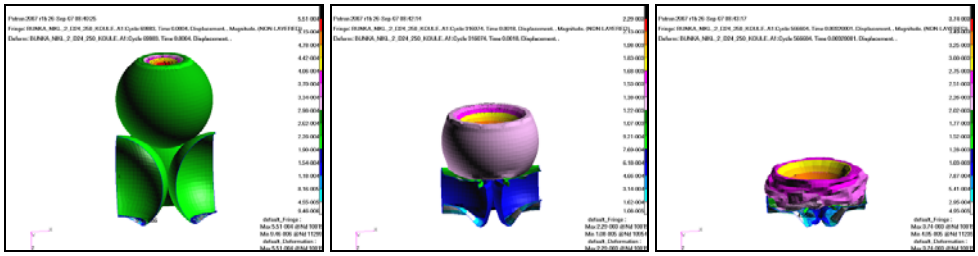

Fig. 2.20. Deformations of the basic cell during compression loading (10%, 40%, 70% of strain)

Small assembling – models

In this case, there was created a system of several layers with dimension 6x6x6 spheres (see Fig. 2.21). The main idea was to better approach to a real structure, which is an irregular and very random structure. For the FEM model generation an MSC.Patran pre-processor was used. A PCL (Patran Command Language) script was used for creation of ideal structure, and randomly degenerate structures. In the case of randomly degenerate structures the cells were randomly omitted by chosen percentage of spheres from a regular structure (red balls at Picture 2.21). For statistical description ten random models were used. For solution 20% omitted spheres was chosen.

For solution a LS-Dyna solver was used. The cells were modelled by shell elements QUAD. Three types of loading cases were solved – tension, compression and shear. The tension and compression loading were solved in three directions - x, y, z axes.

Some types of contact were used depended on the load case. For compression and shear load cases a contact of balls with boundary panel and self-contact of balls was used. The tension loading cases were solved without any contacts (only touching nodes were merged) .

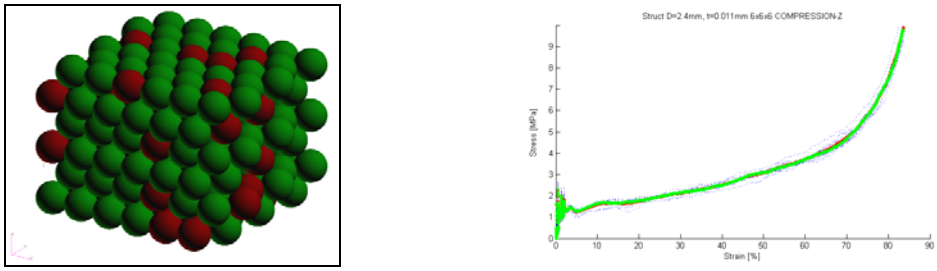

Fig. 2.21. Randomly generated FE model of small assembling(left) and compression response

Impact models of CM structures

In the CELPACT project UBRN investigates sandwich structures with cellular metal cores. In impact analysis task 2.3 a pre-test simulation of the sandwich structure models is undertaken. During the simulations, a projectile with ball shape and another one with cylindrical shape (Table 1) were used. These simulations were done with three types of the numerical models along different level of finite element discretisation from detailed up to homogenized one.

Table 1: Projectile shape and size used for pre-test simulations

Shape	Diameter	Mass	Projectile Energy (initial velocity 100m/s)	Projectile Energy (initial velocity 250m/s)
	[mm]	[g]	[J]	[J]
Ball	10	4.11	20.55	128.45
Ball	20	32.88	164.41	1027.56
Cylinder	20 (13.33 mm High)	32.87	164.37	1027.31

The numerical simulations of the impacted aircraft structures will be done with some type of homogenized finite element models during design process. It may be supposed that the sandwich's core will be modelled by a honeycomb constitutive model coupled by a failure criterion on maximum volumetric strains. The skin will be modelled using simple shell elements and the surface-to-surface contact of the foam core and the skin will be generally used. The results from this impact simulation will be validated using the fine FE model, as well as the experiment.

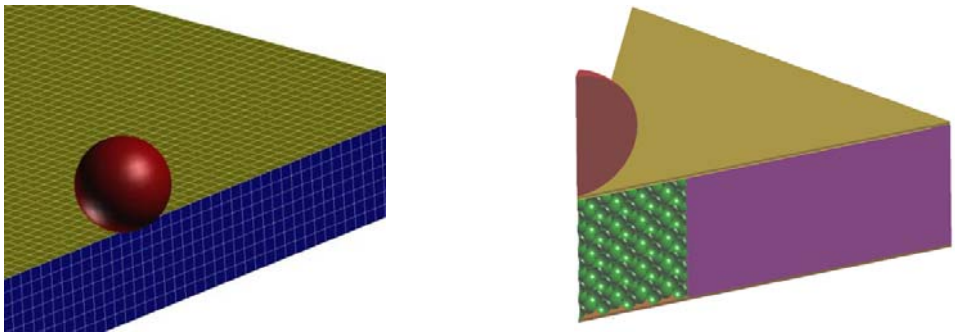

Fig. 2.22 – Homogenized (left) and mixed FE model of sandwich panel used for experiments

Results of simulations

The simulation's results can be divided into two groups. The one is the history curve of projectile deceleration, velocity or energy (is equal to energy absorbed by sandwich panel). The sample of deceleration history of the projectile is shown on Fig. 3.2. Another one is the displacement history of the back skin in the perpendicular direction (displacement history of the back skin in the opposite point of impact), strain or stress history around the opposite point of impact.

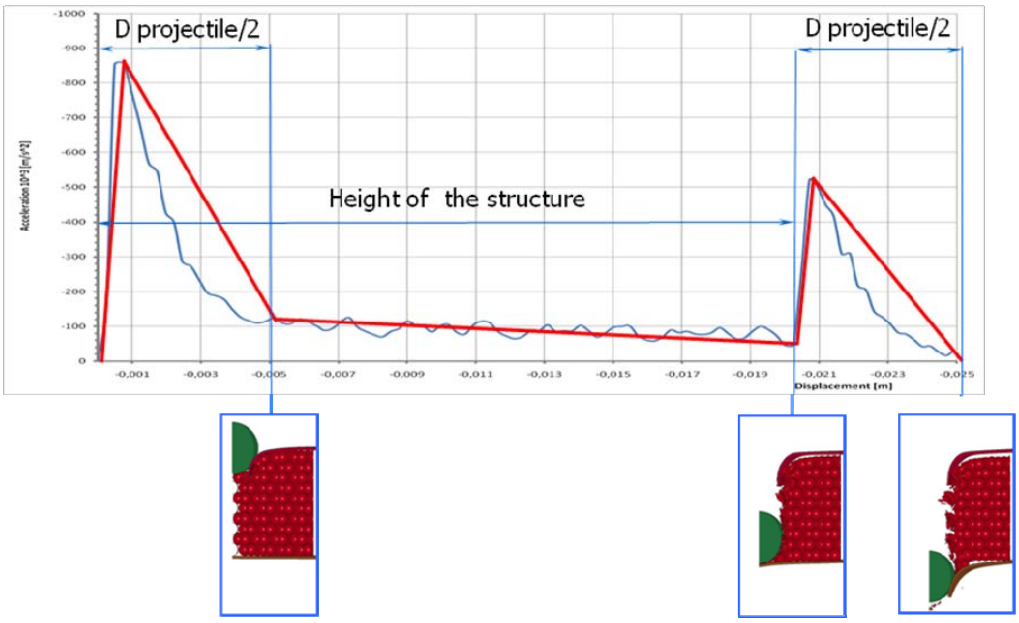

Fig. 2.23 – Acceleration history of the projectile and its position in the sandwich, ball projectile diameter 10mm, impact velocity 250m/s. Testing of fine FE model of sandwich panel with skin thickness 0.5mm, core sphere's thickness 11mm.

ULIV contributions: FE Modelling of Micro Lattice Cores

FE Modelling of Micro Lattice Cores (ULIV)

The beam model

The beam element formulation was based upon the work of Hughes and Liu , and is incorporated into LS-DYNA as the default beam type. This element is formed from the degeneration of the eight node solid element into a two node beam element with an array of cross-section integration points centrally located along the beam axis. Standard shape cross-sections can be defined, as was the case here using a circular section of 16 gauss integration points angularly spaced at 0.6 times the radius to resolve the cross-section stress adequately in bending.

This element generates a constant moment along its length and yielding is only detected at the integration points, which lie midway along the element length. Therefore a single cantilevered beam element subject to bending will yield at too high a force since the fully-plastic hinge develops at the centre rather than at the correct constrained end location. A multi-element mesh of the cantilever reduces this problem as the detected yield location shifts closer to the encastré as the mesh is refined. Table 1 compares the FE model with analytical results for correspondingly finer meshes. This linear elastic analysis shows the 2 element model gives an elastic deflection that is 90% of the beam theory prediction. The slightly overly stiff response is a result of the constant moment along the length of the element. Figure 1 shows the bending moment distribution for two elements.

Number of beam elements representing cell edge	Tip load (N)	End displacement (mm)	Accuracy
2	0.013	0.448	90%
4	0.013	0.471	94%
8	0.013	0.480	96%
Theoretical	0.013	0.500	-

Table 1: Cantilever elastic loading of cell edge. Comparison of elastic tip displacement results for the 2, 4, and 8 element mesh densities.

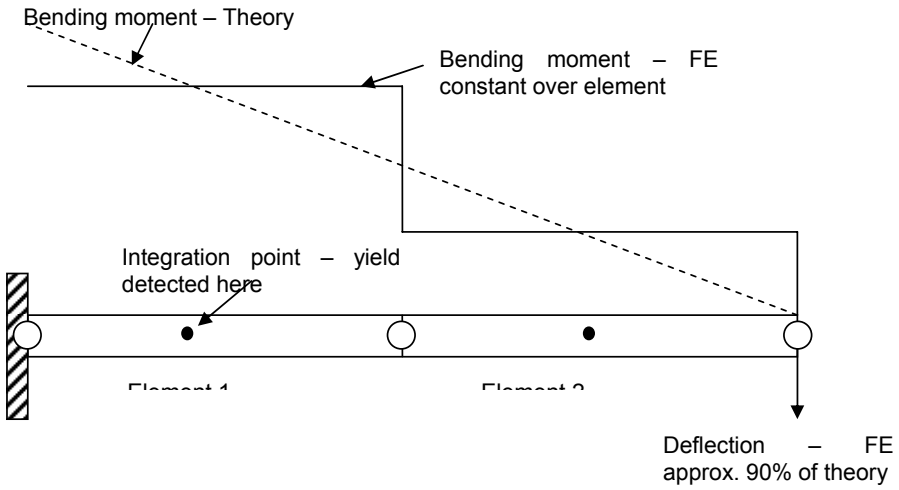

Figure 1: 2 element model of cantilevered cell-edge. Comparison of deflection and maximum bending moment is shown for the FE model and analytical results.

An alternative approach is to select a beam element formulation that generates the correct moment and fully plastic hinge at the correct location along the element length. The Belytshcko-Schwer, B-S, beam satisfies these requirements but has some other limitations with regards to the material models that can be used to represent its behaviour. A single element of this formulation can be used to accurately model the response of a cantilever and so the 2 element cell-edge used in this model should give the correct bending moment and yield at the nodal locations rather than at the centre of the element. Thus the elastic and plastic response will be correct. A 3 element cantilever model ran with Hughes-Liu and Belytshcko-Schwer formulations. The bending moment reported for the elements is the integration point value, which is constant over the length of the beam in the Hughes-Liu case, whilst in the B-S formulation the maximum BM is reported. The accuracy of the B-S can be seen in the comparison of the cantilever deflection results in Table 2.

	Analytical	Hughes-Liu	B-S
Tip load, N	**0.05**	**0.05**	**0.05**

deflection, mm	**0.023684**	**0.02319**	**0.0237**
max BM, Nmm	**At encastré (L=0mm)** **0.125**	**0.104**	**0.125**

Table 2: Comparison of Belytchko-Schwer and Hughes Liu Beams – three beam elements for elastic case

However, an elastic plastic with damage material model cannot be used with Belytchko-Schwer beams and so Hughes Liu beams were used here.

Micro-lattice core model

The geometry of the bcc lattice was created from in-house software which has a library of geometries available. The software generates output manufacturing files for the SLM machine, or it can output LSDYNA formatted node and element data for numerical analysis purposes prior to manufacturing. Figure 2 shows the bcc structure for a unit cell.

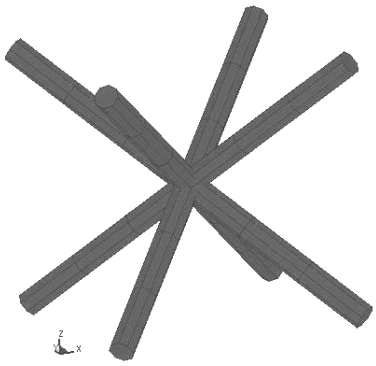

Figure 2: bcc cell (3 elements per strut)

Each strand of the unit-cell is represented by three beam elements. This value is a compromise between the number of integration points along the strand length to capture plastic hinge formation due to bending deformation modes, and the possibility of buckling modes under axial loading of the strands. The bcc unit-cell predominantly carries compression-tension forces when loaded in shear, raising the possibility of a buckling failure mode. A single, one integration point, element cannot simulate the strand buckling mode, thus multiple elements per strand are required. Simulation of a lattice uni-axial compression test indicated that at least three elements per strand were required to capture the stress-strain profile of the test.

The constant bending moment formulation (Hughes Liu) allows for a simple failure criteria to be included in the material model. This criteria simulates strand rupture by reducing beam stiffness as gauss points achieve a critical effective stress, and deleting a beam element when all gauss points are failed. The effective strain is set to the failure strain of a strand subject to uni-axial tension.

A series of experimental tests on lattice strands were performed to establish the mechanical properties of the stainless steel 316L strands and contrast them with bulk 316L properties. The material properties of the strand were determined. This behaviour was approximated using a bi-linear elastic-plastic material model with failure. The value of elastic modulus is 140GPa, yield strength is 250MPa,

Poisson's ratio is 0.3, and tangent modulus is 2.5GPa The failure strain value was determined to be approximately 0.3.

The connectivity between beam elements at nodes is modelled as the default in DYNA, i.e. continuous material properties. Hence, plastic hinge formation and deformation is modelled as if the strut joint was continuous.

An important aspect of the lattice model is the modelling of densification. Experimental observations show that increasing levels of localised crush lead to contact between neighbouring strands of the lattice which produces the rapid increase in stress at densification. To model this, a contact algorithm was incorporated into the lattice model which detects contact between beam elements. The beam stiffness dictates the reaction force generated when this occurs.

Skinless three-point bend

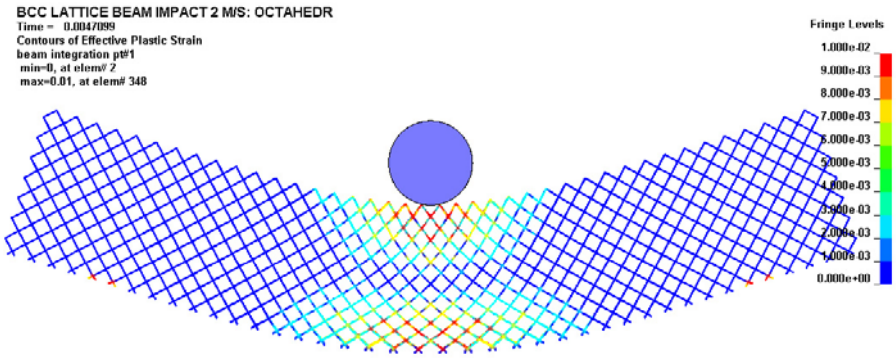

(a) Numerical model of micro-lattice loading in three-point bend. Colours indicate plastic strain formation.

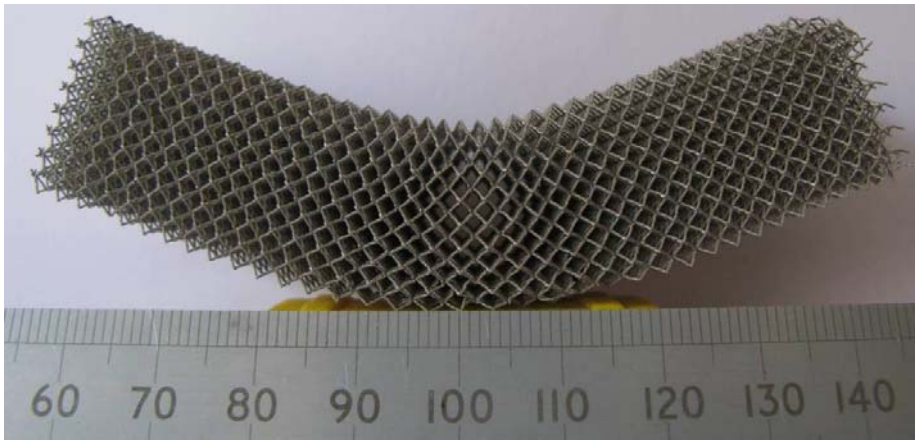

(b) Experimental result at approximately 10 mm permanent deflection.

Figure 3: Validation of large scale global deformation behaviour of the micro-lattice.

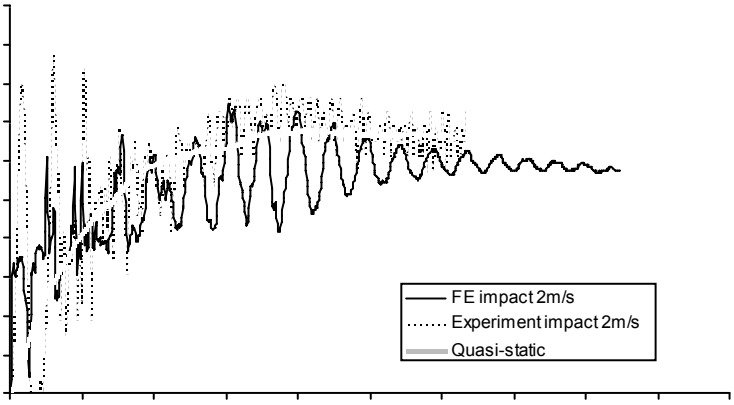

Figure 4: Typical load-displacement results for the experiment and numerical model of the micro-lattice beam loaded in three-point bending.

Uniaxial constrained compression

This was based on experimental tests in which a 20mm3 block is compressed between two flat surfaces.

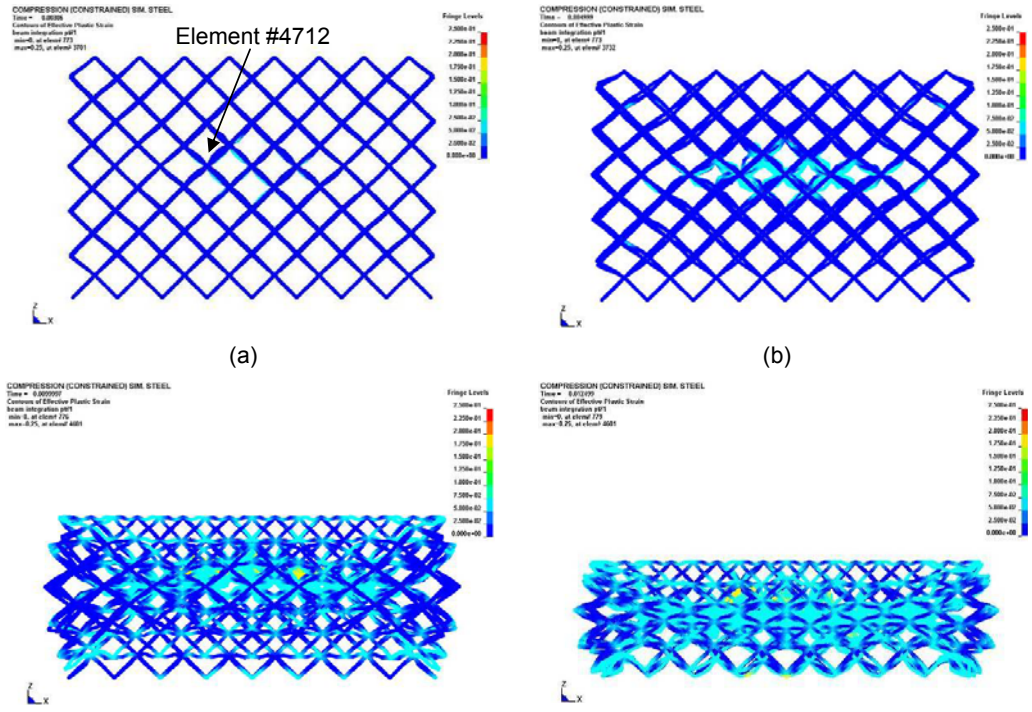

Figure 5: Numerical model of constrained uni-axial compression. The free-edges at the top and bottom are fully constrained.

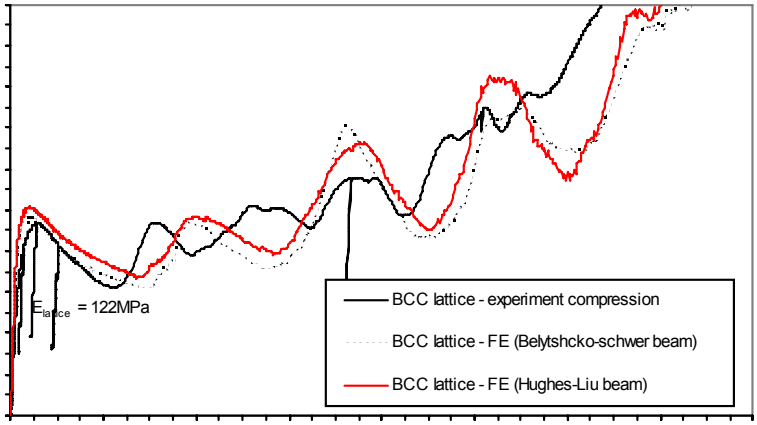

Figure 6: numerical model and experiment results for constrained uni-axial compression of a bcc lattice block.

Indentation simulation

Quarter model of bcc panel subject to low velocity impact. Failure of beam elements characterised by plastic strain to failure value obtained from stress-strain plot of lattice strand uni-axial tensile test data. Trend of the load-displacement curve in good agreement with experimental results. The beam micromechanics of failure is highlighted by the numerical figure, with compression to yield followed by bucking of the strands dominated the behaviour. The final figure shows excellent agreement between the numerical model and experiment in terms of the localised indentation damage spreading to the surrounding lattice at increasing displacements.

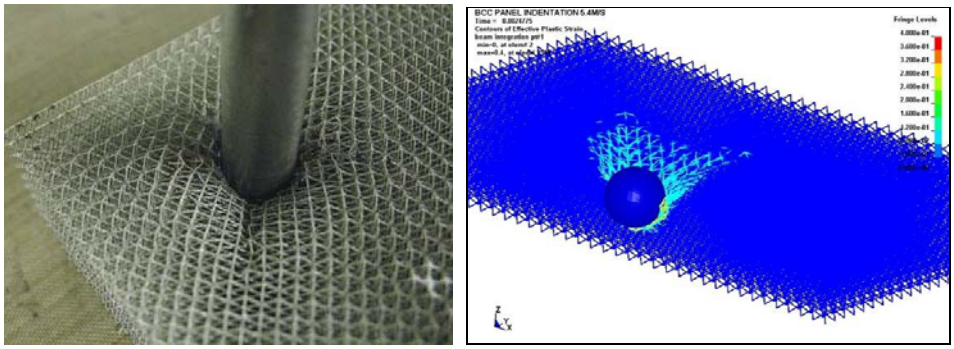

Figure 7: Experiment and numerical indentation of a bcc panel.

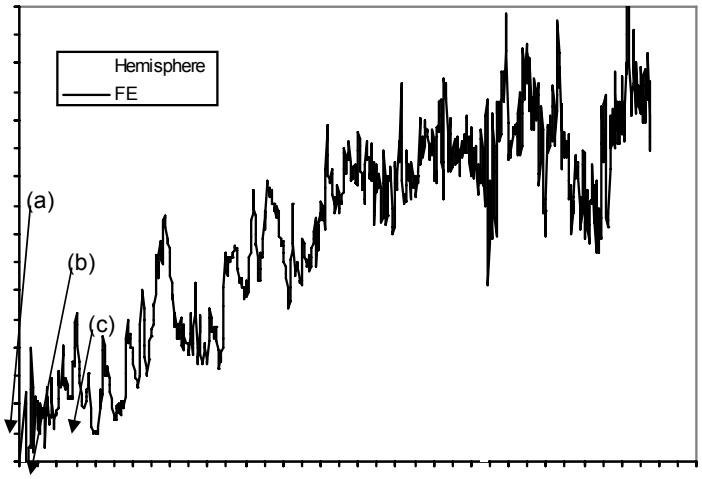

Figure 8: Numerical and experimental results for indentation of a bcc panel using a hemispherical indenter. Experiment is quasi-static whilst the FE simulation is low velocity impact.

(d) BCC panel 0.09J

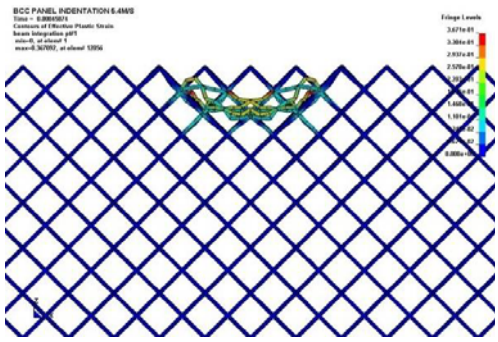

FE BCC panel

(e) BCC panel 0.44J

FE BCC panel

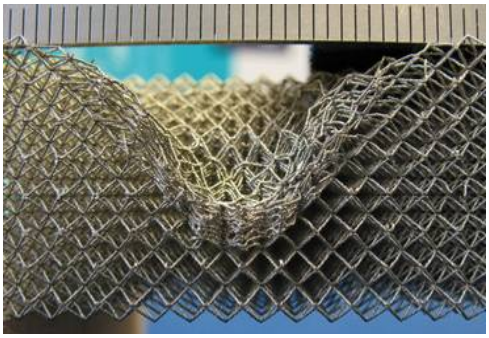

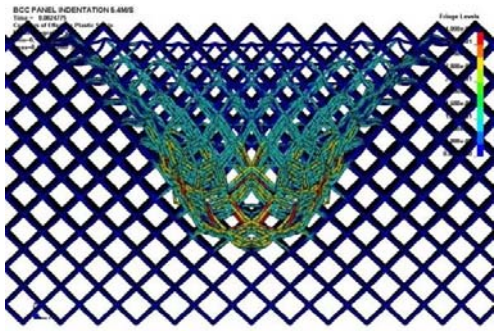

(f) BCC panel 2.11J FE BCC panel

Figure 9: Comparison of experiment and numerical model at several indenter displacements.

Conclusions

The ULIV micro lattice strut model has been validated for BCC Stainless Steel 316l for uni axial compression, global bending and indentation. Material strain rate and inertial effects are secondary.

Modelling hard and soft impact on small SLM panels using DYNA

For details of the micro strut modelling see above.

Carbon fibre composite skin model

There are many approaches possible to model composites in LSDYNA. This approach is based on previous studies which capture the overall behaviour of the composite skin in terms of progressive damage to the composite layers and the related degradation of material properties. There is no attempt to model inter-ply delamination or other complex phenomena such as fibre pull-out or the complex interaction between composite and lattice material at the core-skin interface. As already discussed, the core-skin interface showed excellent resistance to debonding, and so a tied contact interface was used between the skin elements and lattice nodes. The skin itself was modelled with shell elements with length to thickness aspect ratio of 7. Four layers of shells for each panel skin were modelled to represent each of the four plain weave plies. The four plies were tied together with an appropriate contact interface. Each of the shell elements has three integration points through the thickness centrally located in the element plane. Material model Mat 54 was used.

The skin modelled was as follows:

Prepreg material	Skin lay-up	Areal density g/m^2	Tensile modulus (8 ply laminate) GPa	Tensile strength (8 ply laminate) MPa
Plain weave Carbon fibre / epoxy matrix	4 ply - nominal thickness 1.1mm	410 +/-15	58	850

Table 3: Skin material parameters.

Boundary, contact, and load conditions

Support was modelled by rigid sphere, lattice and skin nodes on the symmetry planes given appropriate degrees of freedom. The indenter was modelled with rigid shells and rigid material model with typical properties for steel. Initial velocity applied to indenter.

Rubber Impact on BCC Core Sandwich Beam

A quarter model with perpendicular impact of 20^3 mm^3 rubber projectile. Impact velocity 75 and 135 m/s. Density of rubber 1.12 kg/m^3, Shear modulus, G, 97 MPa. Blatz-Ko rubber model used in LSDYNA. Sandwich beam model same as for 4 point supported impact by hemi-spherical steel projectile.

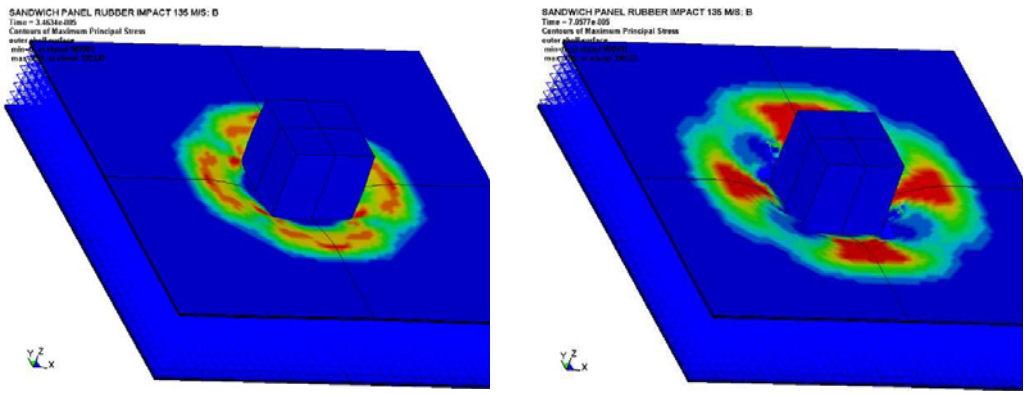

Typical stress profile of upper skin

Figure 10: Sandwich panel model.

Load-displacement data plotted from reaction force of rubber impactor. In the 135m/s impact case the simulation finished before the projectile had come to rest. Hence maximum displacement is not shown on figure . Failure of the skin was not observed in the 75m/s impact. The skin failed completely in the 135m/s impact. The failure points are difficult to characterise on the load-displacement since the rubber projectile undergoes loss of contact during the impact.

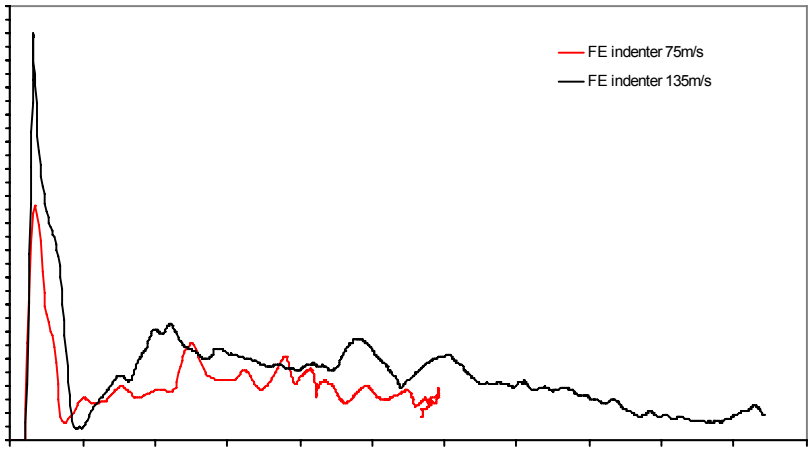

Figure 11: Comparison of load-displacement for 75 and 135 m/s impact.

Figure 12 shows the progressive failure of the skin for the 135m/s impact. The crack propagation is shown to follow the region of maximum principle strain according to the failure criteria of the composite model.

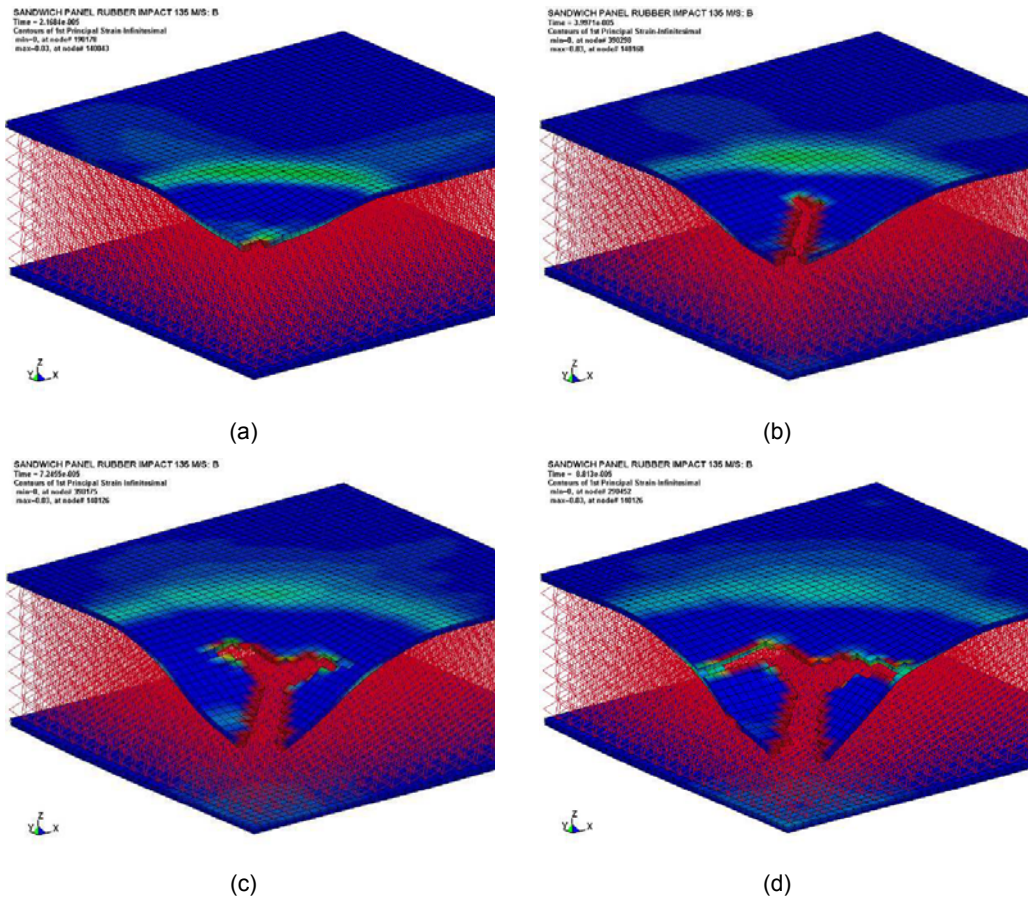

Figure 12: Series of images show the progressive skin failure for the 135 m/s impact. The impactor has been removed for clarity.

BCC Panel Impact 5.4 m/s (13J) hemi-spherical indenter

The core and skin models were the same as the rubber impact case, with the impactor being replaced by a steel sphere.

Results:

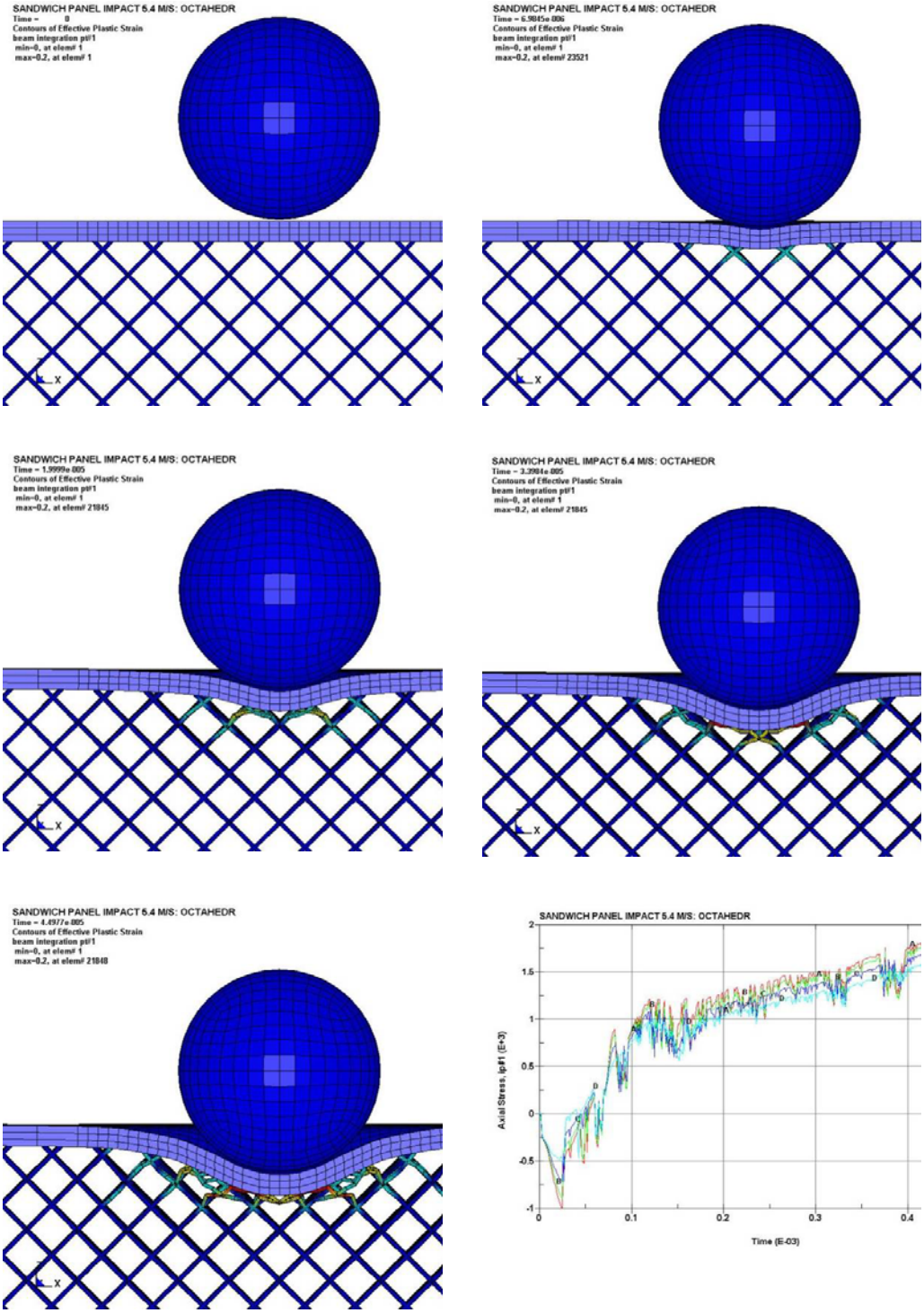

Figure 13: Detail of hard object impact (skin damage not shown)

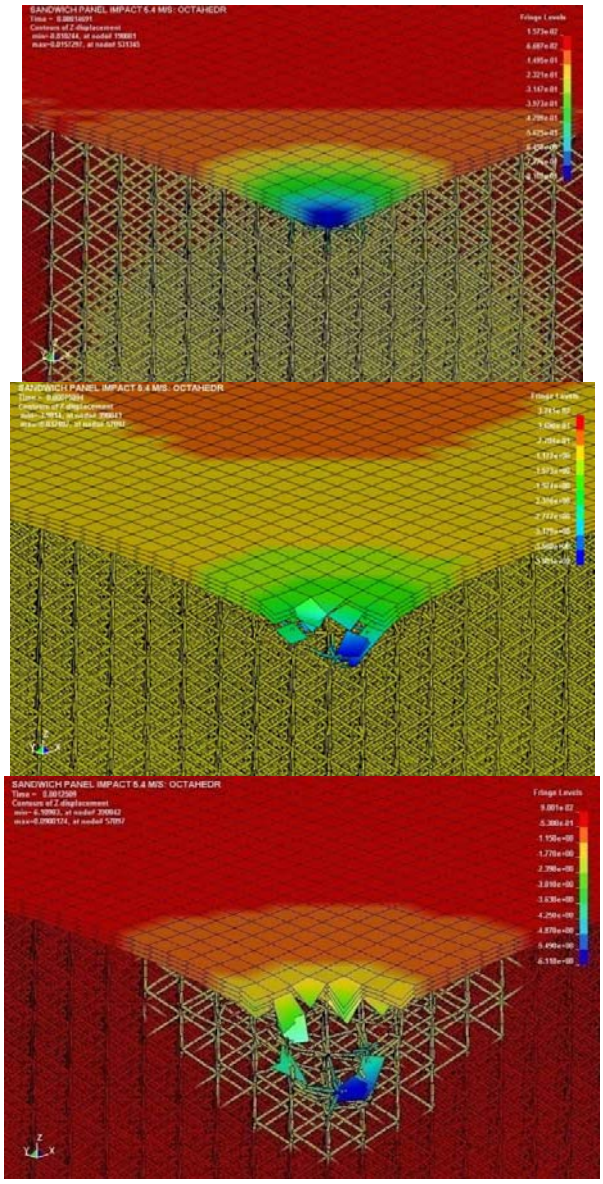

Figure 14: Upper Skin Failure Progression

Conclusions

The micro strut finite element model developed has been shown to be robust and reliable. The skin model use has been shown to give realistic results, which gives us confidence in closely modelling experimental panel tests.

UOXF contributions:

A parametric study was completed to improve the understanding of the resistance of the hollow metallic sphere to compressive uniaxial loading as a function of:

1) wall thickness of hollow spheres (Fig 1), and
2) loading rate (0.008 to 80 m/s) – (Fig 2).

The deformation and failure mode (buckling at different stages etc) were analysed. This modelling activity was required in order to

a) understand better the results of experiments on single spheres both at quasi-static and high rates of strain, and
b) help to relate the unit cell properties to bulk foam (sphere assembly) behaviour (i.e. homogenisation and multiscale modelling in Task 2.2).

The trends in results of numerical models were used to explain the variation in experimental results. This also validated the selection of the mechanical properties of the wall material in hollow spheres.

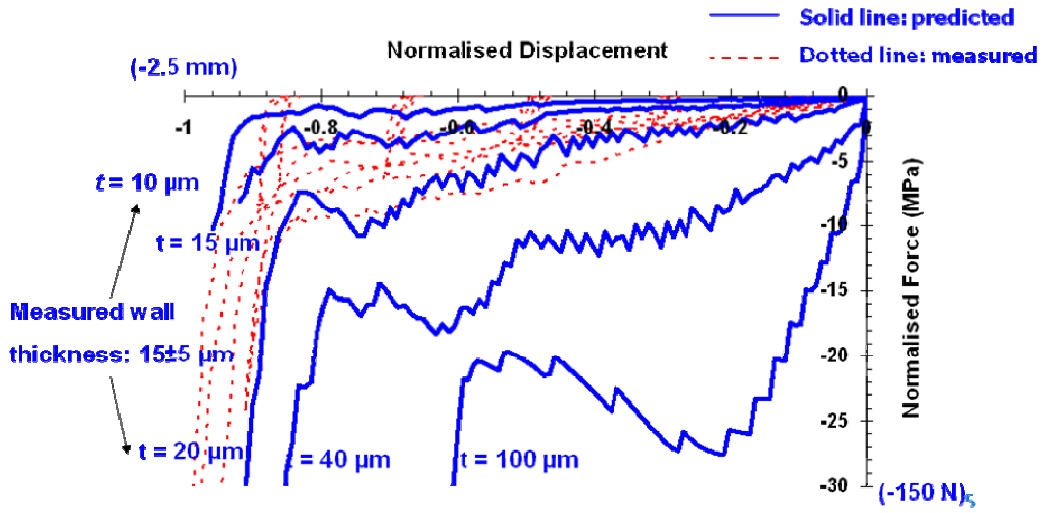

Fig 1. The effect of hollow sphere wall thickness

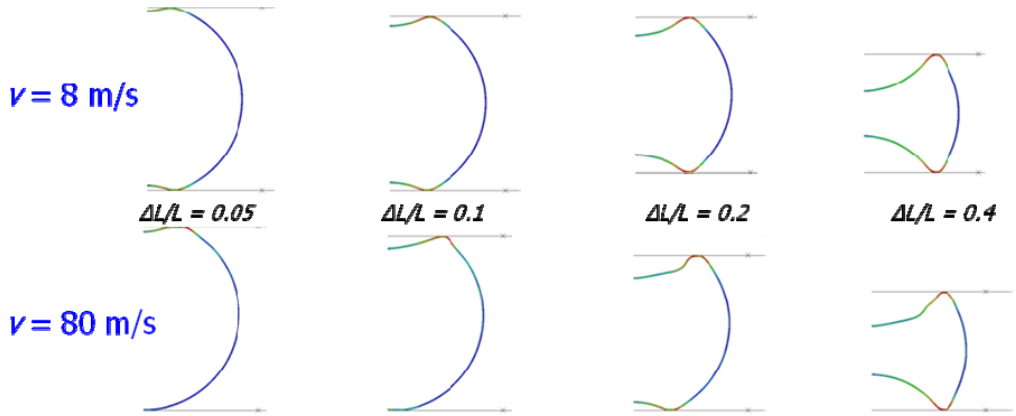

Fig 2 The effect of loading rate – loss of symmetry, excitation of different deformation/buckling modes

Existing foam material models in the literature have been reviewed and a suitable model has been adopted that represents the mechanical behaviour of cellular materials at macroscopic scale. In our work, a crushable foam plasticity material formula in ABAQUS, developed by Deshpande and Fleck, was initially used with the input data obtained from the experiments to simulate the bulk mechanical

behaviour of hollow sphere assemblies under quasi-static compressive loading. The preliminary results illustrate the applicability of the selected models.

Bulk mechanical behaviour of sphere assemblies has also been simulated by linking the mechanical properties of unit cell (single hollow sphere) using hierarchical multiscale modelling strategies (RVE and virtual laboratory). This is required to validate the homogenisation modelling on bulk sphere assemblies (Fig 3). The same technique was used to simulate the behaviour of SLM lattice systems (Fig 4).

Real specimen and Representative Volume Element – Homogenised model

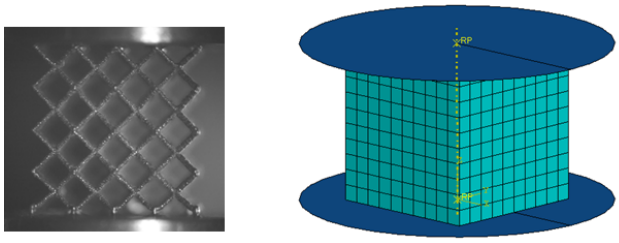

Fig 3 Homogenisation of SLM lattice concept

Fig. 3 shows the SLM lattice core specimen and Representative Volume Element (RVE) of the homogenised model. The validation of the model is seen by the stress-strain curves in compression Fig.4 and the deformation fields in Fig. 5. There is satisfactory agreement in both cases.

Quasi-static Dynamic

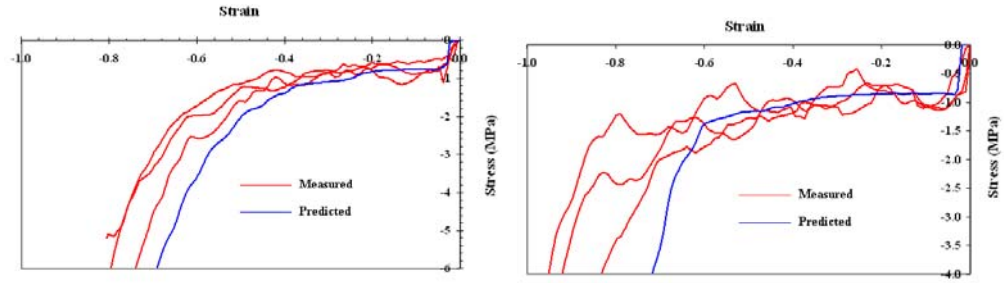

Fig. 4 Comparison of predictions with quasi-static and dynamic test data

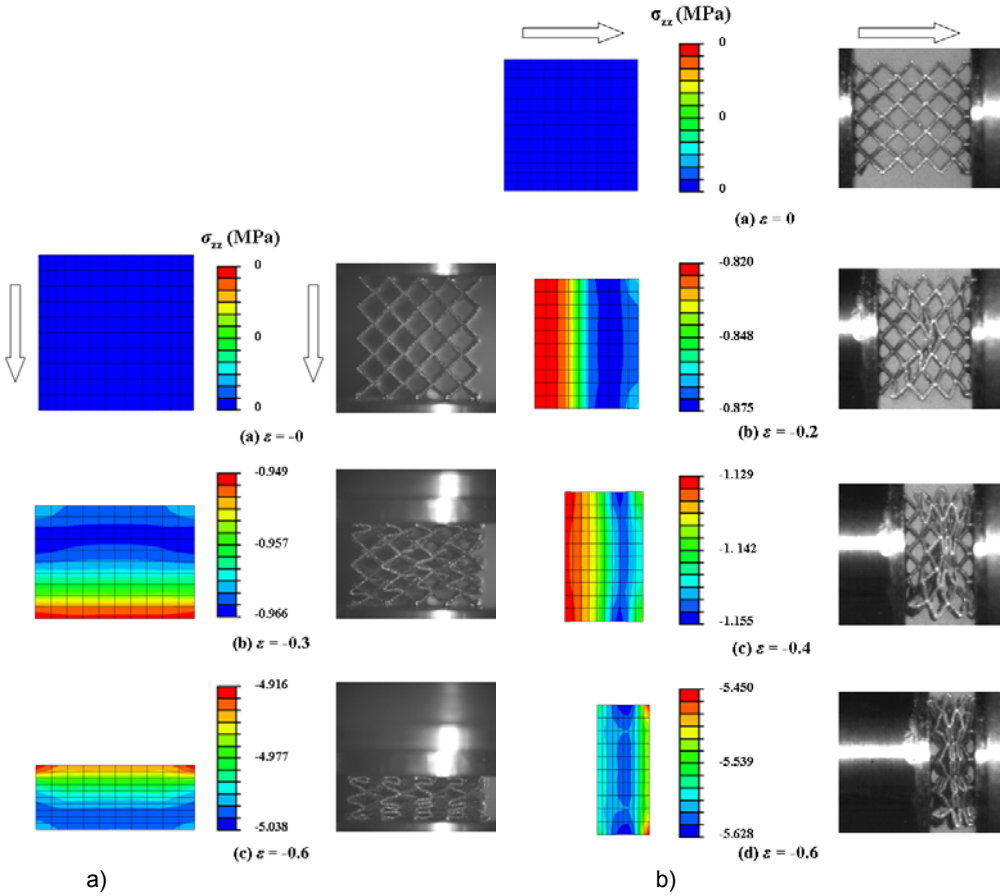

Fig. 5: Comparison of Q/S and dynamic deformation fields with homogenised model

UPAT contributions: Impact models of CM structures

Two types of cellular cores manufactured by different technological processes were investigated. The first core type is produced by Selective Laser Melting (SLM) process using powder stainless steel as constitutive material by ULIV. The second core type (Wadley core type) is produced from stainless steel plated geometry in a stepwise process of slitting folding and brazing multiple layers in a core assembly by ATECA. The investigated unit-cells are presented in figure 1

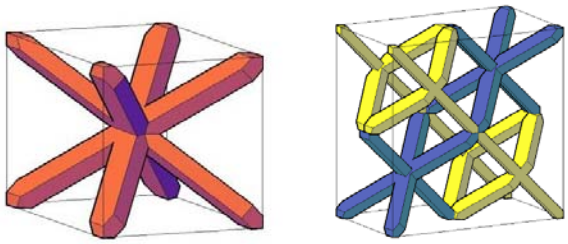

Fig 1 : unit-cell of Wadley and new type of core

Finite Element (FE) models of the unit-cell geometry for both core types (BCC and Wadley) were developed, using beam or shell finite elements. Linear and non-linear response has been obtained by those FE models, i.e. the elasticity module, the plateau stress and the compaction strain The numerical models comprise the basis for a parametric study on the influence of the unit-cell geometrical parameters on the linear and non-linear response of the open-cell metallic structures.

Similar finite element (FE) modes were also created other SLM core types, namely BCC-z and F_2FCC-z type. Improved core designs, in which the strut material of BCC unit cell has been replaced by Titanium, as well as, a new type of Wadley core created by removal of two beams from the original Wadley core have been studied.

The simple analysis methodology developed was proven suitable for the prediction of structural response of compressively loaded cellular cores. It is capable to calculate their elasticity modulus, plateau stress and compaction strain with sufficient engineering accuracy. A non-linear elastoplastic analysis including material plasticity and geometrical non-linearity is required for the proper simulation of the cellular core behaviour, as the basic failure modes are elastoplastic buckling and plastic bending. The critical elastoplastic buckling stress is approximated analytically and introduced into the elastic-plastic material model of the vertical struts, as they are expected to undergo buckling failure. The upper value of the compaction strain is approximated also analytically, in order to avoid the introduction of contact definitions in the numerical simulation.

The obtained numerical results have shown that the structural response is strongly influenced by the strut aspect ratio, as well as unit cell size and shape. Therefore, the capability of the analysis model to predict the structural response is highly dependent on the accurate knowledge of the strut geometrical characteristics and especially the cross-sectional radius. The bcc,z and the f2fcc,z geometries, which have additional vertical struts, exhibit much higher stiffness and critical buckling load compared to the bcc cores. Parametric studies on the influence of the unit-cell size on the non-linear response of cellular cores have shown that the plateau stress of all core-types increases with the decrease of the unit-cell size.

WP2 conclusion

The objective of CELPACT WP2 work package was to be able to simulate the behaviour and to compare different type f cellular cores. Results, mainly shown in WP4, are very good.

In term of virtual material testing, CELPACT partners achieved the same results as in laminates i.e. to be able to predict the behaviour of a core with respect to the good degradation mechanisms. The main additional difficulties was the modelling of defects as it is difficult to distinguish geometrical from material defects as well as their statistical distribution. Based on the microscale modelling, a first optimisation is possible by comparison between potential solutions.

In term of virtual structural testing, the use of a homogenized scale is not straightforward. In fact, the coupling between the homogenized and the microscale descriptions is still an open problem. Concerning the associated numerical solvers, implicit solvers still lead to difficult treatment in case of complex instable behaviours. In the case of non-linear homogeneization or multiscale computational strategies, the major issue is to deal with localization. This point was not properly addressed in CELPACT.

WP 3: Materials and Structures Tests (UOXF)

WP Leader	UOXF
Participants	EADS IW F, DLR, LMT, RWTH, ULIV, UOXF, UPAT

The objectives of WP 3 were to provide the experimental data on the selected materials' behaviour in order to enable the development of numerical models capable of accurate simulation of experimentally observed and measured behaviour. This is aimed to be achieved in two phases a) by performing small scale tests on constituent materials and micro- and meso-scales to provide intrinsic information on the materials' behaviour, and b) by performing medium and large scale experiments to validate the developed numerical modelling methodology.

The main achievements of the WP3 :

a) Completed evaluation of composite core material at LMT, DLR, CRC-G, USTU and RWTH

b) Completed evaluation of cellular metals at EADS IW F, ULIV, UOXF, DLR and UPAT

Composite Core Materials

LMT:

Two main experimental activities have been conducted at LMT. The importance of these two activities has been mentioned during the work done on numerical modelling of USTU folded cores. The first activity concerns the modelling and identification of the aramid paper behaviour in compression and bending. For that, a dedicated experimental setup has been designed. The second activity concerns the modelling and identification of the skin/core bondline properties. A climbing drum peeling test has been used as well as image treatment in order to estimate a local energy release rate.

1. Determination of the paper behaviour in compression and bending

During the loading of a folded core in compression, bending appears very early due to geometrical defects. The paper is then loaded both in compression and bending; this up to high degradation levels of the paper. As it is very difficult to have a high pure compression load, only elastic properties have been studied in compression. A dedicated setup has been designed. It allows both tension and compression loadings on a small curved coupon of paper. Using this test, it has been shown that the paper elastic behaviour in compression is the same as the one in tension (Fig. 1) and also that a single compression test on a small specimen is not sufficient to properly identify the elastic modulus of the paper. This is due to the heterogeneity of the stress field caused by clamped boundary conditions used in this kind of experiment.

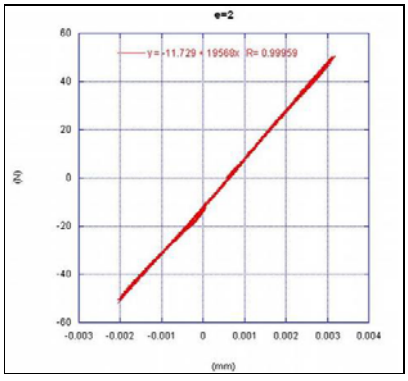

Fig. 1. Load / Displacement curve of a tension – compression test on a 2 mm paper coupon

Concerning the bending behaviour, a dedicated setup has been designed. It is close to the Shanley's structure. This setup imposes proper boundary conditions and allows a simplified treatment of the measured force/displacement to get the moment/curvature data. Different sizes of coupons have been tested. Up to the global load presented on fig. 2, the degradation is supposed to be diffuse in the coupon. A purely damage model has been identified. Its evolution law is shown on fig. 3.

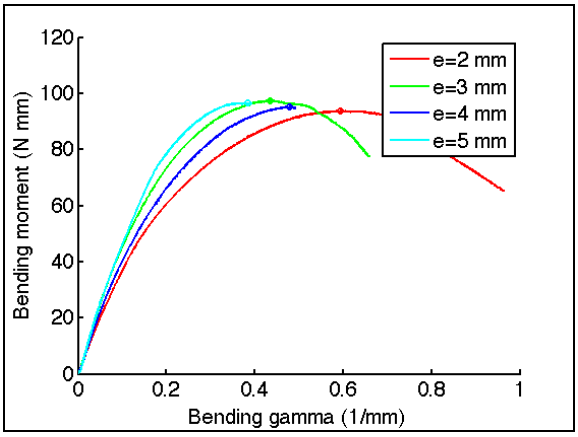

Fig. 2. Bending moment/curvature curves for bending tests on different coupon sizes

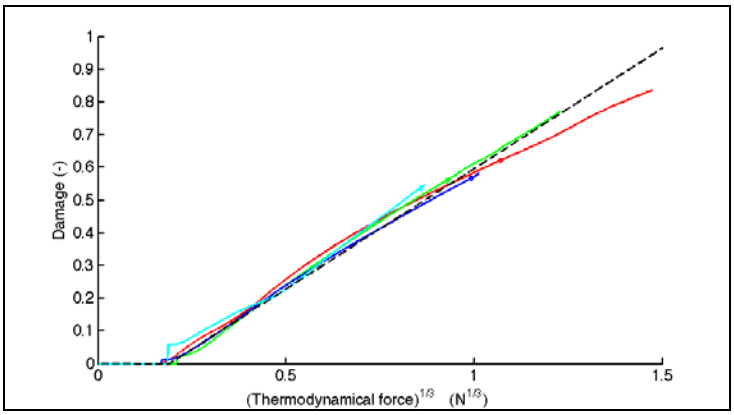

Fig. 3. Damage / (cubic root of the) Thermodynamic force associated to the damage variable curve for bending tests on different coupon sizes

After that peak, localization and plasticity appears and is modelled using a plastic hinge.

2. Determination of the skin/core bondline property

A climbing drum peeling test has been chosen to identify the critical energy release rate of the skin/core bondline. First, this identification leads to macro values depending of the core geometry and of the loading direction. Secondly, using image treatment of the debonded area, the real debonded surface has been used, in addition to the debonding scenario, to identify local energy release rates relative to the debonding of a paper sheet and the skin. These local values (one for initiation and one for propagation) have been used on different geometries and loading directions to predict the associated macro energy release rates.

CRC-G:

CRC-G focussed on composite foldcore sandwich structures and characterised the structures experimentally in compression and shear tests, both statically and dynamically. Additionally, micrographs were generated to have a closer look into the cell wall material, fibre distribution and imperfections. The static tests were conducted on a 500 kN universal testing machine of the type Instron 8803 with a cross-head speed of 1.5 mm/min. A laser extensometer was used for the displacement measurement.

The foldcore structures in the first phase of the project were made from unidirectional carbon/epoxy laminates. Micrographs of the upper folding edge in Fig. 1 show no fibre breakage in the folding edges. Both for the compression tests and the transverse shear tests sandwich specimens of 150 mm x 150 mm were used (Fig. 2).

The compressive behaviour was dominated by a cell wall fracture in the middle of the specimens after initial buckling. The angular geometry leads to a loss of contact and load transfer between the upper and lower side resulting in a drop of the stress level to low values. As the compression continues more cell walls come into contact and are crushed at the opposite side leading to the progressive curve up to the densification region (Fig. 3).

In addition to quasi-static testing, dynamic compression tests at 300 s^{-1} and 500 s^{-1} were conducted on a drop tower facility to investigate the rate-dependency of the compressive behaviour. However, no strain rate effect occurred, i.e. the stress level was not influenced by the loading rate. This could be expected since the crushing stress of CFRP at these strain rates is regarded as not or at most marginally rate-dependent. The shear testing turned out to be limited by the high strength of the CFRP structure leading to a debonding between core and loading plates at some point of the experiment. However, besides the shear stiffness the results of these tests give additional information on the bonding quality.

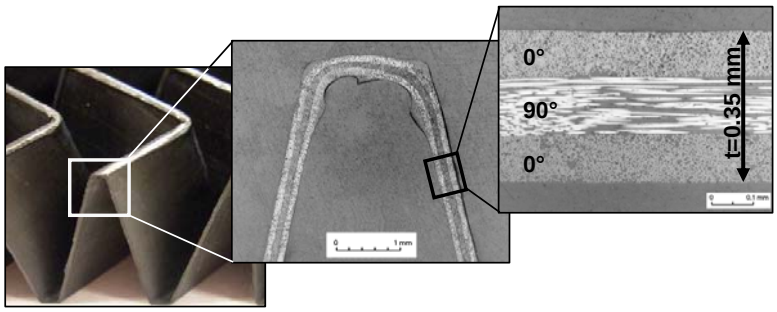

Figure 1: Micrographs of top folding edge and CFRP cell wall laminate

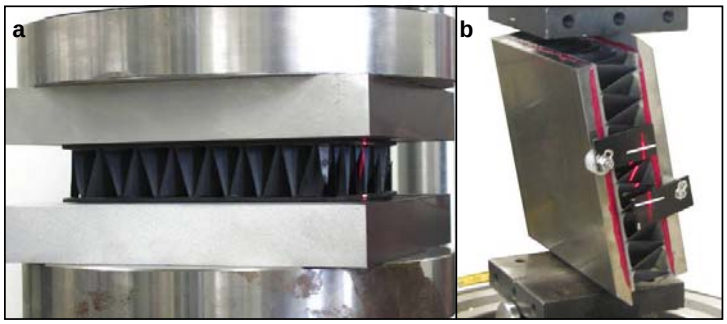

Figure 2: Compression (a) and transverse shear testing (b) of CFRP folded core

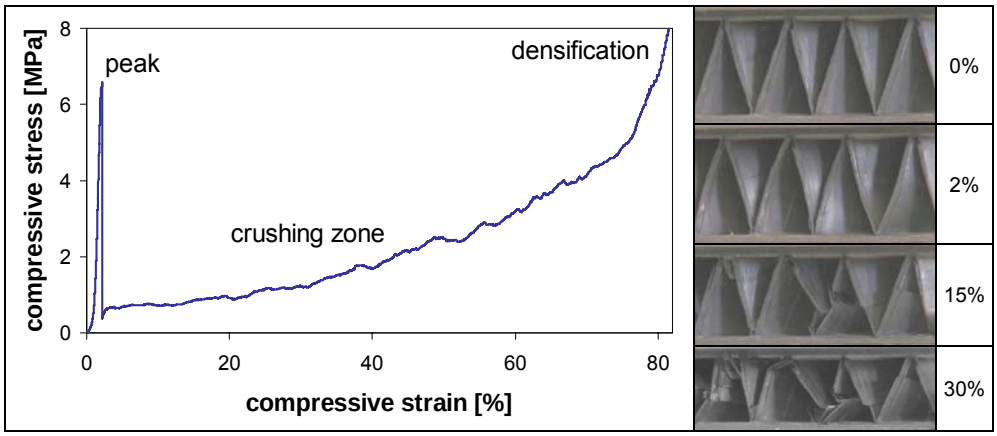

Figure 3: Compressive stress diagram and cell wall behaviour of first phase CFRP folded core (with percentage strain)

Based on the experiences in the first phase of the project CELPACT, new materials and geometries were specified by CRC-G for the foldcore structures in the second phase of the project. Woven aramid fibre and carbon fibre fabric materials were used for the foldcore production with an optimised cell geometry and also in a dual-core configuration.

The cell walls of the ductile aramid foldcore buckle under compression and collapse under an average peak stress of about 3.2 MPa (Fig. 4). Afterwards, the structure is folded up to the densification regime in a comparable way to Kevlar paper foldcores and Nomex honeycomb cores (Fig. 5).

In contrast, the carbon foldcores show remarkably higher stiffness and strength properties, with maximum stresses of up to 8 MPa. Also in this case the cell walls buckle before fracture. After fracture, the stress drops to a very low level and the cell walls are crushed as they come into contact with the opposite skin.

The dual-core sandwich specimens show a sequential two-phase behaviour. First the aramid foldcore fails with ductile deformations. As soon as it is completely densified, the carbon foldcore fails in a brittle way. Different geometrical alignments of the two cores with respect to each other were tested with a minor effect on the result. Comparing the specific absorbed energy, which is the surface under the stress-strain curves divided by the core density, the dual-core and the carbon foldcore show the highest energy absorption potential.

The properties were determined in flatwise compression tests. The compressive stiffness and strength of the second phase foldcore structures could be increased compared to the first phase structures. Especially the crushing stress of the first phase material is much lower compared to the optimised core geometry and also the dual-core configuration. Also the specific energy absorption could be increased significantly.

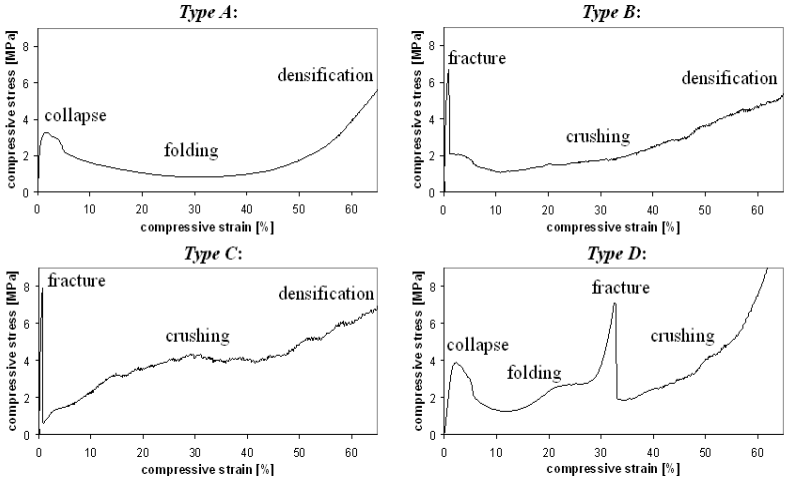

Figure 4: Compressive stress-strain diagrams of four different foldcore types

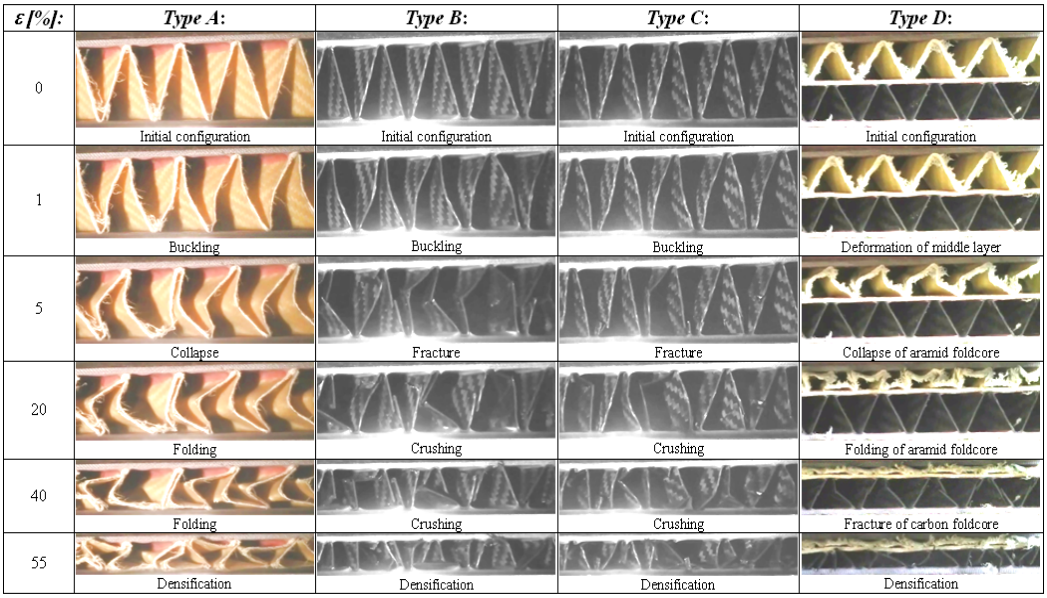

Figure 5: Cell wall deformation behaviour of four foldcore types under compression

RWTH:

Shear and Compression Tests

The aim of this experimental study was the classification of static properties of the foldcores in question. The measured properties were out-of-plane shear and out-of-plane compression, which are the most important static properties for a core of a sandwich panel.

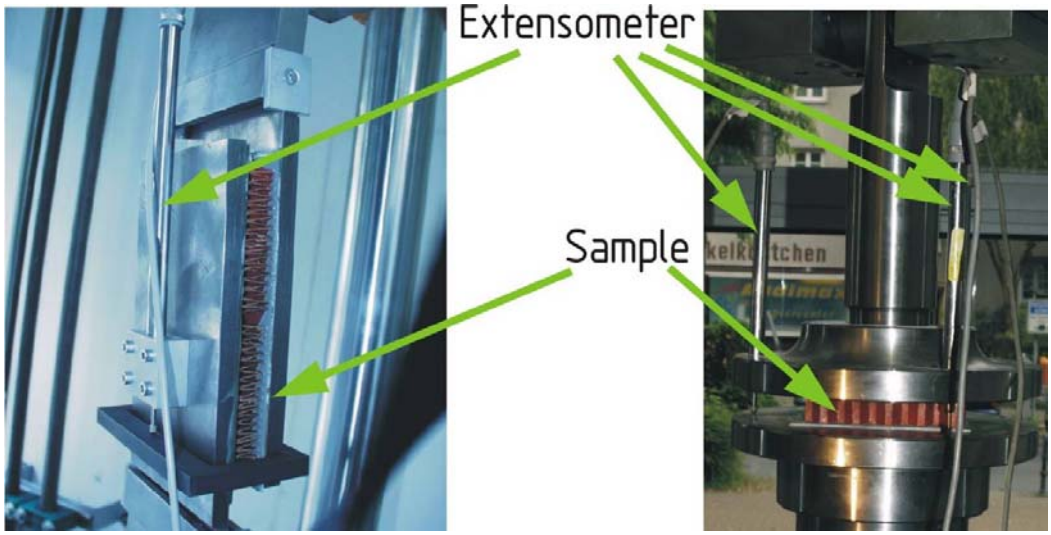

Figure 0-1: Test set-ups for static core characterisations (Left: shear, Right: compression)

The shear tests were performed according to the specification of the standards DIN 53294 and ASTM C273 to measure the shear stiffness and strength of the core in the two main geometrical directions of the core (L- and W-direction). Basically the tested samples are glued between two rigid steel plates. During the tests load is applied to the opposite ends of the steel plates (see Figure 0-1). The load is applied by a universal testing machine.

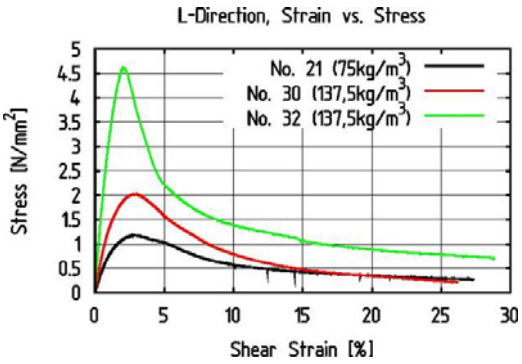

Figure 0-2: Strain-Stress diagrams (different foldcores, shear in L-direction)

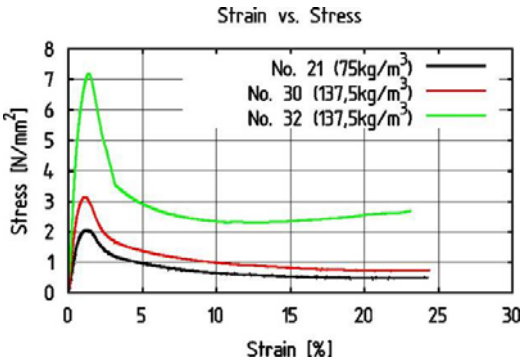

Figure 0-3: Strain-Stress diagrams (different foldcores, compression)

The objective of the performed flatwise compression tests is the determination of the compressive strengths and moduli of the tested sandwich cores in the direction normal to the face sheets. Those properties, as the shear moduli and shear strengths, are fundamental for the design of sandwich panels. The set-up is designed according to the standards DIN 53291 and ASTM C 365-00.
The test sample is compressed during the tests between two rigid steel surfaces. The upper steel plate is connected rigidly with the testing machine. The lower compressing surface is pivoted on a spherical bearing block which is self-aligning (see Figure 0-1).
In both shear and compression tests the specimens were tested up and beyond their ultimate strength to measure as well the elastic as the residual properties after the collapse. In Figure 0-2 and Figure 0-3 some of the acquired results for different core geometries are presented. The compared cores were USTU-type foldcores with different geometrical configurations.
Additionally several Kazan-type configurations were tested to acquire their shear properties.
Low velocity hard body impact tests were performed to investigate the impact tolerance of sandwich panel with folded cores. Different types of USTU and Kazan cores were investigate during the program.

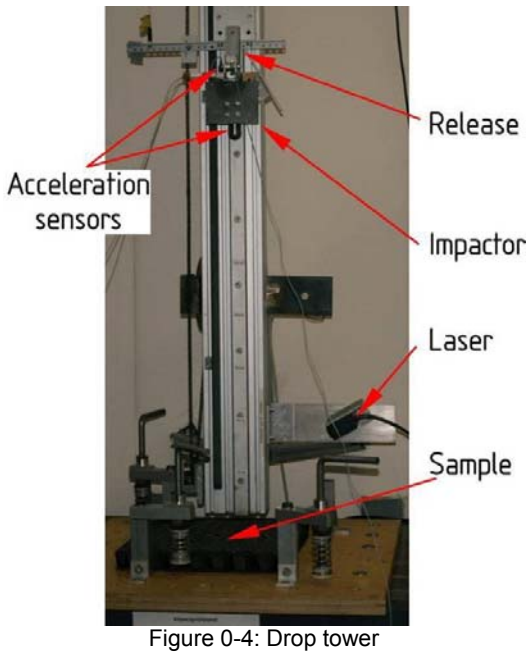

Figure 0-4: Drop tower

All the tests were performed with a drop tower. The main feature of the tower is a 4,5 m long vertical rail. The impactor is able to slide along this rail. The sample is fastened on a table at the lower end of the rail. After the releasing the impactor slides down along the rail and converts his potential energy into kinetic energy. The impactor used during the experiments had a mass of 1,56 kg. The impactor head which actually contacts the sample is ball-shaped and is made of steel. The diameter of the head is 1 inch (25,4 mm). Impact energies up to 60 Joule were tested.
After the impact the damages in the impacted skin were investigated by means of ultrasonic scans (see Figure 0-5). These scans reveal a large amount of delaminations in the skin, whose are is up to magnitude larger than the damage visible from the outside.
The information acquired during these tests were used to validate the numerical model developed to simulate impact events on sandwich panels.

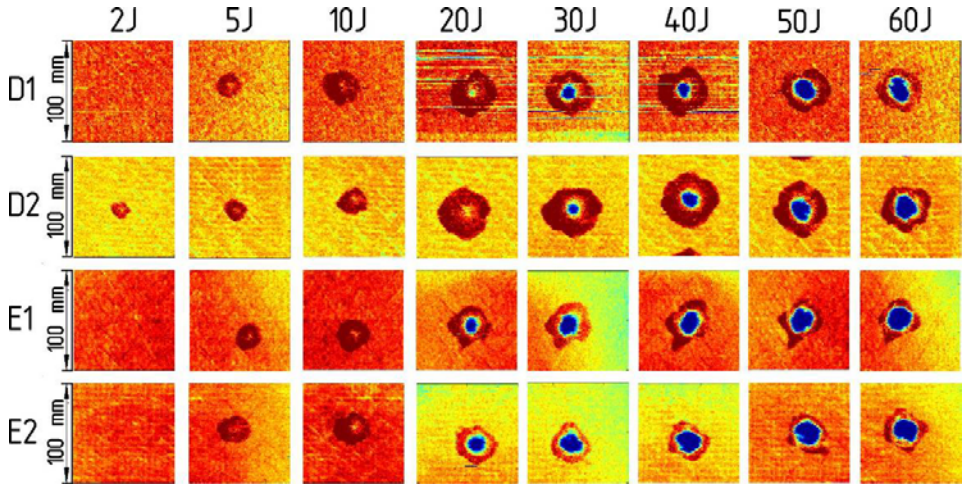

Figure 0-5: Ultrasonic scans of the impacted skin of sandwiches with different foldcores

Some of the impacted sandwich panels were used in subsequent 4-point bending tests. The aim of this investigation was to assess the drop in bending strength due to impact damages.
The set-up used for these tests allows to introduce a pure bending moment into the tested area at the middle of the sample. A schematic drawing of the used set-up are presented in Figure 0-6. The much stiffer filler outside the inner load introductions prevent shear-induced failure there. Due to this design the needed sample length to assure failure in the tested area between the inner introductions can be reduced significantly. The test set-up is designed according to DIN EN 6061.

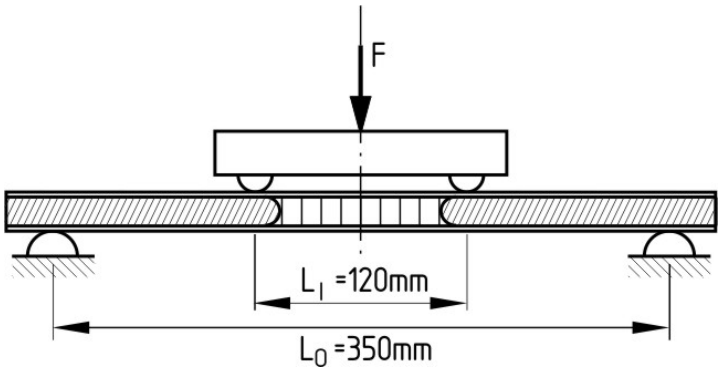

Figure 0-6: 4-point bending test set-up

The influence of low velocity, hard body impact damages on sandwich samples with different USTU type foldcore designs were investigated. Especially the influence on the residual bending strength of the damaged panels was the focus of this test program.

The reduction in bending strength is significant even for very low impact energies which cause nearly invisible damages. In case of the 5 Joule impacts the reduction of bending strength was already between 20 and 40 %. For the highest tested impact energy (40 Joule) the reduction is larger than 60 %. The results for two different USTU-type foldcores are presented in Figure 0-7 and Figure 0-8.
Also this results were the basis for validation of residual strength simulations.

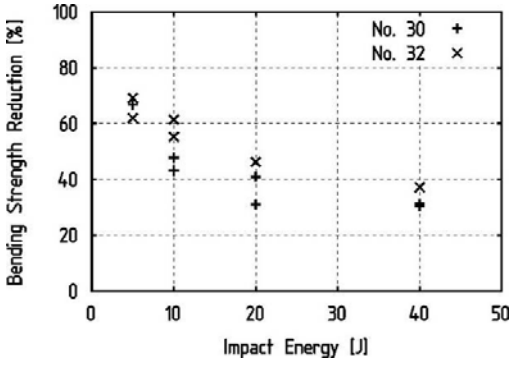

Figure 0-7: Drop in bending strength due to impact (bending in L-direction)

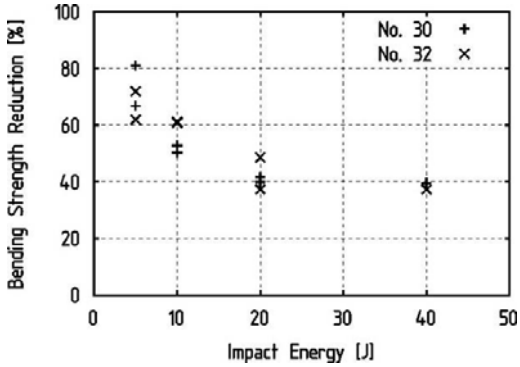

Figure 0-8: Drop in bending strength due to impact (bending in W-direction)

DLR:

HV impact tests on foldcore sandwich panels

This second series of gas gun tests at the DLR was on improved CHC sandwich panels developed in the 2nd phase of CELPACT. The tests were carried out on a range of advanced CHC sandwich panels from CRC-G based on novel Kazan foldcores, with carbon foldcore, and concepts with dual carbon/aramid cores. This was followed by tests on three CHC sandwich panels from USTU with CFRP skins and a higher density blocked foldcore Type 32. A range of impact scenarios were considered mainly relevant to ground or engine debris impact with steel cubes, steel bars, and rubber beams representative of burst tyre fragments. Impact damage was assessed experimentally by X-ray computer tomography (CT) analysis of the impacted panels, as reported in Task 3.3. This technique gives detailed information on internal core damage obtained non-destructively by X-ray methods. Each of the impact tests was documented by a sequence of photographs of the impact event from the HS video camera, photographs of the visible damage on the outer and inner skins and CT images of core and interface damage for selected samples

Two main types of advanced panels were supplied by CRC-G, with carbon fabric foldcore and with dual foldcore concepts. Four carbon composite foldcore sandwich plates (CEL-D1, CEL-D2, CEL-D3 and CEL-D4) had dimensions 400x400x20 mm with ~2.0 mm carbon composite skins (Cytech HTS/977-2, 16 UD plies quasi-isotropic lay up) were provided by CRC-G with carbon fabric composite foldcores of batch D as described in CELPACT D13-2. The foldcore cell walls have about 0.5 mm wall thickness with two plies of Krempel AGBD2008 fabric (2/2 twill weave, bisphenol epoxy). The foldcore height was about 28 mm.

On the carbon foldcore panels the 13.4 g steel cube projectile had impact velocities in the range 63.8 – 137 m/s, whilst the 101.4 g steel bar had velocities 44.1 – 63.3 m/s. The velocity range for the steel cube was chosen to show critical velocities for outer skin damage, core penetration and inner skin damage. Results are summarised in Table 1 in the Task 3.3 report. For the steel bar which usually penetrates the sandwich panels, the aim was to find the velocity when it was stopped by the core. Figs 1a – 1c below show typical results when the steel bar penetrated the sandwich. The bar mass 101.3 g impacted at velocity 52.9 m/s giving impact energy of 141.7 J. As the impact sequence Fig. 1b shows, the bar hit the outer skin end on parallel to the panel foldcore direction and penetrated the outer skin. During the penetration of the foldcore it rotated slightly until it penetrated the inner skin. After

penetration of the inner skin the bar remained stuck in the sandwich which indicates that the impact energy correlates to the energy for complete sandwich failure. The outer skin shows a clean entry slit, whilst the inner skin was extensively torn. Fig. 1a depicts the upper and lower skins after impact and Fig. 1b the test sequence. The CT scans in Fig. 1c show that the bar has stopped after penetrating the lower skin and remains embedded through the complete sandwich. The CT images show how localised this damage is in the foldcore, which reduces the chance that different carbon cores will improve impact response.

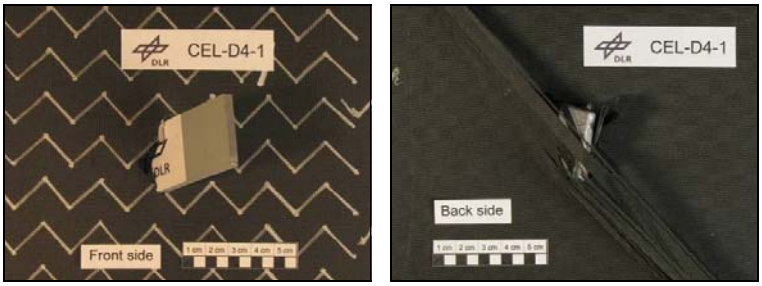

Figure 1a: Front and back side picture of impact area of test shot CEL-D4-1

Figure 1b: Picture sequence taken from the high speed impact video (Picture interval: ~1.17 ms)

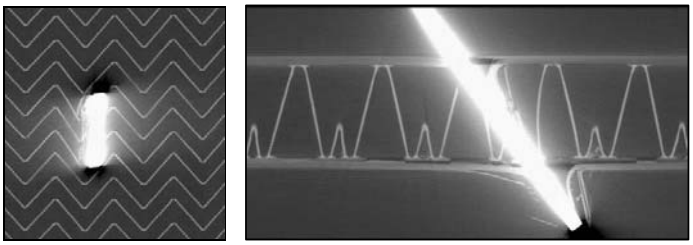

Figure 1c: CT images showing steel bar passed through the sandwich and stayed embedded

The foldcore sandwich panels CEL-E3 and CEL-E4 were impacted with steel bars at an impact angle of 60° to the panel face. The gas gun pressure was 0.8 bar and it accelerated the steel bar to a speed of 44.1 m/s with impact energy 98.5 J. In this case the steel bar penetrated the outer skin and rebounded after damaging the middle skin as seen in Fig. 2a and Fig. 2b. The inner skin showed no visible damage. The CT scans in Fig. 2c show internal damage in the foldcore with extensive bending and folding of the foldcore paper, which absorbs energy. The bar penetrates the outer skin before being stopped by the middle skin, which is damaged. The CT images show clearly the positive influence of the dual core concept with the bar stopped at the middle skin, before rebounding.

Figure 2a: Front and back side picture of impact area of test shot CEL-E3-1

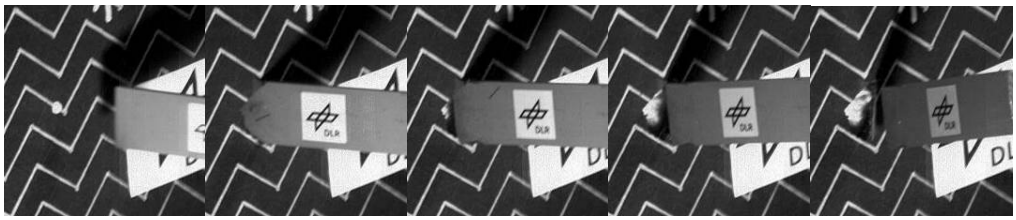

Figure 2b: Picture sequence taken from the high speed impact video (Picture interval: ~2.75 ms

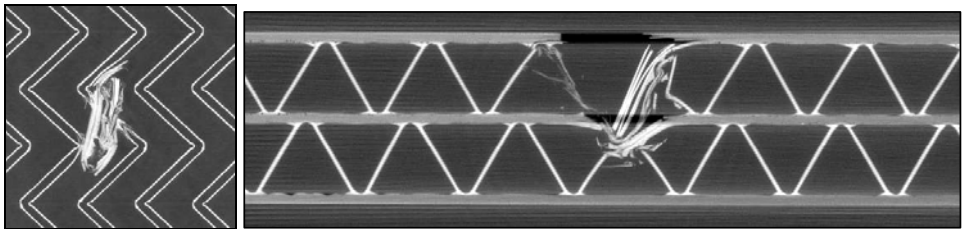

Figure 2c: CT images show bar is stopped at middle skin before rebound in dual core panel

The UST foldcore panels consisted of three aramid paper foldcore sandwich plates (CEL-FC-HV4, CEL-FC-HV5 and CEL-FC-HV6) had dimensions 500x500x20 mm with ~2.0 mm carbon composite skins (Cytech HTS/977-2, 16 UD plies quasi-isotropic lay up) were provided by USTU with blocked foldcore type 32, as described in CELPACT D13-2. They were impacted with steel cube, steel beam and rubber beam at 90° and 60° impact angle and with 2-4 shots per plate, depending on size of damage zone.

As an example of the work Figs 3a – 3c show results from the runner projectile impacting a foldcore panel with block core. In this test the gas gun pressure of 6.4 bar accelerated the projectile to a velocity 135.1 m/s with high impact energy of 937.2 J. There was no visible damage at inner and outer skins. An imprint was visible and the impact area yielded to finger pressure. The CT images Fig. 3c showed foldcore cells with some bending deformation, but no clear core-skin debonding. The cause of the softening at the impact point appears to be due to irreversible kinking in the foldcore struts at the impact point, which are no longer elastic.

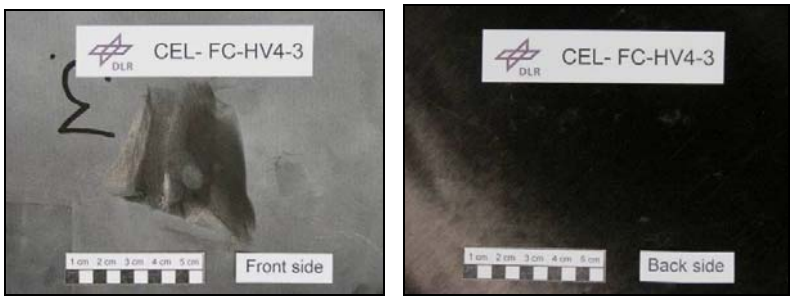

Figure 3a: Front and back side picture of impact area of test shot CEL-FC-HV4-3

Figure 3b: Picture sequence taken from the high speed impact video (Picture interval: ~0.667 ms)

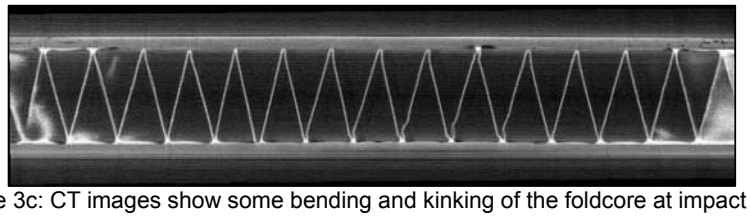

Figure 3c: CT images show some bending and kinking of the foldcore at impact point

The complete results of this gas gun test programme on novel foldcore concepts with carbon, dual core and high density block core are reported in D32-5A/D33-2A.

For sandwich structures it was found to be impossible to study damage inside the core and at the skin/core bond using conventional NDT methods such as ultrasonic C-scan and thermography, since they focus on the outer skin damage. The DLR used X-rays to study damage in the CHC and CM cores arising from the gas gun impact tests reported above in T3.2. Standard X-ray images can be difficult to interpret in a thick structural core as they give a 2D representation of 3D damage. This problem may be overcome with CT, which is based on sequential X-ray scans through the structure, which are then re-assembled by computer image processing to show a 3D image of internal damage across successive planes through the structure. In this way it is possible to display skin debonding and core damage after impact in the sandwich panels.

Examples of the detailed damage information obtained by the technique were shown in Figs 1c – 5c..

The damage studies are required for assessing the robustness of new sandwich panel concepts under impact loads, in particular for comparison of different sandwich panel designs and study of new core microstructures. Of interest here is to define impact velocities and kinetic energies for given projectiles at which first damage appears on the outer skin, when the outer skin is perforated, when there is core penetration, when first damage appears in the inner skin, and finally when the panel is fully perforated. For aircraft sandwich panels this information is directly relevant to damage tolerance criteria and compliance studies. This information is summarized briefly here for the advanced foldcore designs.

Damage level	**Baseline foldcore Type 30, 20 mm 137 kg/m³**	**Block foldcore Type 32, 20 mm 137 kg/m³**	**Carbon foldcore 27 mm core**	**Dual aramid/ carbon foldcore 29 mm core**
Rebound	55.6 m/s 21 J	57.5 m/s 22.2 J	63.8 m/s 27.1 J	50.3 m/s 17.0 J
Outer skin damage				62.5 m/s 26.2 J
Core penetration	82 – 108 m/s 45.2 – 77.2 J	81 - 92 m/s 44 – 57 J	86 - 130 m/s 49.5 - 113.5 J	76.4 - 125 m/s 39 – 105 J
Inner skin damage	109 m/s 79 J			118.5 – 131.5 m/s 94 – 116 J
Inner skin penetration		122 m/s 100 J	137 – 170 m/s 125 – 194 J	

Table 1: Damage velocity and energy levels measured on 4 types of foldcore sandwich panel from gas gun tests with 10 mm steel cubes at 90° impact

The baseline CHC panels tested were high density foldcore (137.5 kg/m³) panels with 20 mm thick core and 2.1 mm CFRP skins tested in earlier work showed damage and energy levels for impact from a 10 mm steel cube weighing ca 13.3 gram, as given in Table 1. Results from the test programme discussed above are added to the table. The table shows that the block foldcore and baseline foldcore from USTU are fairly similar in their impact performance for small hard projectiles, which is

considerably better than earlier DLR studies on low density foldcore with weights 50 kg/m³. Thus an improved resistance to hard body impacts with higher density foldcore is seen, due to the closer packing of the foldcore material which traps the projectile more effectively.

The carbon foldcore and dual core systems provided by CRC-G had core thicknesses 27 mm and 29 mm, respectively, compared with the 20 mm USTU foldcores. The table shows improved impact resistance, with for example a 131.5 m/s impact being stopped by the inner skin of the dual core system, whereas at this velocity sandwich penetration was observed in the block foldcore and carbon foldcore plates. This improvement is due partly to the different energy absorption mechanisms seen in the CT images for the more brittle carbon foldcores, but may also be due to the increase in core thickness.

In the case of the 60° steel bar impact tests, for the baseline foldcore tested previously this was stopped in the core at 39.3 m/s (78.7). For the blockcore sandwich, the carbon foldcore and the dual cores tested here the impacting bar was stopped by the core in all cases at a velocity 53 m/s (142 J). This suggests that the improved foldcore concepts have significant advantages as the impactor size increases.

Metallic core materials

ULIV:

Baseline metal and CM core properties
1st Generation Structures – Stainless Steel 316L

The first generation structures were a result of manufacturing issues, and were not optimized for stiffness and strength in any way. The powder was 316L stainless steel, the strut diameter was 200 microns, and the cell size was 2.5mm. Mechanical properties of these materials are dependent on laser power and exposure time: in this case, they were 140W and 500 microseconds respectively.

As with the previous cellular metals, blocks (of 50 x50 x50mm in this case) were compressed in a servo hydraulic machine. Figure 1(a) shows the collapse mechanism, Figure 1(b) shows collapsed detail. Collapse behaviour was similar to the Wadley type structures, and the structure collapses in a stable manner.

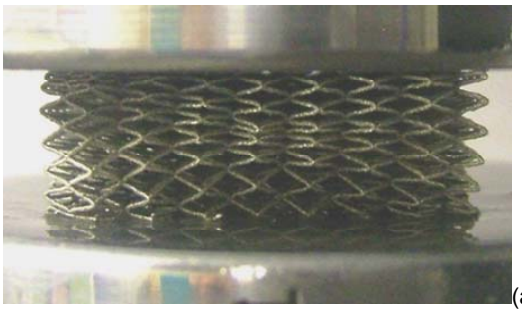
(a)
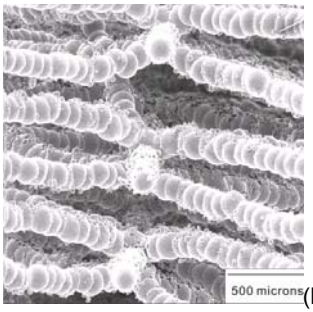

(b)

Figure 1: (a) Block collapse, (b) Detail after collapse

Figure 2 shows the effect of adhering the block to the compression platens. The effect of this is to increase block stiffness and strength. These body centred cubic structures are very sensitive to constraint given their topology. This issue should not be so great for the more three dimensional micro structures of honeycomb and foam.

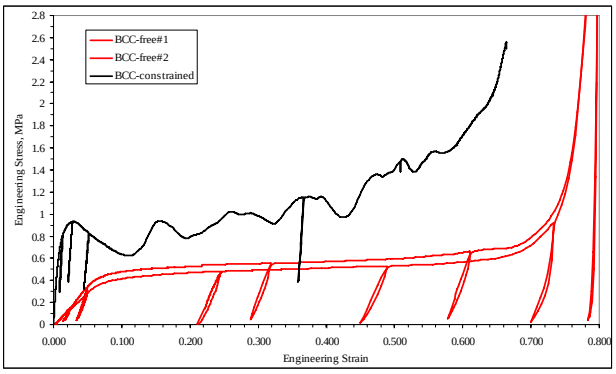

Figure 2: Block compression stress strain curves for constrained (top curve) and unconstrained (bottom curves) blocks

Improved CM core properties
2nd Generation structures – Ti 6 4

A major feature of the CELPACT programme was to review cellular materials at the 18 month point, and to define improved materials for the second half of the project. In the case of micro lattice structures it has been shown that strut diameters can be changed between 150 and 250 microns. It has also been shown that cell size can be changed between 1.5mm and 4.5mm. Also, micro lattice architectures can be extended to bcc,z and f2bcc. A rationale for this has yet to be devised, and so for this work it was decided to replace stainless steel micro powder with Ti 6 4 micro powder (keeping all other parameters the same), with a potential improvement of times 8 in specific strength. Figure 3(a) shows that the collapse mode is different to stainless steel case and Figure 3(b) shows that crush strength increases by a factor of 3 over stainless steel.

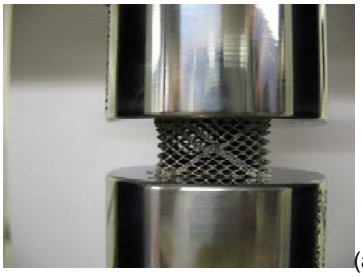
(a)
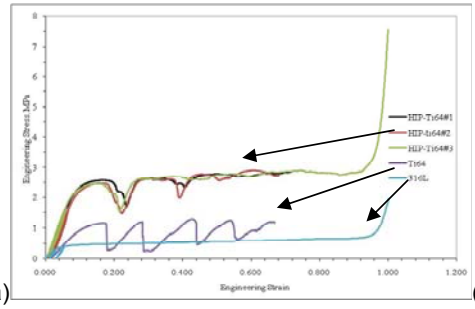

(b)

Figure 3: (a) Block crush, (b) Stress strain for stainless steel, and Ti 6 4, blocks

It should be noted that the Ti 6 4 blocks have to be post treated after manufacture using the hot isostatic process. If this is not done, then the lattice remains very brittle.

COMPARISON OF CELLULAR MATERIALS

The cellular materials are compared in Table 1 from the points of view of compressive specific stiffness and strength.

Property	**Hollow Sph.**	**Type***	**Wadley BCC**	**316L BCC**	**Ti64 Honey**	**Al Foam**	**Al BCC,Z[7]**	**316L**
Density (kg/m3)	288	560	250	170	37	230	394	

Modulus (MPa)	60	18	19	27	273	700	50
Specific Modulus (kPam3kg-1)	208	32	76	160	**7378**	3043	127
Strength (MPa)	0.89	0.4	0.5	2.5	0.7	1.6	1.1
Specific Strength (kPam3kg-1)	3.1	0.72	2	**14.7**	**18.9**	7	2.8

Table 1: Cellular block properties (Unconstrained apart from *)

From the table it can be seen that none of the cellular materials discussed here come close to the specific stiffness of Al. honeycomb, but that the Ti 6 4 micro lattice structure does come close to the specific strength of aluminium honeycomb. It should be noted that the Ti 6 4 configuration has not been optimised for stiffness or strength. Currently, the above comparisons are being conducted for block shear properties. It should also be noted that BCC is inefficient for compression, and with the SLM technique more efficient micro strut configurations (e.g. BCC,Z) can be realised.

Tyre rubber impact on CM panels

Figure 4 gives high speed film from test 6 (v impact = 125 m/s) and Figure 5 gives an approximate evaluation of the force transmitted to the panel. In the latter, the deceleration of a point one diameter length from the rear of the projectile was converted to inertial force using the mass of the rubber projectile. In this, stress waves and internal projectile deformation effects are ignored. Clearly, from Figure 4, this is a major assumption. Figure 6 shows external skin damage for test 6.

(a)

(b)

(c)

(d)

Figure 4: High speed film of rubber impact test 6.

(a) t = -6ms, (b) t = 6ms, (c) t=18ms, (d) t = 30ms

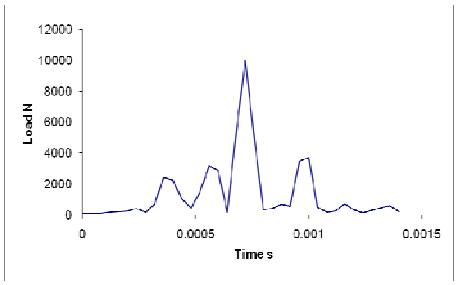

Figure 5: Approximate Force transmitted from rubber to panel in Test 6

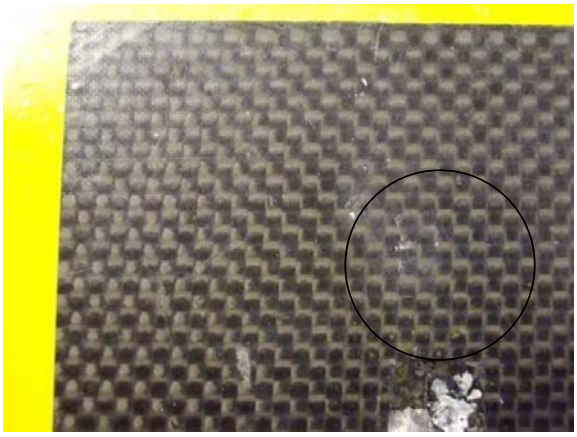

Figure 6: Damage on impacted skin test 6

Hard object low velocity impact on improved CM panels (ICCM17)

STAINLESS STEEL MICRO LATTICE CORE RESULTS

Figure 7 gives force – displacement data for the stainless steel cored four point support case for different impact energies. For the 6.6J case, the upper skin has already damaged and upper skin penetration is about to occur. For the 8.3J impact case, the impactor has penetrated into the core. Figure 8(a) gives cross sectional data for the fully supported panel after impact. It has been shown that impactor penetration for a given impact energy is similar between a fully supported and a four point supported panel. Figure 8(b) gives damage for an Alporas cored panel, and shows that damage for a given energy is similar to the micro lattice case.

Figure 9 summarises dent depth versus impact energy data for the fully supported case. From the four point support case, it has previously been shown that panel response is dominated by local effects. From Figure 6 it can be seen that Alporas aluminium foam is comparable with BCC Stainless Steel, and that impact loading gives a lower dent depth for a given impact energy as compared with the static case.

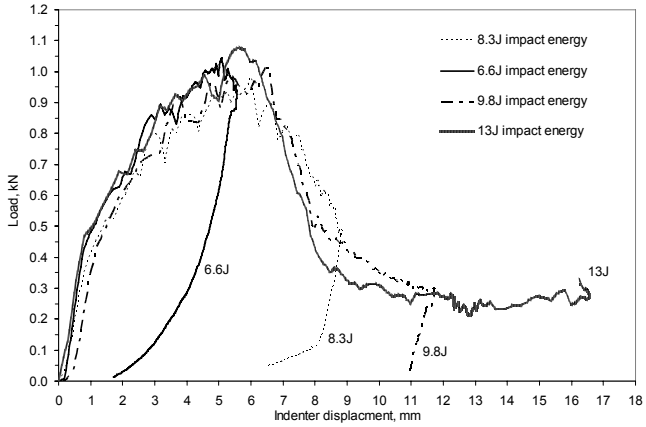

Figure 7: Load versus Indenter Displacement for various impact energies for stainless steel cored sandwich panel under four point support.

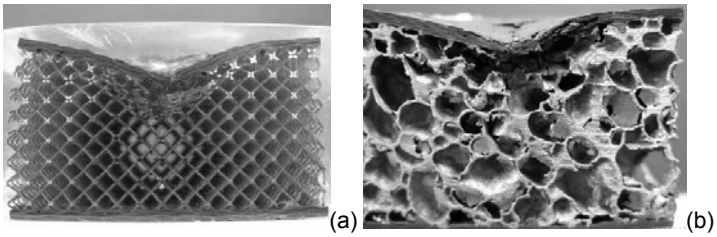

Figure 8: Sectioned fully supported panel (a) Steel micro lattice after 11.5J impact and (b) Alporas after 10J impact

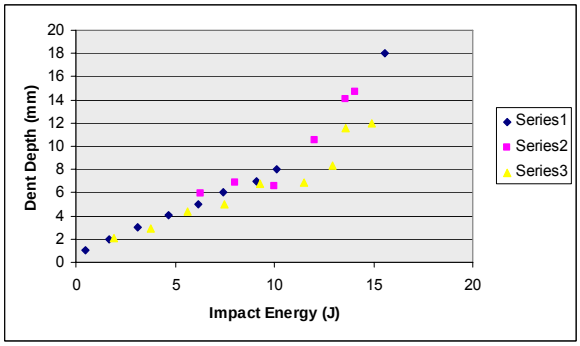

Figure 9: Dent depths for given impact energies. Series 1-BCC, static full support, Series 2-aluminium foam, impact full support, Series 3- BCC, impact full support

Ti 6 4 MICRO LATTICE CORE RESULTS

Similar drop weight tests were carried out with Ti 6 4 micro lattice cores. Core configuration was exactly the same as for the stainless steel case, apart from the change in material. Figure 10 compares the compression block behaviour between the two materials. In Figure 10(c), stress is taken as applied load divided by initial block cross sectional area and strain is based on overall block crushed length. These measures ignore block expansion (See Figure 10(a)) and any strain localisation (See Figure 10(b)).

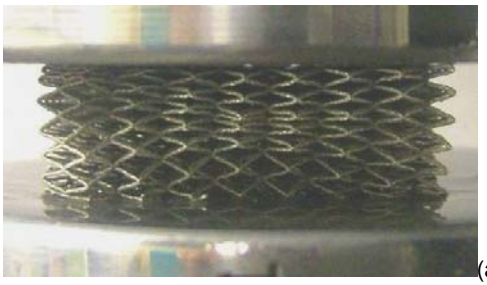
(a)

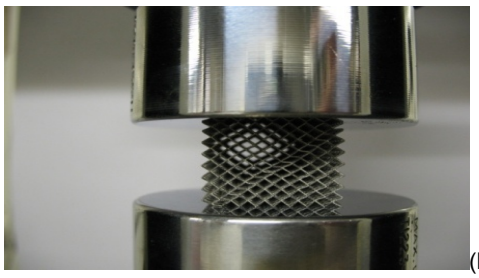
(b)

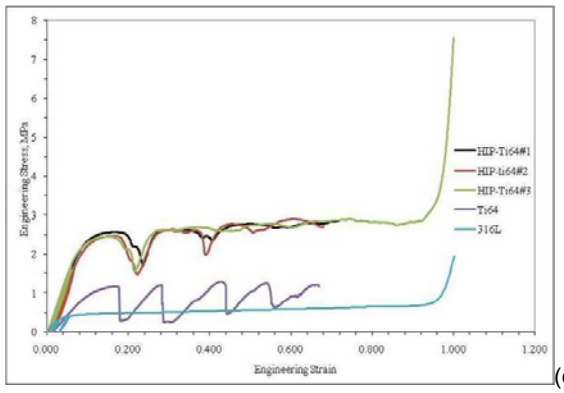

(c)

Figure 10(a) : SS316L block at 50% crush, 7(b) : Ti 6 4 block at 10% crush and 7(c) : Block compression stress strain data for SS316L, Ti 6 4 HIPed and non HIPed

From this it can be seen that the Ti 6 4 block has x5 stiffness and x 5 strength as compared with Stainless Steel 316L. HIP refers to Hot Isostatic Processing. Ti 6 4 is a more complex material as compared with stainless steel, and some post manufacture heat treatment is required. In this case, a component is subjected to both elevated temperature and isostatic gas pressure in a high pressure containment vessel. The pressurizing gas most widely used is argon (no chemical reaction).

As far as the drop weight loading of panels is concerned, Figure 11 and 12 compares Ti 6 4 results with SS316L cored panel results. In Figure 11, tested specimens were sectioned using a diamond saw. This caused some micro lattice damage. A number of specimens are in the process of being CT scanned, which will avoid this problem.

From Figure 11, it can be seen that micro strut damage is much more fragmented for the Ti 6 4 case.

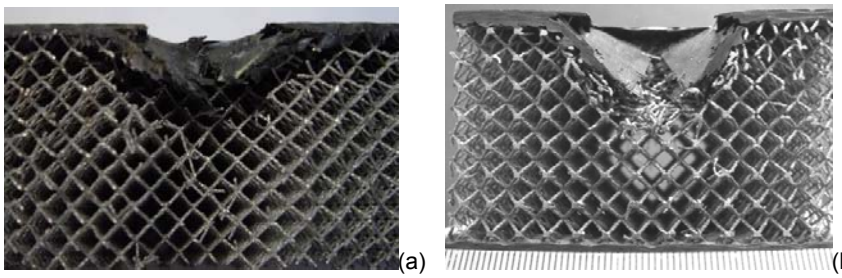

(a) (b)

Figure 11: Comparison of damage for energies given in Figure 9. (a) Ti 6 4, four point support, E_{imp} = 10.2J and (b) SS316L fully supported E_{imp} = 13.6J

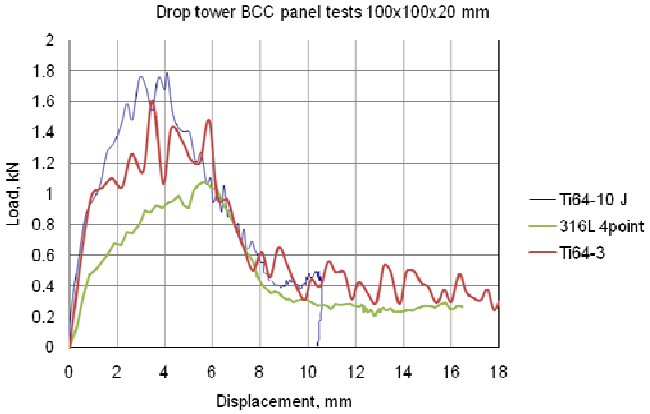

Figure 12: Comparison of load versus indenter displacement four point support, (a) Ti 6 4-10, E_{imp} = 10.2J, (b) Ti 6 4-3, E_{imp} = 20.4J, (c) SS316L, E_{imp}= 13J

UOXF:

UOXF conducted a number of experiments on small scale samples of titanium SLM lattice cores from ULIV, thus providing information on the improved selectively laser melted Ti6Al4V lattice. The results are reported here as comparison with the originally proposed stainless steel. The data are compression stress-strain curves at high rates from quasi-static test (left) and gas gun impact tests (right). The Ti lattice structures have higher crush stresses than the stainless steel lattice structures, and are more rate dependent in their properties.

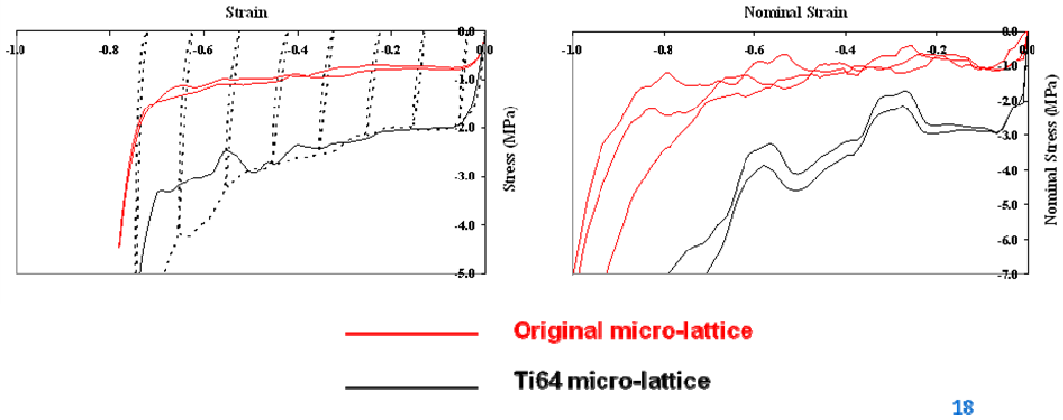

Photogrametric techniques developed specifically for high-speed-digital-photography have been used to quantify more accurately the slow-down of projectiles during the penetration through sandwich systems and related energy dissipation. An illustration of the adopted methodology has been outlined below. By this technique it is possible to measure energy absorption during impact as a function of penetration displacement in the core, as shown in the figures below.

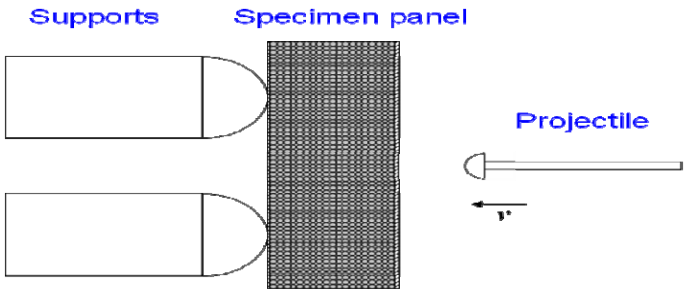

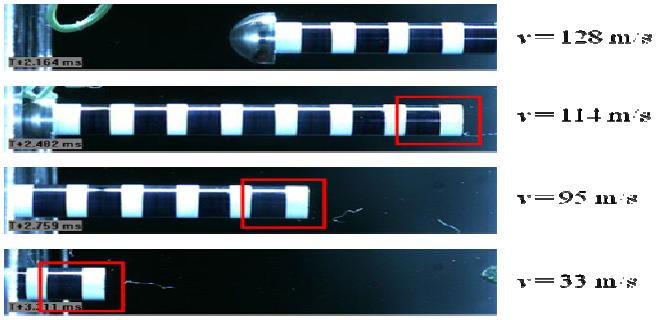

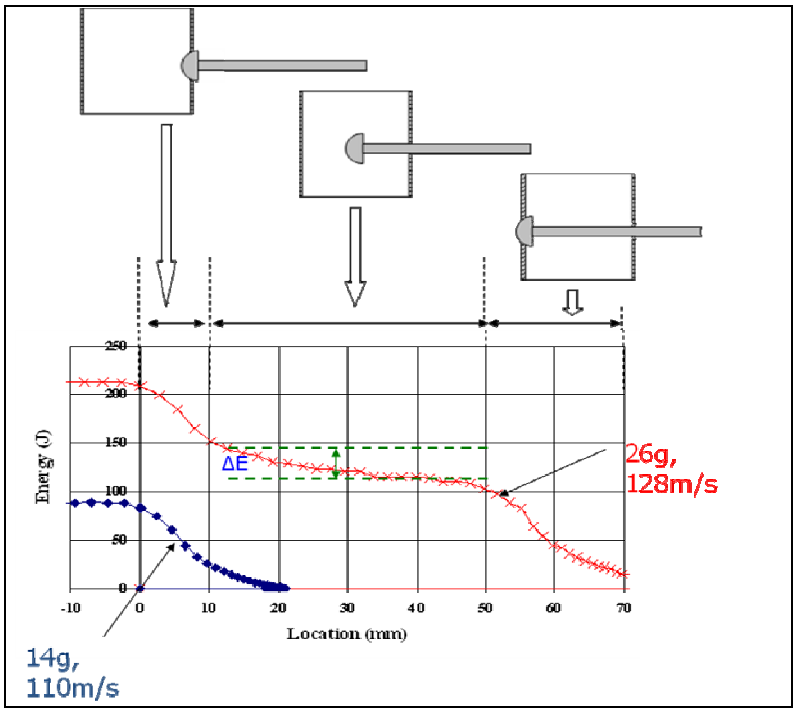

UPAT:

In the frame of CELPACT WP3, UPAT has performed low-velocity (LV) impact tests with hard hemispherical impactor on CM sandwich plates. In figure 1, the Instron Dynatup machine used for the tests is shown.

Fig 1 : The Instron Dynatup machine used for the low-velocity impact tests

This activity is a part of the testing campaign on cellular structures under different impact loading conditions. The results of UPAT tests will be used for the validation of developed numerical models for impact simulations as discussed in the WP4 report below. In the table 1 the testing conditions for tests performed are presented.

a/a	Specimen		Projected Impact Energy (J)	Obtained Impact Energy (J)	Obtained Velocity (m/s)	Drop Weight (kgr)
Test 1	**BCC-Ti64_CFRP1 (Fabric)**		200	198.3533	5.0169	15.3477
	Dimension	150x150x50				
	Core:	Ti64				
	Skin :	Carbon epoxy CFRP (Fabric)				
	Frame:	No				
Test 2	**BCC-Ti64_CFRP1 (Fabric)**		600	590.7886	6.7666	24.79188
	Dimension	140x140x51.5				
	Core:	Ti64				
	Skin :	Carbon epoxy CFRP (Fabric)				
	Frame:	No				
Test 3	**BCC-Ti64_CFRP1 (Fabric)**		800	680.3583	7.7466	26.46162
	Dimension	140x140x51.5				
	Core:	Ti64				

	Skin :	Carbon epoxy CFRP (Fabric)				
	Frame:	No				
a/a	Specimen		Projected Impact Energy (J)	Obtained Impact Energy (J)	Obtained Velocity (m/s)	Drop Weight (kgr)
Test 4	**BCC-Ti64_CFRP2 (UD)**		200	200.5837	4.9407	15.92604
	Dimension	150x150x53.2				
	Core:	Ti64				
	Skin :	Carbon epoxy CFRP (UD)				
	Frame:	No				
Test 5	**BCC-Ti64_CFRP2 (UD)**		800	782.751	7.8597	24.60624
	Dimension	150x150x53.2				
	Core:	Ti64				
	Skin :	Carbon epoxy CFRP (UD)				
	Frame:	No				

a/a	Specimen		Projected Impact Energy (J)	Obtained Impact Energy (J)	Obtained Velocity (m/s)	Drop Weight (kgr)
Test 6	**Wadley-type MO90501-A**		500	470.9982	7.6581	15.93
	Dimension	150x150x51.5 mm^3				
	Core:	Ti64				
	Skin :	Steel 304L				
	Frame:	yes				
Test 7	**Wadley-type MO90501-B**		900	911.24	8.607	24.44
	Dimension	150x150x51.5 mm^3				
	Core:	Ti64				
	Skin :	Steel 304L				
	Frame:	yes				

Table 1 : Tests performed during the period M25 to M37

DLR

HV impact tests on CM sandwich panels

ATECA supplied two types of advanced panels with Wadley type cores and aluminum honeycomb cores. The aim of the test programme was to compare impact response to soft body gelatine impacts of Wadley cors and conventional aluminium honeycomb cores. Four Wadley core sandwich plates (M090603-A, M090603-B, M090603-C and M090603-D) had core dimensions of 200x200x20 mm with ~0.8 mm aluminum skins (Al2024T3 rep. 1092). The second type of panel consisted of four aluminum honeycomb sandwich plates (M090601-A, M090601-B, M090601-C and M090601-D) with core

dimensions of 200x200x15 mm with ~0.8 mm aluminum skins (Al2024T3 rep. 1092). Both 200x200 mm panel types had an integrated aluminum frame (Al 7175 rep 1290) with 30 mm width for bolting to the support frame. Both types of panels were impacted with ca 80 g gelatine impactors at 90° impact angle and with 1 shot per plate. Table 1 summarises the test conditions.

Sample Designation	Number of shots	Projectile Shot angle	Mass [10^{-3} kg]	Velocity [m/s]	Impact Energie [J]
M090601 (Aluminum honeycomb)	3/3	Gelatine 90°	80.0 – 85.0	86.8 – 153.4	301.4 – 1000.0
M090603 (ATECA Wadley)	3/3	Gelatine 90°	82.0 – 83.0	75.8 – 158.5	238.4 – 1030.0

Table 1: Summary of impact tests with 80 g gelatine projectiles on CM panels

In impact test M090601-C on the honeycomb core panel the impact velocity was 153.4 m/s with impact energy of 1000 J. The impactor mass was 85 g. Here the impactor rebounded from the outer skin after forming an extensive dent of 15.5 mm depth at impact location. Buckling deformation of the inner surface was visible, which considerably extended up to the region where it was clamped to the support frame. An imprint of the support frame is visible at the outer and inner skin. Fig. 1a shows front and back side of the impacted sample and Fig. 1b the impact sequence. The impact sequence shows clearly that the gelatine flowed up to the clamps and covered the whole panel during impact. At the CT-scan in Fig. 1c skin-core debonding is visible at the impact location, with the core close to the outer skin crushed. The lower core regions below the impact zone are mainly undamaged.

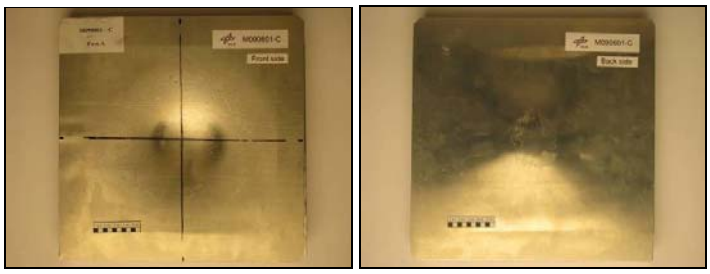

Figure 1a: Front and back side picture of impact area of test shot M090601-C

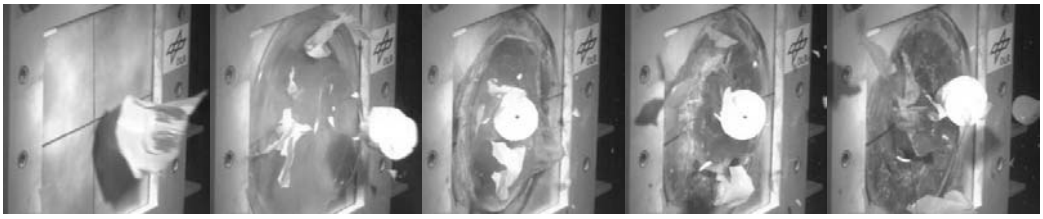

Figure 1b: Picture sequence taken from the high speed impact video (Picture interval: ~2.1 ms)

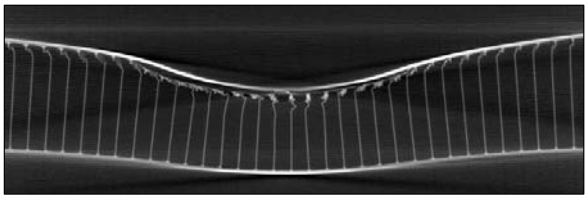

Figure 1c: Side and top CT-scans of impact location of test M090601-C

In impact test M090603-D the impact velocity was almost the same as the previous test being 158.5 m/s with impact energy of 1030.1 J. Behaviour was very similar to that of the honeycomb core. Here the impactor flowed over the outer skin after forming a dent of 17.2 mm depth at impact location, with extensive deformation of the inner surface as seen by the imprint of the support frame at the outer and inner skin. Fig. 2a shows front and back side of the impacted sample and Fig. 2b the impact sequence. TThe CT-scans in Fig. 2c show that the Wadley core is compacted right down at the impact location.

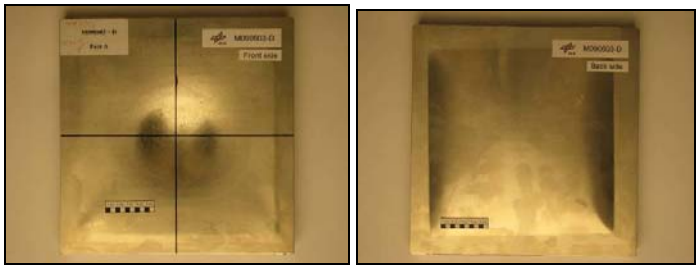

Figure 2a: Front and back side picture of impact area of test shot M090603-D

Figure 2b: Picture sequence taken from the high speed impact video (Picture interval: ~1.0 ms)

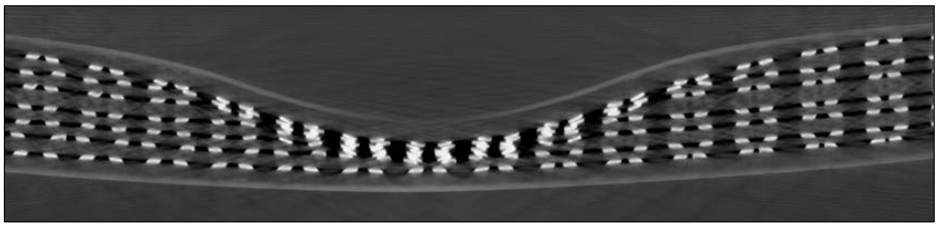

Figure 2c: Side and top CT-scans of impact location of test M090603-D

In these CM tests the impact energy was mainly absorbed by plastic deformation of the outer skin with very local core crushing at the impact position. The CT images in Figs 1c and 2c show clearly for this severe loading (impact energies of ca 1000 J) that the Wadley core crushes down further with the layers of struts beginning to bottom out, whilst the honeycomb core is stiffer and the cells crush down only near the contact skin. For honeycomb core there is visible debonding between core and skin. The maximum indentations on the impacted skins were 15 - 17 mm at 1000 J impact. Since the CT images show different types of core failure, but similar sandwich behaviour, impact response is strongly dependent on skin rather than core behaviour in CM sandwich structures.

WP 4: Technology Validation (WP Leader: CRC-G)

WP Leader	CRC-G
Participants	DLR, ULIV, UOXF, UPAT, RWTH, LMT, USTU, UBRN, A-D, EADS IW F, CRC-G

The objective of work package WP4 'technology validation' was

- to bring together the simulation results from WP2 with the experimental data from WP3 in a validation study and
- to assess the manufacturing methods, simulation tools and core performance of the cellular sandwich structures with respect to their potential application for future aircraft structures.

The following chapter gives an overview of the results generated by the different partners. It is divided into the investigations on 1. cellular metal (CM) core structures and 2. composite hybrid cores (CHC), and a further chapter 3. on the assessment of the core's performance for aircraft applications. Additional sub-chapters describe a) the validation of unit cell and impact models and assessment of simulation tools, b) optimisation studies and c) the assessment of manufacturing methods.

1. Cellular metal (CM) core structures:

Three different families of cellular metal core structures have been investigated numerically within the project CELPACT:

- SLM lattice structures (FE models by UPAT and ULIV)
- Metallic hollow sphere structures (FE models by UOXF and UBRN)
- 'Wadley'-type structures (FE models by UPAT and UBRN)

a) Validation of CM unit cell and impact models and assessment of simulation tools

UPAT:

Two types of open metallic cores covered with composite or aluminium skins have been tested by UPAT on a drop-tower testing facility. Sandwich panels with SLM cellular cores of 150 x 150 x 50 mm^3 dimensions, fabricated by Univ. Liverpool for low-velocity impact testing. The unit-cell of this structure is of BCC (Body Centred Cubic) type and has dimensions 2.5 x 2.5 x 2.5 mm^3. The struts have circular cross section of about 0,1mm radius. The constitutive material is sintered powder stainless steel 316L with elasticity modulus of 140 GPa and density of 8000 kg/m^3. The skins covering the cellular core are produced of carbon/epoxy $[0/90]_4$ fabric composite material.

The sandwich panels fabricated by ATECA consist of 'Wadley'-type metallic open cell core placed between two aluminium skins and have dimensions of 150 x 150 x 50 mm^3. The Wadley-type core is fabricated from 304L stainless-steel sheets (density of 8000 kg/m3 and elasticity modulus of 193 GPa) using the punching and folding technique for fabrication of layers, which are then stacked and brazed to form the cellular core. The representative unit-cell for this core type is an irregular BCC of dimensions 10.7 x 8.7 x 6.55 mm^3 and strut cross-section of 1.6 x 0.55 mm^2. The panels were subjected to low velocity impact in a drop tower facility, with impact velocities ranging from 1m/s to 10 m/s and impact energies ranging from 20 J to 1000 J. Numerical simulation methods for low-velocity impact of sandwich panels were developed, focusing in a successful simulation of the response of the above described panels under drop-mass loading.

The sandwich panel skins and core structure were modelled by UPAT using the PAM-CRASH code. The core models comprise beam or shell elements with isotropic elastic-plastic material law. The carbon/epoxy skins are modelled by a multilayer shell material model developed in a previous project and verified against experimental data. Self-impacting contact interfaces are defined in the core to simulate the core compaction during impact. Results comparison between experimental and FE models for different values of impact velocity and impact energy has been performed, indicating a satisfactory accuracy. The FE model for sandwich panels with SLM cellular cores and 'Wadley'-type metallic open cell core in Pam-CRASH code is shown in Fig 4.1.

It was concluded from the investigations that application of the explicit dynamic FE code PAM-CRASH FE can lead to successful simulations of low-velocity impact on sandwich cellular open lattice panels.

Development of a quarter symmetry models of the tested specimens, by applying appropriate boundary and loading conditions can facilitate the simulation effort, otherwise huge models (i.e. of the order of MDOFs for small unit-cell sizes) should be solved. The spherical supports can be modelled as infinite mass rigid walls, while an impactor model as a rigid body with one degree of freedom in the direction of impact is sufficient. Node-surface contact definition is required between the impactor and the sandwich panel core-skin system in the region of impact.

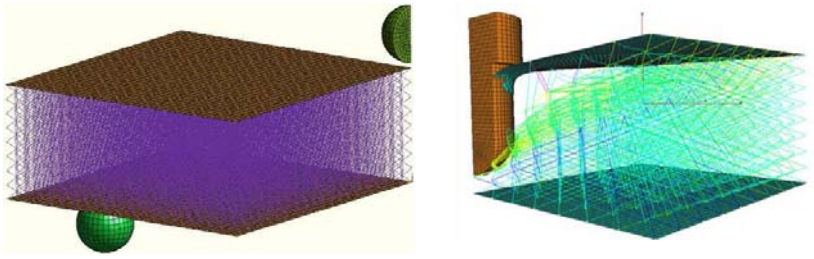

a) SLM cellular cores b) 'Wadley'-type metallic open cell core

Fig. 4.1: FE model of sandwich panel with SLM core (a) and 'Wadley'-type metallic open cell core (b)

For the SLM core sandwich panels, the core is well-bonded to the composite skin and no interfacial is observed in the experiments. Hence, the bond between the core and the skin in the numerical model is assumed to be perfect, which means that no interface failure needs to be included. The perfect bond represents the actual experimental response of the SLM-type panel, which is also reflected in the impact simulations.

For the Wadley-type core sandwich panels, a tied interface definition with tensile and shear rupture criteria is applied between the skin and the Wadley-type core. This was found necessary in order to model the experimentally observed failures of brazed bonds between the core and the skins. The rupture model associated to this interface should be given special attention and should be supported by appropriate experimental data. The introduction of the tied interface represents well the actual experimental response, which is also reflected in the simulation results for the Wadley-type structure.

In general, the numerical simulation tools developed for the low-velocity impact simulations on the metallic open-core sandwich panels are capable to provide good correlation with experimental data. It is concluded that the modelling features investigated in the numerical models for the BCC and the Wadley-type sandwich panels can be successfully used in the structural analysis and partly for the structural design of any type of open lattice cellular core sandwich panels under impact conditions. Application of homogenization and multi-scale approaches (not investigated so far for these types of structures) is expected to increase computing efficiency.

ULIV:

The ULIV sandwich panels were placed on four hemispherical supports and subjected to drop weight impact from a 10 mm diameter hemisphere attached to a drop weight machine, see Fig. 4.2. Force versus displacement data was obtained using a laser Doppler velocimeter and a high speed camera. Also, post impact test damage was quantitatively assessed. Dent depth was measured using a clock gauge. A numerical model of the panel was developed with beam elements for the micro struts and standard composite models for the carbon epoxy skin. The explicit finite element code, LS-DYNA was used (Fig. 4.3). Conclusions are that the FE model is robust and models the basic physics (Fig. 4.4).

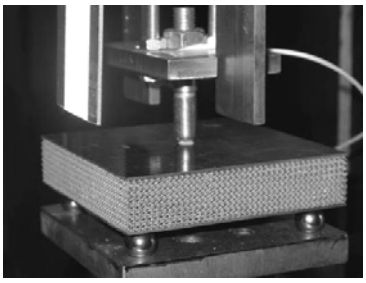

Fig. 4.2: Panel supported at four corners

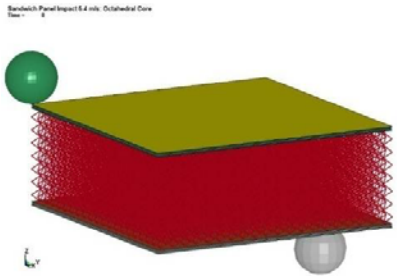

Fig. 4.3: LS-DYNA model

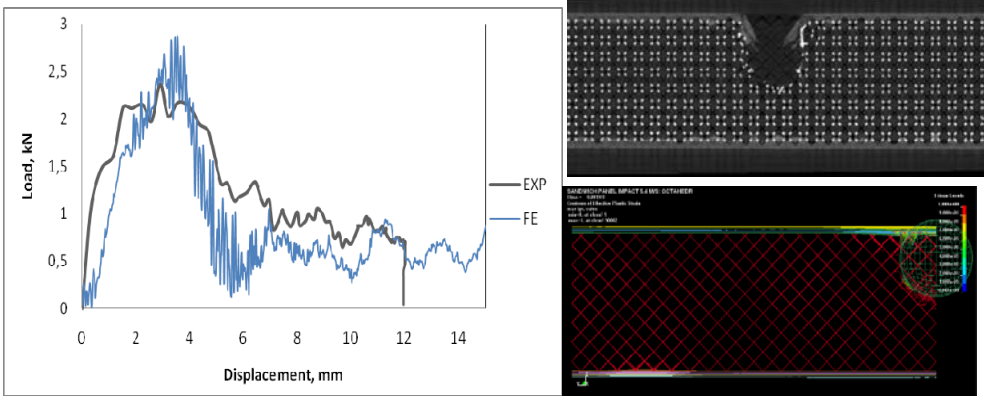

Fig. 4.4: Left: Ti6Al4V - comparison of FE and experiment in four-point supported micro-lattice core sandwich panel impact test. Right: Comparison of cross section of CT scan and Test Ti6Al4V #6

UBRN:

At the beginning of the project the response of the micro-structure of the hollow sphere core under compression loading was studied by UBRN. During this early stage different FE models and approaches were used. Those were a single sphere, regular structure and irregular structure made of omission some spheres from the regular structure. The hollow spheres are made of nickel, and for simulations an LS-DYNA elastic-plastic material model was used. After testing the modelling approaches was changed, because previous results were overestimated. Real structures were very random, and ways or tools how to include maximum or all of the imperfections described below were needed found. The one possible way is to simulate real manufacturing process. The global imperfection can be included using a randomly generated spheres with random diameter and random thickness. Those spheres are arranged in the grid, and are moved and rotated about their all axes (see Fig. 4.5). Then a free drop simulation into rigid cylinder for generation of much randomized structures may be used. Included was self-contact and contact between the spheres with friction. After a numbers of simulation steps we can get a nest of spheres which can be used for estimation of compression behaviour. There was shown that the compression behaviour of FE models of those randomly generated structure is much realistic and better that the irregular structure.

There must be say that the correlation between simulations and experiments is good only for the early stage of loading, let's say up to 50-60% of strain. This is due to compaction and densification of the buckled and crushed spheres in reality. In the simulation the compaction or densification of the hollow spheres core cannot be modelled, because segments of the spheres are eroded, while in real assemblies still exists. Another problem the bonding connection of single spheres is. In real structures the resin contributing to the densification. In the FE models there was solved using contact algorithm with tiebreak which is only numerical tool, so any material of the resin occupying the space between spheres was not modelled.

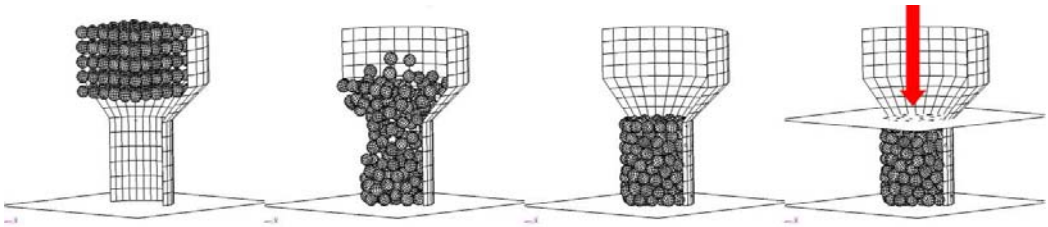

Fig. 4.5: Generation of the randomized hollow sphere structure and final loading

The imperfections which are present in the real structures can be categorized as a global (random distributions of spheres in space, different median diameter, median thickness of wall, size of the bonding region, mechanical properties of the resin) and local imperfections (irregular sphere geometry, thickness distribution on one sphere, distribution of the resin in the middle-sphere space, differences in material characteristic). After the assembling process a definition of the bonding follows and can be done using some tied or tiebreak contact. In our cases a LS-DYNA tiebreak contact definitions was used. This type of contact includes friction conditions as well as a tensile and shear failure of the resin. A thickness of the region which is considered as glued can be also defined. Once again all of the parameters defined in the tiebreak contact may not be constant over whole structure but can vary. Together that allowed us to define for each sphere in the structure an individual bonding connection with each other sphere. This may be much exacting and time consuming work, but it was reduced by constant failure stresses and the thickness of the resin over the structure. The some calibrations to the experiment results for determination of those characteristics were needed. During our work a properties introduced by the producers of the resin were used. Thickness of the bonded region was estimated as equal to the wall thickness of the spheres. The local imperfections can be modelled using different diameter of particular spheres as well as the thickness. An individual sphere can have diameter randomly selected from the defined range. If the nodes of those ideal globe are moved in all three axes (node shaking) again randomly from the selected range there is gotten an irregular globe. Next the wall thickness not have to be constant over the sphere, can be varied.

Validation of simulation was done after testing of single hollow-spheres, and the small assemblies on different loading velocity. The results of single hollow-spheres were used for calibration of material properties, or material parameters identification. Glued spheres in the randomized structures were connected using tiebreak contact with tension and shear strength limits. Thicknesses of glued regions were considered and all contact parameters were identified using calibration to the test results.

During the second stage of the project a simulations of sandwich panel with core made of the hollow spheres and the Wadley structures under impact conditions were undertaken. The numerical simulations of the impacted aircraft structures will be done with some type of homogenized finite element models during design process. It may be supposed that the sandwich's core will be modelled by a honeycomb constitutive model coupled by a failure criterion on maximum volumetric strains. The skin was modelled using simple shell elements and the surface-to-surface tiebreak contact of the foam core and the skin was been generally used. This allows to including an effect of bonding connection (and of course failure) between skins and core. All numerical models used for simulations therefore will consist of three parts, the projectile, skins and the core. Rigid and soft projectiles was be used during the studying of impact cases. Based on the experience with the hollow sphere structures under static compression loading, the detailed and large FE models of the sandwich were created too. Computation time of these panels under high velocity impact conditions was about ten hour whereas using homogenised model there was needed about one hour. Detailed model get us good information's how the core is deformed during the impact. Sandwich face sheets of both panels (hollow spheres and Wadley core) were produced of aluminium 2024 T3, so an elastic-plastic material model with failure based on a plastic strain was used. Two types of material model of the skins were tested. One was a continuum damage mechanics model LS-DYNA MAT_104 whose parameters were calibrated up to results of experimental tension test and the second one was MAT_024 into which a stress-strain response from tension test was supplied. Material model of the core used in the homogenized FE model was set to MAT_HONEYCOMB. The material data necessary for honeycomb material model can be supplied as results from the real compression test of the core foam or from the fine FE simulations.

During the project the high velocity impact (HVI) using soft projectile which can simulate a bird-strike impact were focused on (Fig. 4.6). Originally this work had had to simulate a sandwich panel with the

ATECA-WADLEY core, but the developed of FE models (with homogenised core) was useful for other types of cores. Therefore was planned to use common FE models for comparison of different cores developed during the project. That means only changes in the compression (stress-strain) curves of the core. During the simulations, a projectile of cylindrical shape with hemispherical ends was used. There are number of ways to solve soft impact to some panel. There include classical Lagrange-Lagrange simulation (L-L), Smooth Particle Hydrodynamics (SPH) and Arbitrary-Lagrangian-Euler (ALE). Using ALE the simulations can furthermore be done using single Eulerian material or multi-material fluids. For comparing of different ways an L-L, SPH and ALEMMG were undertaken (the ALEMMG was solved using both LS-DYNA and MSC.Dytran packages). There was shown that ALE and SPH giving much better results than classical Lagrange, mainly at higher velocity of projectile. SPH gives better results if more particles are used so finally we use hundred thousandth particles and we get differences from ALE about 1% up to speed of 250 m/s.

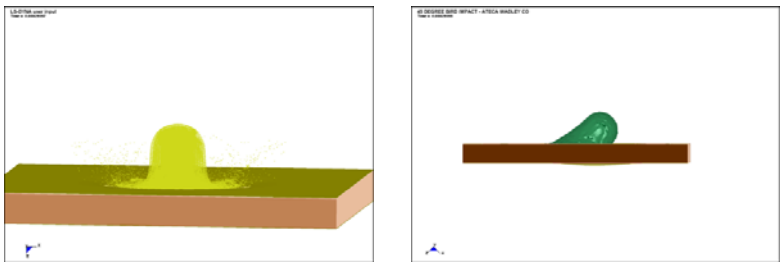

Fig. 4.6: a) FE model of SPH projectile b) FE model of projectile using ALE approach

For experiment setup purpose a simple case study, which maps the influence of impact velocity on the damage of sandwich panel, was done. The aim of this study was to find two levels of velocities, which will destroy the sandwich panel by different way. The simulations started with an impact velocity of 250 m/s and that was changed based on results by the method of bisection. Of course the transfer velocity can be found exactly. The transfer velocity denotes a critical impact velocity on which the damage level changes from full penetration to no penetration or partial penetration.

b) Optimisation study of CM cores

ULIV:

Within constraints of manufacture (SS316L, BCC, 0.2 mm strut size) what is optimal block compression specific stiffness and strength? Note manufacturing parameters are all important. The suggested nomenclature is:

Architecture/Parent Material/Laser Power (W)/Exposure Time (µs)/Strut Diameter (µm)/ Cell Size (mm)/Unit Cell

which in this case would be:

BCC/SS316L/140/500/200/2.5/Cubic.

Mechanical properties can also be improved using different parent materials, e.g. Ti 6 4 versus SS 316L… E: x 0.55, Density: x 0.56, Strength; x 4.3. From experimental results (Fig. 4.7) we assume a specific deformation mode (Fig. 4.8).

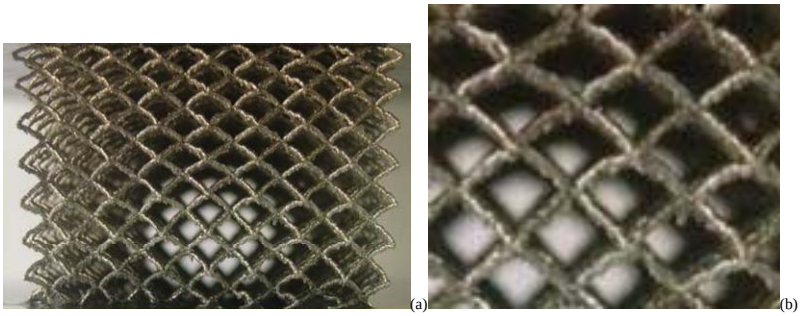

(a) (b)

16% compression, cell size 2.5mm, unconstrained

Fig. 4.7: Compression of stainless steel BCC block

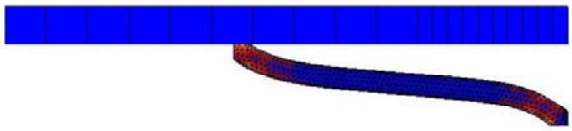

Fig. 4.8: Assumed micro strut deformation mode

Taking into account the deformation mode, an analytic model was developed for the elastic and elasto-plastic behaviour of micro struts. The predicted variation of block specific stiffness and strength is shown in Fig. 4.9, where the cell size (L) is the variable and d is the diameter of the strut. Conclusions from parametric modelling:

- Parametric modelling is complex given multiple failure modes
- Failure modes dependent on cell size, parent material, and mode of loading
- Need to include shear effects
- Need to include effect of block constraint
- Analysis needs to be extended to block shear, multi axial loading

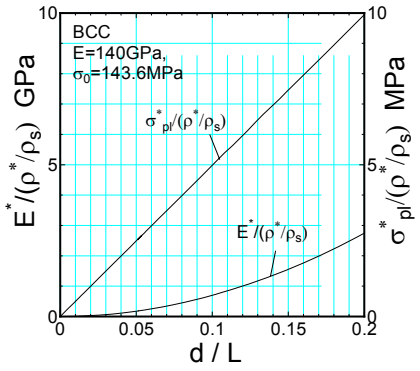

Fig. 4.9: Results from parametric model.

UBRN:

It is not surprising that the optimisation of some component in the aeronautical industry is the most important part of the design process. The critical point is the good definition of the optimisation, so definition of the variables which have been found and their range, definition of the response, constraint and the objective which is wanted to minimize. Those data need to be defined exactly because optimal structure can be different for different condition, for example one goal is to found a panel for impact in normal direction, whereas the another goal needs found an optimum for impact under angle of 45°. First will search optimal structure with the objective of minimal deflection and second use as the objective a condition not allowed plastic deformation and so on. Always we get different structure.

During the final part of the project the optimisation task was conducted by UBRN during which optimal sandwich panel with dimension about 800 x 800 mm was founded. This panel was supported at two opposite edges and was impacted using a spherical projectile with mass of 1.8 kg in the normal direction at velocity 100 m/s. The objective function the panel mass was minimised for constraints of minimal deflection of the inner skin and the maximum allowable plastic strain in the middle part of the inner skin, which was set to very low value. There were a large number of design variables, totally forty-three, nine of those were depended and thirteen was constant, so the task was very complex. Those were for example thickness and material properties of the skins, tension and shear strength of the bonding between the skin and the core, density of the core and so on. During the first part of the project we found that the compression characteristics of the hollow sphere core depends only on the density of the core or differently told that the specific stress-strain response of the core is constant (or nearly) for the same base material. Density of the hollow sphere core is depended on the diameter to thickness of the sphere's wall ratio. In optimisation task the stress-strain responses for different density were recalculated from the measurement one in the density ratio. A LS-OPT optimisation package which is supplied with the LS-DYNA was used. In this solver a large number of optimisation methods were included. Results comparison of two optimisation methods were done, the response surface methodology (RSM) and neural network combined with genetic algorithm, because the optimisation process always crash after a few optimisation loops and the task to not converged. Thus the RSM appears to be better even if a large number of panels must be solved.

Different optimal panels were founded for two different optimization constraints. In the first case (minimum deflection of the inner skin) the optimum configuration of panel was thick outer skin, thin inner skin and core with lower limit of the density (core with lowest compression curve). This means a panel without the core application, because all projectile's energy is absorbed by the outer thick skin which deflection is lower that thickness of the panel. In the second case (maximum allowable plastic strain of middle inner skin about 0.1%) the optimal panel had thinner skins than in the first case and the core had a real density. Can be declared that about fifty percent of the energy was absorbed by the core, inner skin was deformed mainly elastically so no permanently deformation cannot be viewed. If little modification and increase the specific stress-strain response of the core two times is made (suppose better core) and run the optimisation process once more other panel is received. Thickness of the inner skin stay approximately same, thickness of the outer skin was two times lower and density of the improved core is approximately same, so two times strength of the core was used. This means that more energy was absorbed by the core. Finally it can be declared that if the core with two times higher specific strength than about 18% of the mass can be saved. This cannot be say generally, but only for our optimisation task. Different results will be probably taken for different impact cases, mainly for the different angle of impact.

c) Assessment of CM manufacturing methods

ULIV:

Details of manufacture of SLM microstructures in SS 316L and Ti 6 4 have been given elsewhere (see Mines R, Tsopanos S, CELPACT Deliverable D 123, February 2009). Essentially, various micro lattice configurations can be realised, covering body centred cubic (bcc) (see Fig. 4.10), face centred cubic and other geometries. It was decided to focus on bcc here. For the purposes of CELPACT, blocks of dimension 50 mm cubed, 100 x 100 x 20 mm³ (small panel) and 150 x 150 x 50 mm³ (large panel) were made from both stainless steel 316L and Ti 6 4 powder.

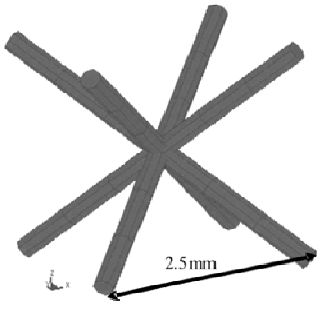

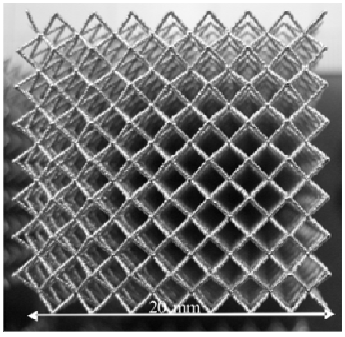

Fig. 4.10: Geometry of the BCC unit-cell and an example of a micro-lattice block.

Small panel and large panel blocks were then combined with carbon epoxy skins on a hot press. Pressure was applied at approximately 1 bar, and a temperature of 120°C for approximately 2 hours. Careful control of the pressure was required to prevent yielding of the lattice core but was still high enough to bond the prepregs together. Fig. 4.11 gives detail of the skin core bond line, it can be seen that there is good bonding between core and skin.

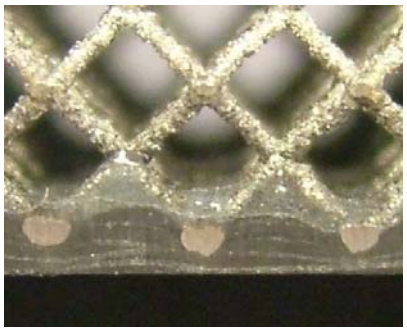

Fig. 4.11: Core skin bond detail.

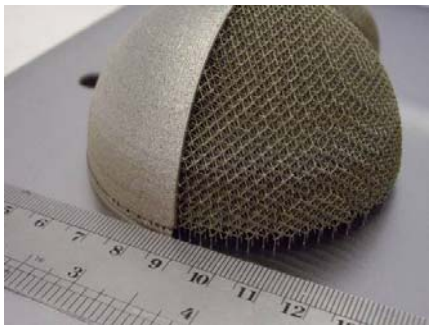

Fig. 4.12: Example of the 3D complexity that can be achieved using the SLM process.

The constraints of the manufacturing procedure are as follows. The process of SLM is time consuming – it takes about 5 hours to manufacture the small panel, but a number of cores can be made at the same time and the whole process is automated. The current build envelope is 200 x 200 x 250 mm³, but a larger machine (500 mm cubed build envelope) is being built. It should be noted that 3D structures with integral metallic skins (see Fig. 4.12) can be built. It can therefore be concluded that currently the process is most applicable to small, high value added, components. For example, the process has applicability to aero engine components. However, in the longer term, the process should become faster, more cost effective with larger panels being able to be produced. One possible item for future work is the welding together of lattice blocks to create larger structures. It should also be noted that micro lattice configurations can be adjusted to optimise core properties (see: Mines R, Tsopanos S, CELPACT Deliverable D 413, March 2009).

2. Composite hybrid core (CHC) structures:

Two different families of composite foldcore structures have been investigated numerically within the project CELPACT:

- 'Stuttgart'-type foldcores made from aramid paper (FE models by DLR, LMT and RWTH)
- 'Kazan'-type foldcores made from CFRP or AFRP (FE models by CRC-G)

a) Validation of CHC unit cell and impact models and assessment of simulation tools

DLR:

The first DLR foldcore micromodel used shell elements with an isotropic elastic-plastic material law and numerical investigations were carried out to assess element type, mesh size, loading rate and mesh distortions. The model showed the feasibility of simulating the microcell buckling, element folding and compaction in compression. As test data became available on the aramid paper properties and from unit cell tests it was decided that this model was oversimplified, since it did not contain the brittle failure behaviour seen in tension tests of aramid paper. Microscopy studies by LMT indicated that the foldcore paper consisted of aramid paper coated on each face by a phenolic resin layer, which led to an improved 4-ply shell model for the resin-impregnated aramid paper, consisting of a bi-phase composite model (with different tensile and compression properties) for the aramid paper ply, with an elastic-plastic model for the outer resin plies.

Final validation was achieved by simulating DLR/USTU compression tests and RWTH shear tests on foldcore SW plates. Fig. 4.13 shows results for the TL shear direction for foldcore type 21 with 5 x 19 unit cells, which corresponds to the RWTH shear test. In this model fracture of the aramid paper at

high strains is now observed and the global shear response is also well represented and load-deflection curves agree well with test data.

The foldcore micromodel described above was developed further by addition of laminated composite skins to the basic core micromodel and used for validation studies under low and high velocity impact. The setup of the FE model is based on a 250 x 250 mm² sandwich panel, with 20 mm thick foldcore impacted at the centre by a 50 mm diameter spherical impactor, which represents a DLR low velocity impact drop test with spherical impactor head. For high velocity impacts (HVI) discussed the projectiles selected are steel cubes and bars. The CFRP sandwich skins are modelled as single layered composite shell elements where delamination failures were not included, or by 4 stacked shells with 3 cohesive interfaces where delamination failures were important.

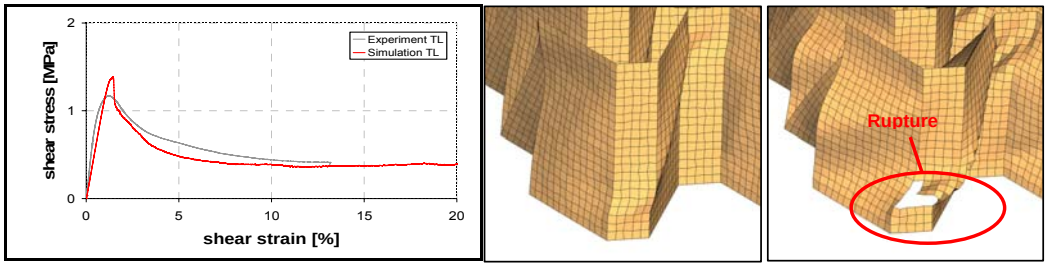

Fig. 4.13: Simulation of RWTH TL shear test with improved 3-layer shell foldcore model

In the drop tower tests three impact velocities with impact energy levels ranging from 70.8 J to 456 J were selected, to provide information on different failure modes, ranging from rebound of the impactor at the upper skin to penetration of the core and high core energy absorption. Typical results in Figs. 4.14 – 4.15 show simulation of the intermediate velocity test LV2 (M = 25 kg, V = 3.55 m/s, E = 157.5 J), where the impactor rebounded after penetrating the skin, with impact energy absorbed by the core. In this simulation delamination damage is included in the skins, and is also visible in the CT images. The model gives reasonably predictions of failure mode and load pulses measured in test. The FE models often overestimate observed damage, making them conservative for design analysis.

For validation of the impact models under high velocity impact (HVI) loads, 5 HVI tests with the DLR gas gun representing characteristic sandwich damage conditions were modelled. The cases considered represent runway debris impacts from steel cubes and bars. The three steel cube impact scenarios show impactor rebounding (HV1-2), outer skin penetration and core crushing (HV1-1) as well as penetration of outer skin and core with impactor stopped by the inner skin (HV1-4). Typical simulation results are shown in Fig. 4.16 for the steel cube test HV1-1. The FE simulation predicts the skin penetration and embedding of the cube in the foldcore in good agreement with CT test results of the damage.

The main assessment of the core “microscale” models is that they provide an accurate and detailed reproduction of local deformation and failure in the foldcore which arises in local indentation, microbuckling and impact penetration. Due to the implemented small element size and large number of elements the model has high computational costs. This limits the efficiency of the model to reproduce large-scale load cases such as crash modelling of whole structures.

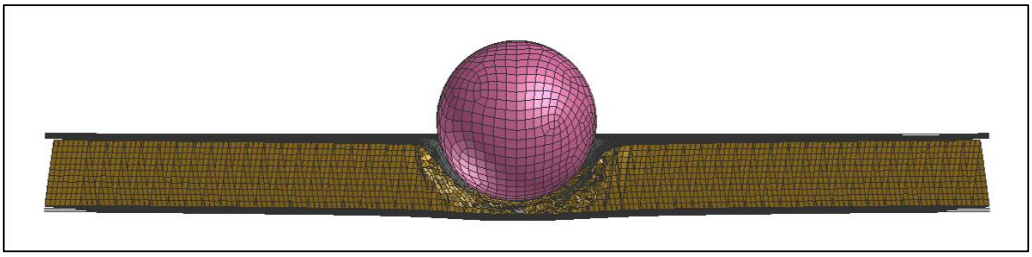

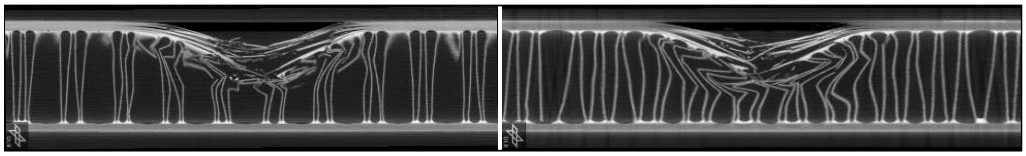

Fig. 4.14: Cross section of FC-LV2 specimen at impactor rebound and cross-sectional CT-scans of FC-LV2 specimen in foldcore L- and W-direction

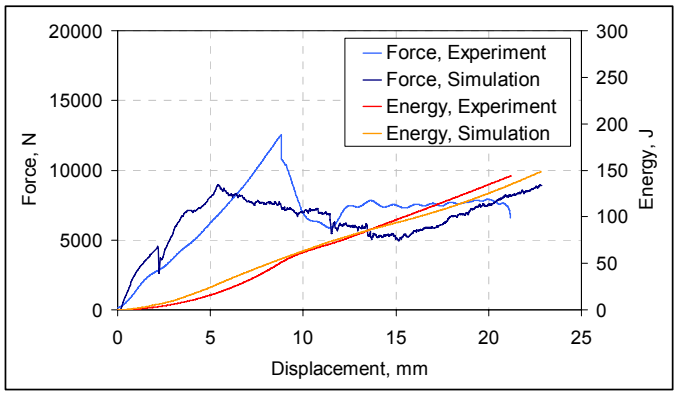

Fig. 4.15: Load-deflection curve and absorbed energy of simulation and experiment

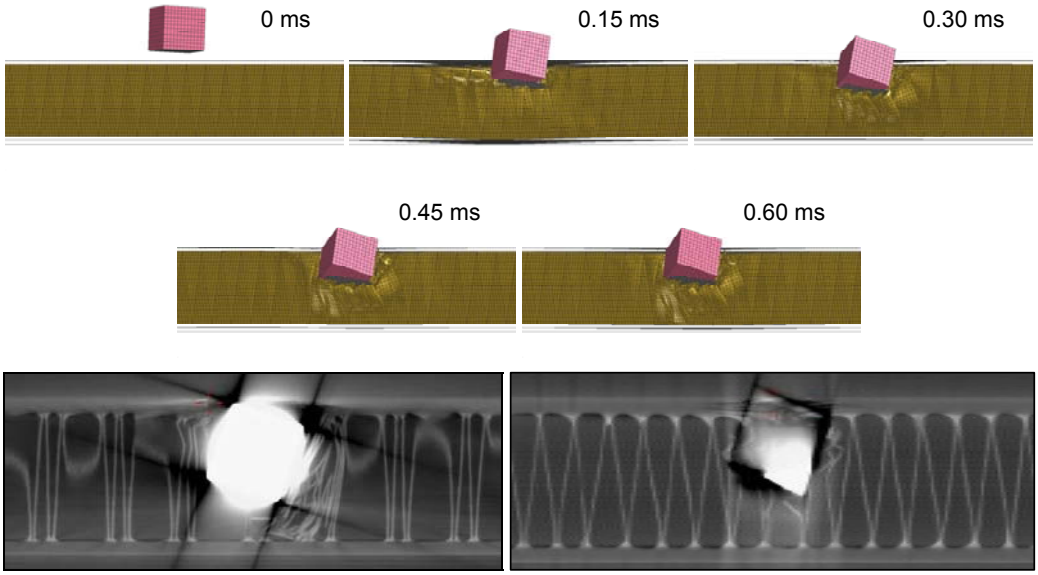

Figure 4.16: Image sequence of HV1-1 (81.8 m/s, 45.2J), with CT-scan of damage in foldcore

A homogenisation approach was developed to reduce the computation time of FEM models by simplifying elemental and mesh organisation. DLR investigated an approach where the detailed 'microscale' foldcore model is substituted with a homogenised model with larger solid elements. The fundamental idea is to input the global foldcore behaviour into the constitutive law of the 'homogenised'-type elements. Particularly the softening behaviour of the foldcore at collapse initiation is difficult to reproduce. However, the homogenized models are suitable for simulating foldcore structures away from the damage region, where behaviour is dominated by elastic waves in impact, rather than material failures.

For larger structures multimodel coupling (MMC) was investigated where the 'local' micromodels and

‘global’ homogenized models are linked by interfaces in the model across which nodal loads and forces are transmitted. By running the model parts in parallel processors and exchanging data at the interfaces, it is possible to reduce CPU time in explicit code simulations. In summary the MMC approach performed satisfactorily. For impact test simulations on small sandwich plates the size of a potential simplified model region is limited so that the benefits of a sub-cycling approach are often negligible. However if the impact load scenario were on a large fuselage panel with frames, then the MMC method would demonstrate its efficiency.

DLR final activities are the ‘Design guides’ on sandwich structures, which aim to summarise the simulation methods developed in CELPACT in a simplified form as a recommendation to aircraft engineers for design of such structures.

LMT:

LMT has focused his effort on validating the mechanical understanding and modelling of the CHC core (pattern 31 from USTU) behaviour under an out-of-plane compression load. For that ABAQUS Standard computations have been used. The numerical model is considered validated if its results are not to far from the experimental results, with respects to criteria to be defined. These criteria are defined regarding to the final objective of the model that could be:

1. A good description of the experimental data (global shape of a response curve, local criteria…)
2. A good prediction, i.e. a good description of the experimental data and of the degradation mechanisms.

In the case of shape optimization, the second objective has to be reached.

The next question concerns the exploitation of a set of experimental data both for identification and validation. A set of degradation mechanisms and a scenario of degradation are identified on a part of the experimental data set. The validation will focus on another part of the experimental data set (complementary to the one used for identification) but respecting the set of degradation mechanisms previously defined. Thus, a model can be identified on a part of experimental data and validated on another part.

First, a nonlinear material model has been developed and implemented in an ABAQUS UMAT subroutine. This model is able to represent the tensile and bending behaviour of a sheet of aramid paper. It has been identified using different kinds of data, available at different scales. The paper laminated structure relies on microscopy observations but the thickness of the different layers of the paper is only partially identified at this scale. In fact, relevant information is also available at the upper scale. Thus, the paper structure and elastic properties come from morphology analysis, from quasi-static tensile tests on paper sheets and from vibrating bending tests on paper sheets. Concerning the non-linear behaviour of the paper, in bending, a damage evolution law is identified from a dedicated test. This test setup is very close to the Shanley’s column. During this test, the damage evolution law is very reproducible while the elastic bending stiffness is less reproducible due to the thickness scattering of the sheets of aramid paper. In conclusion, very different data have been used in order to build, identify and validate a mechanical modelling of the behaviour of the paper. The validity range of this model is known and each piece of information that has been used has been carefully chosen and represents the most relevant information at the most relevant scale.

Secondly, geometrical defects coming from folding issues have been modelled. Concerning the pattern 31, the density of the core is quite high and folding becomes more difficult. In the case of the out-of-plane compression of a folded core, the initial geometry of the core is of major importance. It has been chosen to model these defects by taking into account the folding process. For that, a folding pattern is built on a sheet of paper. This folding pattern does not respect the ideal embossing geometry but slightly differs (in a range of physically observed defects). This strategy is illustrated on the following Fig. 4.17, where one node of the ideal pattern (on the left) is moved (on the right). The Folding process is then simulated using ABAQUS standard for three complete rows of cells (3x5 cells).

It leads to a folded geometry that is very similar to the real one. Generated defects are of the same magnitude as observed ones. In fact, these defects mainly rely on the fact that folded edges do not remain straight after folding. This tremendously decreases the stiffness of the folded core structure.

With these two ingredients, the out-of-plane compression behaviour of a folded core can be represented up to the global instability load. After the global instability load, the modelling of the material mechanical behaviour is no more relevant. The following figure, presenting the evolution of

the force versus displacement, shows a good agreement between experimental data and numerical results (Fig. 4.18, denoted “Simulation, damage, defect”). It has to be noticed that experimental defects play a major role during ¾ of the global instability load while the mechanical behaviour only plays a role around this instability load.

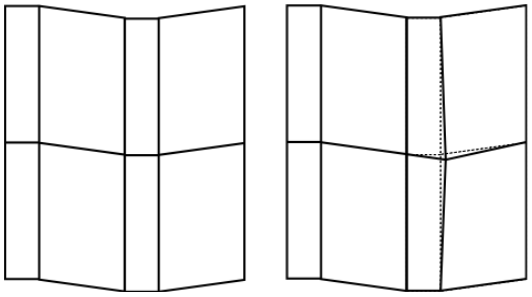

Fig. 4.17: Distortion of folding edge node

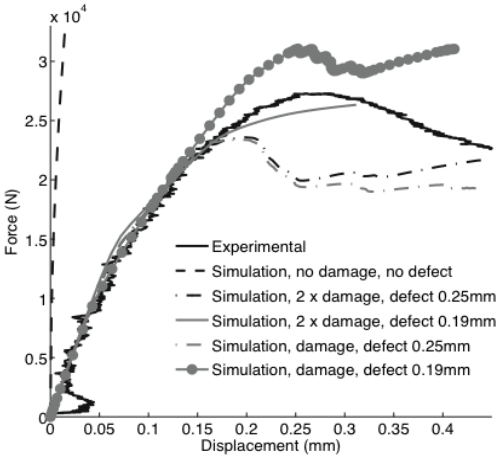

Fig. 4.18: Force-displacement-curves: experiment vs. simulation

RWTH:

A procedure to perform subsequent impact and residual strength simulations was developed by RWTH. During this procedure first an impact simulation with an explicit finite element code (LS-DYNA) is performed. After this simulation the computed residual deformations are transported into a new model. Additionally the damages in the skin due to impact are analysed and used to degrade the material properties in the associated elements of the new model. Then this new model is used to perform static non-linear residual strength computations with ABAQUS (Fig. 4.19).

To validate this numerical procedure subsequent low velocity impact tests and 4-point bending tests were performed with sandwich panels with USTU-type No.30 cores. During this experimental campaign sandwich panels were exposed to low velocity impacts with energies between 5 and 40 Joule (Fig. 4.20). A hard ball-shaped body with a mass of 1.56 kg was used as an impactor. After the impacts 4-point bending tests were performed with the impacted and non impacted samples (see Figure 4.21). During this test the samples were oriented in both main directions of the foldcore (L- and W-direction). All the experiments are repeated numerically using the described procedure. In detail the measured and simulated impact forces and the impactor position were compared. For the 4-point bending set-up the bending strength of the pre-damaged panels and the collapse mode were used for comparison. The comparison between the simulations and the experimental results is very promising. The predicted forces and indentions measured during an impact events are in very good agreement with the results predicted by the impact simulations (Fig. 4.22). In case of the 4-point bending the agreement is also good for most cases (Fig. 4.23).

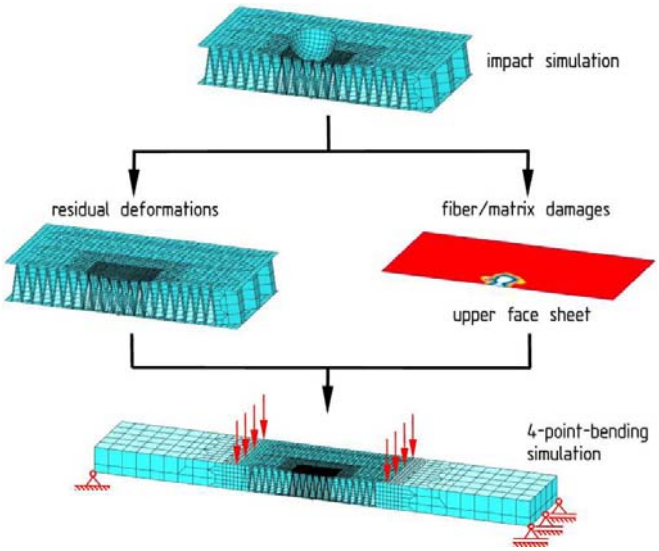

Fig. 4.19: The scheme for the 4-point-bending residual strength simulations

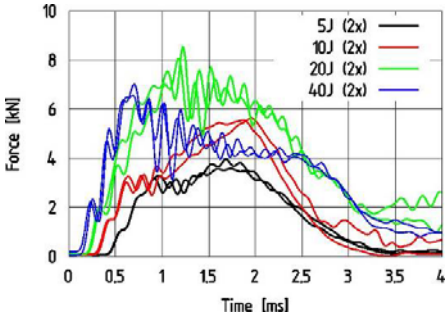

Fig. 4.20: Contact forces (Impact)

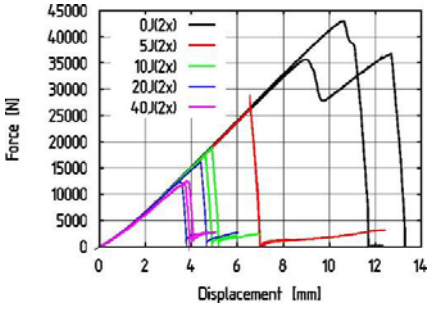

Fig. 4.21: Force-displacement diagram (4-point bending tests, L-direction)

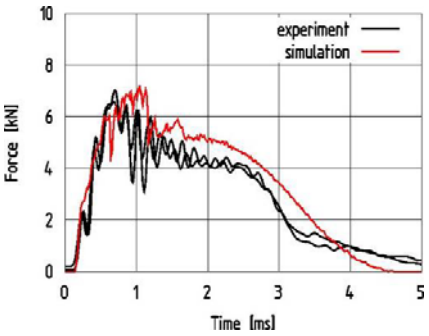

Fig. 4.22: Contact forces (Impact, 40 Joule)

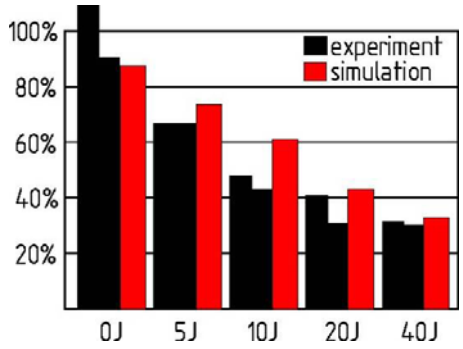

Fig. 4.23: Drop in bending strength due to impact damage (4-point bending tests, L-direction)

The results of the performed simulations provide useful observations of the investigated sandwich panels. The investigated approach has the potential to be a valuable tool in the design process of new core and skin configurations. The necessary experimental program could be reduced and simplified. Also the influence of local structure of the core regarding the impact position (for example the

differences between an impact above a folding edge of the core and an impact above a gap in the fold core) can be investigated easily.

CRC-G:

In the CELPACT project CRC-G developed unit cell model of discontinuously produced CFRP foldcores of the 'Kazan'-type in LS-DYNA based on the composite material model MAT54. The comparison of the FE model and basic compression and shear test data allows for a critical judgement of the abilities of the finite element model with respect to a correlation of mechanical properties and failure mode representation.

In the experimental flatwise compression tests the structural behaviour of the CFRP foldcore was mainly characterised by a cell wall buckling followed by a material failure in the middle of the cell walls and a crushing of the cell walls when they come into contact with the opposite skin surface (Fig. 4.24). This behaviour could be represented in the numerical simulation with a good correlation, although the element erosion led to some discrepancies at high deformations.

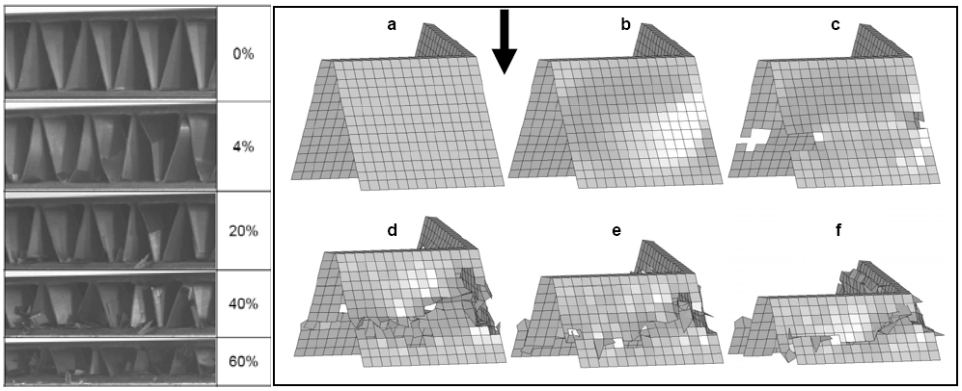

Fig. 4.24: Cell wall failure in experiment and simulation

Further validation studies were conducted with respect to the impact simulations on 2nd phase foldcore sandwich structures with LS-DYNA. For the textile-reinforced composite cell walls as well as the Kevlar® middle layer of the dual-core sandwich structure the continuum damage mechanics (CDM)-based material model Mat_Laminated_Composite_Fabric (MAT58) was used in combination with reduced-integrated shell elements. Identical material behaviour in 1- and 2-direction of the lamina can be defined, which is important for fabrics, where no specific fibre and matrix direction exists. Element erosion after failure is controlled by the definition of maximum effective strain values. The UD laminate of the skins was modelled with reduced-integrated shell elements and Mat_Enhanced_Composite_Damage (MAT54). In contrast to the CDM model, this constitutive law assumes linear elastic behaviour until the failure criteria of Chang and Chang are met. Then the stress level is kept constant until defined failure strains are reached. Element erosion is again controlled by failure strain values. Since shell elements are unable to cover delamination failure, a stacked shell approach was applied for the upper skin. In this approach, two shell elements, each representing a sublaminate, are connected by a delamination contact interface, which allows for interlaminar failure and the separation of the sublaminates. A simple tiebreak contact interface with failure option was also used for the connection of skin and core elements in order to cover skin/core debonding.

The low velocity impact tests were simulated using a rigid body for the spherical impactor and boundary conditions similar to the experiments. These simulations are especially valuable as a quantitative comparison between experiments and simulations in terms of force and energy plots is possible – these data are not available for the HVI tests. Fig. 4.25 exemplarily shows the results of the 60 J low velocity impact simulation on the dual-core sandwich. The qualitative correlation of the damage pattern and the indentation depth appear to be very good. Also the force and energy curves are consistent, although the expectation of a perfect correlation would not be justifiable due to the high complexity of the models and potential imperfections in the structure. However, the general correlation can be judged as very satisfactory, making the models useful for parameter studies and their extension for high velocity impact simulations.

The high velocity impact simulation shown here is limited to the steel cube impactor, which was also modelled as a rigid body with an initial velocity according to the experiments. Unlike in the low velocity case, no force or energy data for a quantitative correlation of test and simulation are available, as their measurement is not possible due to the high oscillations involved in the test. But this makes the evaluation of the numerical results especially helpful, as it allows for the analysis of data that are not available from the experiments. This is shown in Fig. 4.26 for the example of a penetrating impactor in a dual-core foldcore model. First of all, the correlation of the damage pattern compared to the cross-section of the real specimen is very good. The upper skin and middle layer are penetrated with a crushed carbon foldcore. Interesting is the evaluation of the impactor's kinetic energy plot in the simulation, as it allows to quantify, how much energy is absorbed by penetrating through the skin or by crushing the foldcore. In Fig. 4.26 it can be seen that the skins absorb much more energy as for example the compression of the aramid foldcore between points (b) and (c). Almost all of the initial kinetic energy is absorbed by the sandwich structure, only a small amount is returned as elastic spring-back. This example shows the advantages of such numerical models in the detailed evaluation of result data, which are not available from the experimental tests.

Assessing the modelling methods of foldcore sandwich structures, the major issues are seen in: foldcore cell wall material modelling, foldcore imperfection modelling, sandwich skin material modelling, skin/core debonding modelling and contact modelling. At the end of the project many experiences were gained and the impact simulation results correlated well with the experimental data, but still some uncertainties and possibilities for improvements are seen, especially in the composite material and interface modelling.

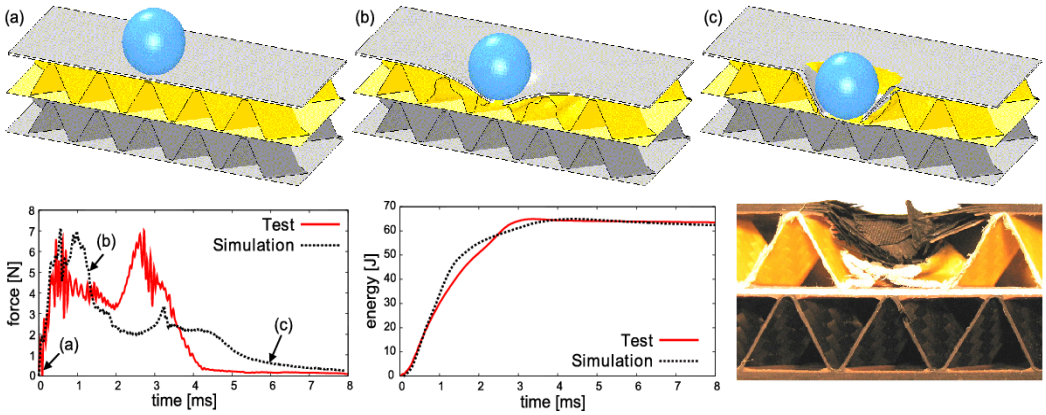

Fig. 4.25: Validation of low velocity impact simulation on dual-core sandwich

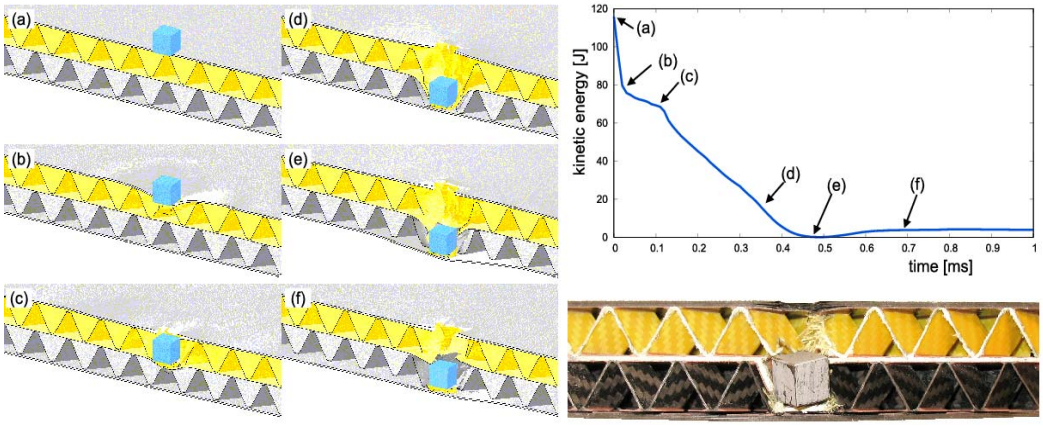

Fig. 4.26: Validation of high velocity impact simulation on dual-core sandwich

b) Optimisation study of CHC cores

DLR:

A study to investigate optimised foldcore geometries was performed by DLR by linking parametric FE models of a foldcore cell to the optimisation program PAM-OPT, which in turn controlled PAM-CRASH solver runs with changed parameters. The study investigated optimum foldcore configurations under compression, shear and impact loading. The study incorporated a deterministic parameter-variation and an optimisation in which the foldcore geometry was optimised for mass specific energy absorption and mass specific peak load in case of shear and compression loading and for maximal impact depth in case of impact loading. Fig. 4.27 shows the optimised cell geometries for foldcore under compression and shear loads, based on 20 mm core thickness, with optimisation criterion the maximum mass specific energy absorbed. This led to development of improved foldcore structures with 'block core' similar to the middle geometry in Fig. 4.27.

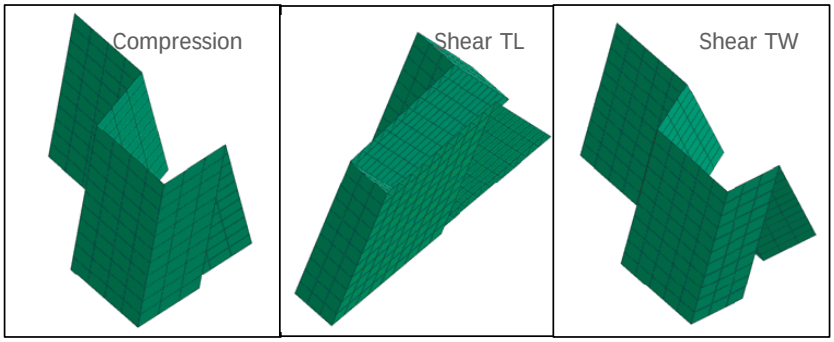

Fig. 4.27: Optimised foldcore geometries for core compression and shear loads, based on mass specific energy absorbed

CRC-G:

The cell geometry of the CFRP foldcore investigated by CRC-G in the first phase of the CELPACT project was based on experiences by the foldcore manufacturer KSTU (Kazan State Technical University). To find an improved geometry for the second phase of the project, CRC-G performed a geometric optimisation study on a numerical basis. The goal was to find a geometry with improved mechanical properties under flatwise compression while maintaining the same global density of the foldcore structure. A parametric foldcore model in PATRAN was the basis for the optimisation of the foldcore cell geometry. The aim was to investigate the influence of changing single geometric parameters like edge lengths and to identify a geometry, which had the same core height and density but higher mechanical properties under compression loads, which is most favourable for an impact optimised core structure. The shear properties were allowed to be slightly lower. Another boundary condition was to keep the producibility of the core, i.e. the cell walls should not be too small that a discontinuous manufacturing would be impossible. In a first step, the single geometry parameters were changed and the resulting stress-curves, obtained in compression test simulations in LS-DYNA, were divided by the resulting density. This was necessary, since the parameter change affected the overall density, and an improvement in compressive strength is no benefit for a lightweight core structure if the density increases as well. In a second step, two parameters were changed at the same time, while the third one was kept constant. The other two were changed in such a way that the overall density always was constant (102 kg/m³). With the help of this information an improved geometry could be defined, which is shown in Fig. 4.28. Compared to the original geometry the cell walls are smaller, which means higher buckling loads, and the vertical angle is lower, which leads to an orientation more parallel to the load direction. As can be seen the buckling load could be increased by 66%, the compressive strength by 29% and the compressive stiffness by 2% while maintaining the same density and core height. In the second phase of the CELPACT project foldcore samples based on this geometry were manufactured and tested, proving the correctness of these simulation results.

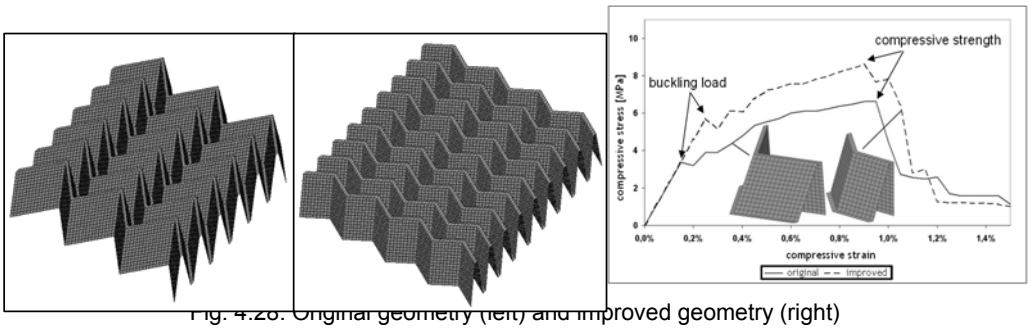

Fig. 4.28: Original geometry (left) and improved geometry (right)

c) Assessment of CHC manufacturing methods

USTU:

During the project, a number of foldcores were successfully produced by USTU. Used base materials were aluminium foil and aramid paper. Also different unit-cell geometries were used, zigzag unit-cells, 3-HAP unit cells and blocked configurations. The foldcores with different geometries and base materials are shown in Fig. 4.29.

The achieved quality of the foldcores was good. The geometrical imperfections (for example deflections in height) were low. The desired core density and core height were achieved. It is noted that density and height of a foldcore can be varied in wide ranges by changing the unit cell geometry. The cores were used to build up various sandwich samples together with aluminium, GFRP and CFRP face sheets. Bonding of the foldcores to face sheets with a film adhesive was possible without problems. New unit-cell geometries like the blocked configuration and new materials like aluminium foil were successfully introduced to the production methodology. Also cores with high densities of more than 100 kg/m³ were built. Before this, typical core densities were below 75 kg/m³. The production methods allow also the manufacturing of foldcores with varying unit cell geometry (Fig. 4.30). So the core can be tailored in order to fit to the surrounding geometry. Also continuous manufacturing is possible which allows building cores for large panels in a cost-effective process (Fig. 4.31).

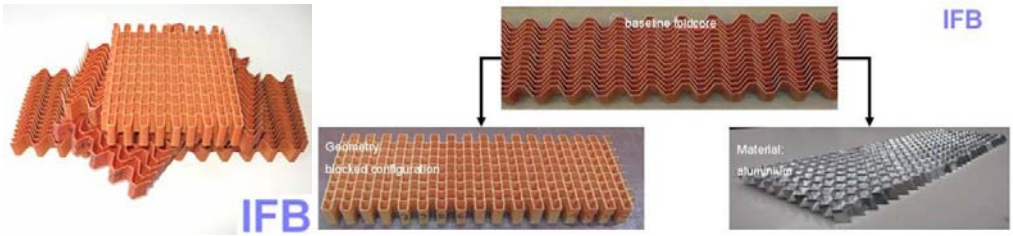

Fig. 4.29: Some of the foldcores produced during CELPACT

Fig. 4.30: Foldcore with varying unit cell geometry

Fig. 4.31: Continuous produced foldcore

CRC-G:

The basic principle of the discontinuous folding technology by the Kazan State Technical University used for the foldcore manufacturing in the CELPACT project is to convert a flat sheet of material into the final foldcore shape by folding or locally bending the material without elongating it, by the use of transformable matrices.

The discontinuous CHC manufacturing process is in general rather simple but very robust and effective. The choice of potential materials or geometries is almost unrestricted. All materials that are foldable and available as flat sheets can be used, like metals, composites, polymers, paper, cardboard etc. Some examples of different CHC folded cores made of composite materials are shown in Fig. 4.32.

The foldcore geometry can also be changed in a number of different ways. The length measures of the simple Z-crimp geometry can be changed arbitrarily. Therefore, the foldcore height can also easily be changed and the limitations arise only due to a worsening of the buckling behaviour. Beside the regular Z-crimp configuration also other geometries can be folded. Furthermore, unsymmetrical or non-uniform configurations as well as curved geometries can be folded.

This manufacturing technique is rather simple and a variety of different configurations and materials can be folded. If a new geometry is to be folded, new tools have to be built. Those are the transformable matrices and the post-curing mould. The foldcore specimens cannot be produced in an infinite size using the discontinuous manufacturing technology. The specimen size is limited by the size of the folding tool and by the size of the autoclave for post-curing. The quality of the foldcore with respect to the uniformity of its cell geometry depends on the quality of the transformable matrices. The metallic parallelograms have to be cut and joined with high precision. These discontinuously produced foldcore specimens are not suited as core structures for large panels but rather for smaller structures. The main characteristics of carbon fibre-reinforced Z-crimp foldcores are the high weight-specific stiffness and strength values as well as the ventability.

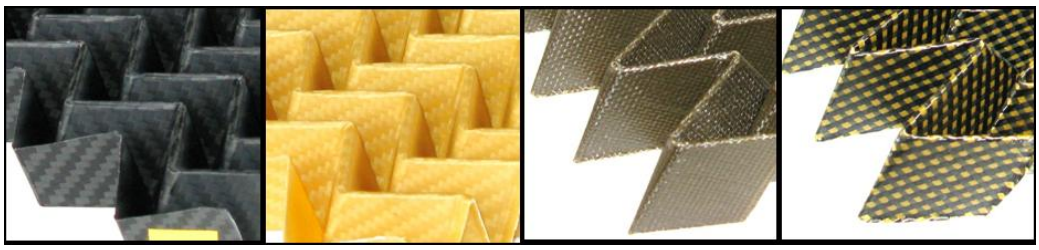

Fig. 4.32: Foldcores made of woven carbon fibre fabric prepreg, woven Kevlar fibre fabric prepreg, woven basalt fibre fabric prepreg, woven carbon/Kevlar fibre fabric prepreg (f.l.t.r.)

3. Assessment of CM & CHC performance for aircraft applications

A-D:

A-D reviewed all test and simulation results in CELPACT with respect to proven performance regarding impact resistance and specific energy dissipation and compared it with conventional honeycomb sandwich applications. According to a given zoning of an aircraft for impact statistical threats and by distinguishing between low and high velocity and low and high energy impact scenarios, a list of structural components was compiled for potential application of new cellular structures. Current general limitations and requirements for using sandwich in primary and secondary aircraft structures and in sacrificial shielding applications were highlighted. Depending on the design drivers of a specific application of cellular structures the current industrial sandwich sizing process at Airbus was reviewed w.r.t. to necessary changes required, e.g. for replacing semi-analytical procedures valid only for honeycomb, by analytical and numerical modelling approaches as developed in CELPACT.

EADS IW-F:

CM core structures have been tested according a multiscale approach to assess the quasi-static and dynamic properties of the materials, the understanding of the materials behaviour, the robustness of the testing and modelling. From the tests, the following Table 4.1 is providing recommendations on the performance of the materials according the following parameters:
- resistance to soft impacts
- resistance to hard impacts
- resistance for structural design
- convenience for high velocities impacts
- convenience for low velocities impacts

More specific tests are for sure needed to complete this first overview and notably the evaluation remaining for the cases without any mark. Next step can also be dedicated to check the capacity of each material to answer specific requirements.

Table 4.1: Recommendations for use

Materials	resistance to soft impacts	resistance to hard impacts	resistance for structural design	convenience for high velocities impacts	convenience for low velocities impacts
Al honeycomb	2	tbc	1	2	2
Ateca-Wadley struc.	2	tbc	4	2	tbc
Al folded cores	tbc	tbc	4	tbc	tbc
Hollow spheres	1 but heavy	tbc	3	1	2-3 but heavy
SLM Stainless steel	tbc	tbc	2	tbc	3
SLM Ti	tbc	tbc	2	2	3

1 : very good behaviour 2 : good behaviour 3 : can be efficient 4 : Not efficient tbc : to be checked

WP 5.2: Road Map to Applications (task Leader: A-D)

WP Leader	A-D
Participants	DLR, ULIV, UPAT, RWTH, USTU, A-D, EADS IW F, CRC-G

The aim of this task is to focus on the uptake of the CELPACT CM and CHC technologies by the aircraft industry: in particular, the new fabrication routes for composites and metals, the novel twin-walled structural concepts and improved design analysis tools.

Recommendations were made for the Technology Assessment Reports and Design Guides being written in T4.3, which aim to summarise the CELPACT results in a form suitable for aircraft structural

designers. A ‘Road Map to Applications Reports’ was produced at the Mid-term Critical Design Review and at the end of the project.

Within WP5.2, the main activity of the ‘Road Map’ Working Group was to review the progress and achievements made with CM and CHC technologies with respect to readiness level requirements defined by the three industrial partners: A-D, EADS IW F and CRC-G. The critical assessment of the technology readiness level (TRL) reached was performed for the various cellular materials separately also taking into account the level of validation achieved for the corresponding analysis techniques.

According to the basic definitions of TRLs, the focus was set on TRL3, for which a set of assessment criteria was defined and evaluated for each of the categories performance, value & risk, engineering, manufacturing and operation.

With the input from the technology assessment performed in WP 4.3 on the potential areas of application, the road-map was created defining the next steps on the way to industrial application, but also identifying potential limitations or show-stoppers.

2. Dissemination and use

List of **Publishable** results of the Final plan for using and disseminating the knowledge :

	WP	Exploitable Knowledge (description)	Exploitable product(s) or measure(s)	Sector(s) of application	Timetable for commercial use	Patents or other IPR protection	Owner & Other Partner(s) involved
1	WP1, WP4	*Novel structural concept of open lattice metallic cellular cores*	*The design concept (material systems and structural details)*	*1.Aeronautics – energy absorption sectors* *2. Automotive* *3. Research Establishments* *4. Education establishments* *5. Airworthiness authorities*	*2010* *2011*	*A concept patent is planned for year 2010*	***ULIV (owner)*** ***CRC-F*** ***ATECA***
2	WP1, WP4	*Novel structural concept of closed metallic cellular cores*	*The design concept (material systems and structural details)*	*1.Aeronautics – energy absorption sectors* *2. Automotive* *3. Research Establishments* *4. Education establishments* *5. Airworthiness authorities*	*2009 (ATECA)* *2010* *2011*	*A concept patent is planned for year 2010*	***CRC-F*** ***ATECA*** ***(owners)***
3	WP1, WP4	*Foldcore composite structural concept*	*The design concept (material systems and structural details)*	*1.Aeronautics – energy absorption sectors* *2. Automotive* *3. Research Establishments* *4. Education establishments* *5. Airworthiness authorities*	*2011* *2012*		***USTU*** ***CRC-G*** ***(owners)***
4	WP2	*Unit-cell microscale models*	*Analysis methods, software, guidelines*	*1. Aeronautics, 2. Marine,* *3, Automotive, 4. Packaging* *5. Education establishments* *6. Research Establishments*	*2009* *2010*	*No patents are foreseen*	***DLR,*** ***CRC-G,*** ***RWTH,*** ***ULIV,*** ***UOXF,*** ***LMT,*** ***UBRN,*** ***UPAT***

	WP	Exploitable Knowledge (description)	Exploitable product(s) or measure(s)	Sector(s) of application	Timetable for commercial use	Patents or other IPR protection	Owner & Other Partner(s) involved
							(owners)
5	WP2	*Homogenisation and multiscale models*	*Analysis methods, software, guidelines*	*1. Aeronautics, 2. Marine,* *3, Automotive, 4. Packaging* *5. Education establishments* *6. Research Establishments*	*2009* *2010*	*No patents are foreseen*	***DLR,*** ***CRC-G,*** ***RWTH,*** ***ULIV,*** ***UOXF,*** ***LMT,*** ***UBRN,*** ***UPAT*** (owners)
6	WP2, WP4	*Impact models for technology validation*	*Analysis methods, software, guidelines*	*1. Aeronautics, 2. Marine,* *3, Automotive, 4. Packaging* *5. Education establishments* *6. Research Establishments*	*2009* *2010*	*No patents are foreseen*	***DLR,*** ***CRC-G,*** ***RWTH,*** ***ULIV,*** ***UOXF,*** ***LMT,*** ***UBRN,*** ***UPAT*** (owners)
7	WP3	*Experimental results of the mechanical behaviour of the cellular materials and structures*	*Experimental technique know-how, mechanical properties, guidelines*	*1.Aeronautics,* *2.Marine,* *3.Automotive,* *4.Consumer* *5. Education establishments* *6. Research Establishments*	*2009* *2010*	*No patents are foreseen*	***DLR,*** ***CRC-F,*** ***CRC-G*** ***UOXF,*** ***RWTH,*** ***UPAT*** ***LMT*** ***(owners)***
8	WP1, WP4	*Selective Laser Melting for manufacturing complex three dimensional open lattice structures*	*The SLM manufacturing process know-how*	*1.Aeronautics – energy absorption areas* *2. Automotive* *3. Education establishments* *4. Research Establishments*	*2009* *2010*	*A patent is planned for year 2010*	***ULIV (owner)***
9	WP1, WP4	*Manufacturing process of cellular metallic structures out of thin sheets (bonded type)*	*The adhesive (or brazing) manufacturing process know-how*	*1.Aeronautics – energy absorption areas* *2. Automotive* *3. Education*	*Hollow spheres already commercially available*	*No patent planned for hollow spheres (existing technique)*	***CRC-F*** ***ATECA*** ***(owner)***

	WP	Exploitable Knowledge (description)	Exploitable product(s) or measure(s)	Sector(s) of application	Timetable for commercial use	Patents or other IPR protection	Owner & Other Partner(s) involved
		and hollow spheres adhesively bonded (or brazed)		*establishments* *4. Research Establishments*			
10	WP1, WP4	*Manufacturing process for folded composite cell structures from paper and prepregs*	*The foldcore manufacturing technology know-how*	*1.Aeronautics – energy absorption areas* *2. Automotive* *3. Education establishments* *4. Research Establishments*	*2009* *2010 ?*		***USTU*** ***(owner)***
11	WP1, WP4	*Design and fabrication of functional sandwich structures with the innovative cores*	*The manufacturing of sandwich cellular structures know-how*	*1.Aeronautics – energy absorption areas* *2. Automotive* *3. Education establishments* *4. Research Establishments*	*2009* *2010*	*A materials patent is planned for year 200x*	***(owner)***

Commentaire [ALMA, StO1] : Insert a name